Removal or Immobilization of Arsenic by Stabilized Magnetite Nanoparticles in Water, Soil and Poultry Litter

by

Qiqi Liang

A dissertation submitted to the Graduate Faculty of
Auburn University
in partial fulfillment of the
requirements for the Degree of
Doctor of Philosophy

Auburn, Alabama
May 5th, 2013

Keywords: Arsenic, Magnetite, Stabilized Nanoparticles,
Roxarsone, Fe-Mn

Approved by

Dongye Zhao, Chair, Huff Professor of Environmental Engineering
Mark Barnett, Malcolm Pirnie Professor of Environmental Engineering
Ahjeong Son, Assistant Professor of Environmental Engineering
Yucheng Feng, Professor of Agronomy & Soils
German Mills, Associate Professor of Chemistry & Biochemistry

Abstract

Stabilized magnetite (Fe_3O_4) nanoparticles were synthesized and extensively tested for enhanced removal of arsenate, As(V), from water, and for in situ immobilization of arsenic in soil and poultry litter. Two low-cost and "green" polysaccharides, a water-soluble starch and sodium carboxymethyl cellulose (CMC), were used as stabilizers to facilitate particle size control and enhance adsorption capacity. Results indicated that particle size, morphology, soil mobility and arsenic sorption capacity can be controlled by manipulating the stabilizer type and concentration. Starch at ≥0.04 wt.% or CMC at ≥0.005 wt.% can stabilize 0.1 g/L (as Fe) of the nanoparticles. While CMC-stabilized magnetite displays a highly negative zeta (ζ) potential, starch-stabilized magnetite shows a nearly neutral surface. Starch-stabilized magnetite offers much faster sorption rate and greater capacity than CMC-stabilized magnetite. Increasing starch concentration from 0 to 0.04 wt.% doubles arsenate uptake, yet the nanoparticles remain settleable by gravity. Further increasing starch concentration to 0.1 wt.% results in fully dispersed nanoparticles and an increase in arsenate uptake by 14%. The sorption kinetics can be modeled using an intraparticle-diffusion model. The sorption capacity increases with decreasing pH. Dissolved organic matter at 20 mg/L as TOC decreases arsenate uptake by 19%. When aged for >1.5 years, the nanoparticles did not show any arsenate leaching or particle dissolution.

As(V) immobilization in soil using starch-stabilized magnetite nanoparticles was investigated through a series of batch and column experiments. Batch sorption tests showed that the nanoparticles could effectively immobilize As(V) in As(V)-laden sandy soil with As

distribution coefficient for nanoparticles of 9999.5 L/g, which is >5 orders of magnitude than for the sandy soil. As leachability based on TCLP (Toxicity Characteristic Leaching Procedure) was reduced by 80% upon the nanoparticle treatment. Column tests showed that water-leachable As(V) from the sandy soil containing 31.45 mg/kg As was reduced by ~93% and the TCLP leachability by >83% when the soil was treated with 34 pore volumes (PVs) of a 0.1 g/L Fe_3O_4 nanoparticle suspension. The starch stabilizer was able to facilitate the soil deliverability of the nanoparticles, and the effective travel distance of the stabilized nanoparticles can be manipulated by controlling the injection flow rate. Once delivered, the Fe_3O_4 nanoparticles are retained by the soil matrix within a limited distance (<10 cm) under natural groundwater flow conditions (velocity $\leq 2.2\times10^{-7}$ cm/s).

Magnetite and Fe-Mn binary oxide nanoparticles were prepared and tested for reducing arsenic (As) leaching from poultry litter (PL). At a magnetite dosage of 2.5 g/L as Fe, or Fe-Mn dose of 0.5 g/L as Fe, >93% of ~150 mg/L soluble As in PL leachates was removed from the aqueous phrase within 24 hours. The Fe-Mn binary oxide particles, which act as an oxidizing agent and an high capacity adsorbent, showed 3.8 times higher arsenic sorption capacity than the magnetite particles based on batch tests. The arsenic sorption for both magnetite and Fe-Mn oxide particles was pH-dependent. 18% and 12% more of As was removed by magnetite and Fe-Mn, respectively, from aqueous phrase when pH was dropped from 10 to 4. The use of polysaccharide (a water-soluble starch and carboxymethyl cellulose) enhanced arsenic sorption at different extent. Column tests that simulate field application of PL suggested that amending PL with the nanoparticles reduced the total leachable arsenic by more than 91% compared to untreated PL. The results indicated that amending PL using low-cost and “green” particles may greatly mitigate adverse environmental impacts associated with land application of PL.

Acknowledgments

I would never have been able to finish my dissertation without the guidance of my committee members, help from friends, and support from my family.

In the first place, I would like to express my greatest gratitude to Dr. Dongye Zhao for his excellent guidance, caring, patience, and providing me with an excellent atmosphere for doing research. His truly scientist intuition has made him as a constant oasis of ideas and passions in science, which exceptionally inspired and enriched my growth as a student, a researcher and an engineer. I am indebted to him more than he knows.

I gratefully acknowledge enlightened guidance from my committee members Drs. Mark Barnett, Yucheng Feng, German Mills and Ahjeong Son for their encouraging words, thoughtful criticism, time and attention in their busy schedules. I would also like to thank Dr. John Blake, who let me experience the research of poultry litter in the field and practical issues beyond the textbooks.

I would like to thank Jinling Zhuang for the analytical and mechanical assistance. It is also a pleasure to pay tributes to my fellow students in the environmental engineering program here at AU for their research advice and for creating a supportive environment. It would have been a lonely lab without them.

Finally, I would like to thank my parents and friends for their support and encouragement throughout this work.

Table of Contents

List of Tables

List of Figures

Chapter 1. General Introduction

1.1 Background

Arsenic is ranked first on the most recent priority list of Superfund site (ATSDR, 2011). The presence of arsenic (As) in soil and water is widespread. The U.S. EPA estimates that approximately 2% of the U.S. population receives drinking water containing > 10 μg/L As (Holm, 2002), and the Natural Resources Defense Council estimates that ~56 million people in the U.S. drinking water with As at unsafe levels.

Arsenic has been associated with various cancerous and non-cancerous health effects (An et al., 2005). According to a recent report by the National Academy of Science (NAS) and National Research Council (National Research Council, 2001), even at 3 μg/L of As, the risk of bladder and lung cancer is between 4 and 7 deaths per 10,000 people. At 10 μg/L, the risk increases to between 12 and 23 deaths per 10,000 people (National Research Council, 2001).

Triggered by risk concern, the U.S. EPA announced its ruling in October 2001 to lower the maximum contaminant level (MCL) from the prior 50 μg/L (established in 1942) to 10 μg/L with an effective date of January 22, 2006 (An et al., 2005). This ruling poses tremendous impacts on water utilities. Approximately 4,100 water utilities serving ~13 million people are affected by this law (Environmental Protection Agency, 2001b). The compliance costs have been estimated to be ~$600 million per year using current treatment technologies (Frey et al., 2000).

In soil and groundwater, As predominantly exists in two oxidation states, As(V) and As(III), with specific forms influenced by pH and redox (Amini et al., 2008) conditions. It has

been quite common for both species to coexist. Consequently, simultaneous removal of As(V) and As(III) are often required in drinking water treatment.

Adsorption has been one of the most employed technologies for removal of trace levels of As (Jang et al., 2006). Numerous studies have showed that various types of iron oxides can effectively adsorb both As(V) and As(III) (Bissen and Frimmel, 2003; Farquhar et al., 2002; Pierce and Moore, 1982; Raven et al., 1998; Zhang et al., 2007). Moreover, researchers found that reducing the size of the adsorbent particles to the nanoscale can substantially increase As uptake because of the much gained specific surface area. For instance, decreasing particle size from 300 nm to 12 nm can increase the adsorption capacity for both As(III) and As(V) by nearly 200 times (Yean et al., 2005). However, the nanoparticles without a stabilizer or surface modifier tend to agglomerate rapidly into micron-scale or larger aggregates, thereby greatly diminishing the specific surface area and As sorption capacity.

To prevent particle agglomeration, various particle stabilizing techniques have been developed in recent years (He and Zhao, 2005; Si et al., 2004; Yean et al., 2005). Of many stabilizers reported, polysaccharides such as starch and carboxymethyl cellulose (CMC, molecular weight = 90, 000) have been found not only effective in facilitating size control of various metal and metal oxides nanoparticles, but also cost-effective and environmentally benign. The proper use of stabilizers can maintain a high specific surface area and high reactivity of the nanoparticles. Furthermore, the stabilizers can facilitate manipulation of the morphology of the nanoparticles suitable for desired environmental cleanup applications.

1.2 Synthesis of polysaccharide bridged or stabilized magnetite nanoparticles

For water treatment, two features of nanoparticles are desired: 1) the particles should offer high adsorption capacity; 2) the spent particles should be amenable to easy separation from water and must not cause any harmful effect on the treated water. To this end, the desired form of magnetite would be a water-based suspension, in which magnetite nanoparticles are present as inter-bridged flocs. The bridged nanoparticles offer the advantages of high As sorption capacity and easy separation after the desired use. Alternatively, fully stabilized magnetite nanoparticles may also be used for water treatment. However, an external magnetic field will need to be employed to separate the spent nanoparticles (Yavuz et al., 2006). For in situ As immobilization, the prerequisite is that the nanoparticles must be deliverable in the soil. Therefore, fully stabilized nanoparticles are required.

There have been two main schemes for preparing magnetite nanoparticles: a) decomposition of organic iron precursors at high temperatures, and b) aqueous-phase coprecipitation of ferrous-ferric ions at elevated pH. In the organic decomposition scheme, for instance, Yean et al. demonstrated that at 320 ^{o}C the reaction of FeO(OH) in oleic acid and 1-octadecene resulted in magnetite nanoparticles with an average size of 11.72 nm (Yean et al., 2005). The main drawback of this approach is the use of organic solvents and the high energy input. In contrast, the aqueous coprecipitation scheme is rather straightforward. It is conducted at room temperature and only requires pH adjustment in the aqueous phase without involving any organic solvents. Yet, without a stabilizer, this method fails to control the particle size and aggregation of the resulting nanoparticles (Sun and Zeng, 2002).

The following modified scheme was proposed for preparing polysaccharide bridged or fully stabilized magnetite nanoparticles:

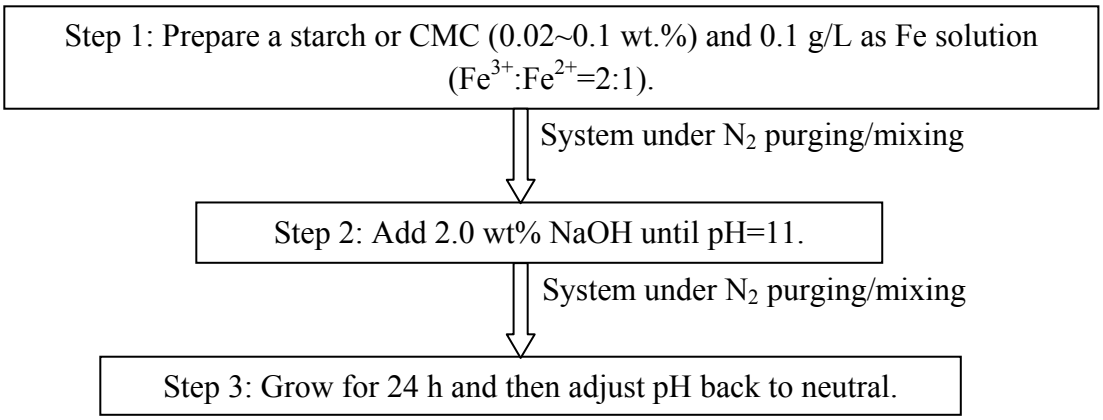

As rapid precipitation of $Fe(OH)_2$ occurs after addition of sodium hydroxide solution to the mixture of Fe^{3+}-Fe^{2+}, the magnetite formation begins with oxidation of $[Fe(OH)]^+$ (the dissolved form of $Fe(OH)_2$ (solid) in water). Subsequently, the oxidation brings about the intermediate product $[Fe_2(OH)_3]^{+3}{}_{(aq)}$, which can combine with another $[Fe(OH)]^+$ to form $[Fe_3O(OH)_4]^{2+}{}_{(aq)}$ that has the same Fe^{2+}/Fe^{3+} ratio as magnetite. **Eq. 1.1-3** depicts the key chemical reactions involved (Manning et al., 2002; Roonasi and Holmgren, 2009):

$$Fe(OH)_{2\ (solid)} \leftrightarrow [Fe(OH)]^{+}{}_{(aq)} + OH^- \quad \textbf{(Eq. 1.1)}$$

$$2[Fe(OH)]^{+}{}_{(aq)} + \frac{1}{2}O_2 + H_2O \rightarrow [Fe_2(OH)_3]^{+3}{}_{(aq)} + OH^- \quad \textbf{(Eq. 1.2)}$$

$$[Fe_2(OH)_3]^{+3}{}_{(aq)} + [Fe(OH)]^{+}{}_{(aq)} + 2OH^- \rightarrow [Fe_3O(OH)_4]^{2+}{}_{(aq)} + H_2O \quad \textbf{(Eq. 1.3)}$$

At highly oxidizing environment or low pH, $[Fe_3O(OH)_4]^{2+}{}_{(aq)}$ will further oxidize to goethite or ferric hydroxides. On the other hand, at low dissolved oxygen (DO) and high pH, $[Fe_3O(OH)_4]^{2+}{}_{(aq)}$ will nucleate and/or crystallize to form magnetite particles:

$$Fe_3O(OH)_4{}^{2+}{}_{(aq)} + 2OH^- \rightarrow Fe_3O_{4(solid)} + 3H_2O \quad \textbf{(Eq. 1.4)}$$

In the absence of a stabilizer, the magnetite particles will agglomerate into micron scale or larger aggregates that will settle out of the aqueous phase by gravity. However, in the presence

of an effective stabilizer such as starch or CMC, the growth rate and extent, and thus, the size, of the nanoparticles can be controlled (He and Zhao, 2005; 2007; He et al., 2007). Researchers at Auburn University (An et al., 2011a; He and Zhao, 2007; Liang et al., 2012a) also demonstrated that the particle size and surface chemistry can be manipulated by means of starch and/or CMC stabilizers at various concentrations, molecular weights and degree of substitution.

1.3 Soil contamination and As-leaching from poultry litter

Arsenic is a natural component of surface soils and soil is a complex matrix providing 90% of all human food, livestock feed, fiber and fuel (Belluck et al., 2003). Arsenic is naturally abundant in sulfide-bearing mineral deposits, especially those associated with gold mineralization, and it has a strong affinity for pyrite (Nordstrom, 2002) and hydrous iron oxides. Arsenic, despite its toxicity, is readily used by a great diversity of prokaryotes for cell growth and metabolism (Stolz et al., 2006). Thus, the mechanism for As release into drinking water and soil typically involves the reductive dissolution of ferric(hydr)oxide minerals and/or the reduction of arsenate to its more toxic compound arsenite (Saltikov et al., 2005).

It was also reported that 28,400-94,000 tons of As was released annually to soil from anthropogenic sources, which widely included coal burning, mine tailings, smelters, agriculture, chemical manufacturing, urban and forestry wastes, etc (Belluck et al., 2003). Background concentrations of As are variable based on local geological and habitation characteristics. Typically, average or mean background levels usually are in the low parts per million range worldwide, unless elevated by local high As contained minerals or anthropogenic activity. For example, the background As concentration in soil is 7.5 ppm in the United States (Belluck et al., 2003). As soil retention times are variously estimated at 1000-3000 years in moderate climates and a default half-life estimate is 10^8 days (Belluck et al., 2003). Arsenic chronic numerical

limits in soil, based on cancer end points, range from about 0.4 ppm to about 40 ppm to one-in-ten-thousand incremental cancer risk range (Abernathy et al., 1999). In the United States, there are 1300 sites on the National Priority List (NPL) for the treatment of contaminated soils, indicating the extensiveness of soil contamination. Arsenic is not only present in groundwater in all 50 states, but also found in soil and mineral deposits. Arsenic in soil results from human activities including pesticide use, mining and ore processing operations, operating coal burning power plants, and waste disposal (Belluck et al., 2003). Contamination in excess of 1000 As mg/kg has been recorded at many sites throughout Australia. Similar contaminated sites also exist in the United States (Smith et al., 1998). Sites of former tanneries, which make leather from animal hides, have large amounts of arsenic in the soil. The persistence of As residues in soil and toxicity to both plants and animals is of concern.

Roxarsone, 3-nitro-4-hydroxyphenylarsonic acid, is an organoarsenic compound that is used extensively in the feed of broiler poultry to control coccidial intestinal parasites, improve feed efficiency and promote rapid growth (Garbarino et al., 2003). Generally, poultry litter (PL) has been applied at the rate of 8.96-20.16 mg/ha on agricultural lands (Christen, 2001) with the mean total As concentration in PL of 14-76 mg/kg (Arai et al., 2003). It has been estimated that around 70% of domestically raised broiler chickens receive roxarsone (Chapman and Johnson, 2002), totaling between 1.7 and 2.2 million pounds of this drug added to poultry feed each year (Wallinga, 2006). It is confirmed in a market basket study (by Institute of Agricultrure and Trade Policy) of uncooked and prepared chicken tissue that detectable levels of arsenic were found in a variety of poultry products (Wallinga, 2006). While some roxarsone remains in chicken tissue, much of the drug has been demonstrated to be excreted in the waste (Rutherford et al., 2003a).

Typically, PL was repeatedly and intensely disposed onto local farmland to minimize the cost of disposal, thus introducing a substantial amount of As into the environment at up to 250 g/ha with every application (Garbarino et al., 2003). Furthermore, since most PL was stored outside, the wetting of PL during storage by rainfall will promote endemic microbial activities that could influence the stability of Roxarsone, resulting in the increase of As mobility through leaching. Research by The US Geological Survey (USGS) has shown that the majority of As in PL is rapidly converted once in the environment through both biotic and abiotic processes into more leachable inorganic forms (Garbarino et al., 2003).

Currently, there is no state or federal regulation on annual total metal(loid) inputs on agricultural lands via PL amendments. Since 70 to 90% of the As present in PL is water-soluble, the fate and transport of As was of most importance. The water soluble components are available for uptake by plants and other soil organisms. Concentrated As in soil water can contribute to elevated arsenic concentration in plants, which might become phytotoxic or lead to accumulation in human or animal that consume them.

It was established that Roxarsone in PL would quickly degrade into inorganic As (Rutherford et al., 2003a). Extraction of PL-amended soils indicates that weakly bound As mobilized by water associates with element C, P, Cu and Zn, while strongly bound As correlates with Fe (Rutherford et al., 2003). The extent of As desorption from PL increased with increasing time and pH from 4.5 to 7 (Arai et al., 2003). Interestingly, it was reported by Arai et al., (2009) that less than 15% of total As was desorbed after 5 replenishments at pH 7, which seems to be contradictive to the conclusion by Jackson and Bertsch (Jackson and Bertsch, 2001) that over 92% of total As, mostly roxarsone, was soluble after 2 hr of water extraction. Another study also showed that the distribution of arsenic in soil with 20 years' history of PL application was

indistinguishable (Morrison, 1969) or not significant (<15 mg/kg). However, the difference could be attributed to the photodegradation and biodegradation of roxarsone into arsenate anions, based on the findings that the biodegradation of roxarsone into arsenate anions was a function of incubation time and water content (Garbarino et al., 2003).

1.4 Objectives

The overall goal of this research is to investigate the feasibility of applying innovative technologies for remediation of groundwater and soils contaminated with As. The specific objectives of this research are to:

1. Synthesize a class of well dispersed nano-scale magnetite particles stabilized with "green" polysaccharides including a water soluble starch and sodium carboxymethyl cellulose (CMC). Characterize the nanoparticles using TEM, XRD analysis, zeta potential, UV-visible spectra and test the effect of stabilizer type and concentration on arsenate uptake by starch/CMC stabilized magnetite nanoparticles. The effects of water chemistry such as pH, DOM (Dissolved Organic Matter), competing ions on As(V) uptake by stabilized magnetite nanoparticles, as well as the leachability and long term (around 1~2 yrs) particle stability of stabilized magnetite nanoparticles, will be elucidated.

2. Design and carry out experiments to investigate the effects of stabilizer on As sorption kinetics with starch or CMC-stabilized magnetite nanoparticles. Probe various empirical sorption kinetics models such as the first/second order, power function, Elovich and parabolic diffusion models to describe arsenic sorption kinetics with stabilized magnetite nanoparticles. Construct and test proper film diffusion controlled models and intraparticle diffusion models to interpret sorption kinetics data.

3. Conduct batch equilibrium and kinetics tests with stabilized magnetite nanoparticles to test the effectiveness of starch-stabilized magnetite nanoparticles for immobilization of arsenate in As-contaminated soil. Determine the maximum transport distance (radius of effect) of stabilized magnetite nanoparticles by model in porous media through column breakthrough tests and transport modeling.

4. Investigate the effectiveness of magnetite and Fe-Mn nanoparticles amendment for reducing arsenic leachability from poultry litter through batch and column experiments.

1.5 Organization

This dissertation includes five chapters. Except for Chapter 1 (General Introduction) and Chapter 5 (Conclusions and Suggestions for Future Research), each chapter of this dissertation is formatted in the journal style of Water Research. Chapter 1 outlines the background and objectives of this dissertation. Chapter 2 introduces the synthesis of stabilized magnetite nanoparticle and their characterizations by TEM, DLS, XRD analysis, zeta potential and UV-visible spectra; it further investigates the arsenate sorption capacity, kinetics, the effect of stabilizer type and concentration, as well as the effects of water chemistry. This chapter is based on the information that has been published in Industrial and Engineering Chemistry Research (Liang et al., 2012). Chapter 3 describes the immobilization of As by stabilized magnetite nanoparticles in As-contaminated soil and calculates the maximum transport distance of stabilized magnetite nanoparticles. This chapter is based on the information that is going to be submitted in Water Research. Chapter 4 investigates the effectiveness of magnetite and Fe-Mn nanoparticles amendment for reducing As leachability from poultry litter. This chapter is based on the information that is to be submitted to Journal of Hazardous Materials. Chapter 6 gives a summary of major conclusions of this research and suggestions for future work.

Chapter 2. Effects of Stabilizers and Water Chemistry on Arsenate Sorption by Polysaccharide-Stabilized Magnetite Nanoparticles

This chapter studies magnetite nanoparticles, which were successfully synthesized with starch and sodium carboxymethyl cellulose (CMC) as a stabilizer, and tested for enhanced arsenate removal in water. The prepared nanoparticles were characterized with transmission electron microscope (TEM) and dynamic light scattering (DLS). Sorption kinetics and isotherms, effects of starch and CMC concentrations, pH, DOM (Dissolved Organic Matter) on stability of magnetite nanoparticles, As sorption capacity, and arsenate leachability are investigated through a series of batch tests.

2.1 Introduction

Arsenic (As) is a priority contaminant due to its potent toxicity and widespread contamination of groundwater across the globe (Amini et al., 2008). Chronic exposure to elevated levels of As has been associated with skin, bladder, and lung cancers (World Health Organization, 2000). Arsenic contamination of drinking water has been a serious problem in many regions worldwide, in particular, in the Bengal Delta of Bangladesh and India (Manning et al., 2002), the Red River Delta of Vietnam (Berg et al., 2001), South America (e.g. Chile and Argentina), and many other areas including the western United States (Welch et al., 1988). The World Health Organization (WHO) guideline value and the European maximum permissible concentration (MPC) for As in drinking water are both set at 10 μg/L (World Health

Organization, 2008). Effective in January 2006, the United States Environmental Protection Agency (Environmental Protection Agency, 2001b) lowered the maximum contaminant level (MCL) of As in drinking water from 50 to 10 μg/L.

To mitigate human exposure to As, a variety of technologies have been studied for arsenic removal from water, including coprecipitation (Gulledge and Oconnor, 1973), enhanced coagulation (Cheng et al., 1994), adsorption (Clifford, 1999), membrane filtration, anion exchange (An et al., 2005), reverse osmosis (Kang et al., 2000), bubble/foam flotation with colloidal ferric hydroxide (Kang et al., 2000; Peng and Di, 1994) and biological sequestration (Chen et al., 2011). However, it remains highly challenging to comply with the MCL of 10 μg/L in a cost-effective manner.

A number of studies have shown that iron oxides can effectively adsorb both As(V) and As(III) (Bissen and Frimmel, 2003; Pierce and Moore, 1982; Raven et al., 1998). Inner sphere surface complexation has been held responsible for the strong interactions between As and various iron oxides (Farquhar et al., 2002; Manning et al., 1998; Waychunas et al., 1993) .

Yean et al. (Yean et al., 2005) and Mayo et al. (Mayo et al., 2007) noted that the size of magnetite particles strongly influenced As adsorption capacity. For example, as particle size decreased from 300 nm to 12 nm, the sorption capacity for both As(III) and As(V) increased by nearly 200 times. However, magnetite particles prepared using traditional methods tend to agglomerate rapidly into micron scale or larger aggregates, greatly diminishing the specific surface area and As adsorption capacity.

There have been two main schemes for preparing magnetite nanoparticles: organic solvent-phase decomposition of an organic iron precursor at high temperatures and aqueous-phase coprecipitation of ferrous-ferric ions by a base (Gnanaprakash et al., 2007; Molday, 1984;

Si et al., 2004; Sun and Zeng, 2002; Woo et al., 2004; Yean et al., 2005). In the organic decomposition scheme, for example, Sun and Zeng (2002) demonstrated that at 265 °C, reaction of ferric acetylacetonate, $Fe(acac)_3$, in phenyl ether in the presence of alcohol, oleic acid and oleylamine resulted in magnetite nanoparticles of the size from 4nm to 20nm (Sun and Zeng, 2002). The primary drawback of this approach lies in the use of organic solvents and the high energy input. The aqueous coprecipitation scheme is rather straightforward, which only requires pH adjustment and produces no hazardous wastes. However, this method has limited success in controlling the particle aggregation and size (Sun and Zeng, 2002).

To prevent particle agglomeration, various particle stabilizing techniques have been tested (Gnanaprakash et al., 2007; Si et al., 2004; Sun and Zeng, 2002; Woo et al., 2004). Some recent work (He and Zhao, 2007; He et al., 2007; Si et al., 2004) has shown that the presence of polymeric stabilizers during the particle synthesis may effectively facilitate size control in aqueous solution. Consequently, we hypothesized that applying proper stabilizers to the coprecipitation approach may prevent particle aggregation, facilitate particle size control and result in much smaller nanoparticles. For environmental cleanup applications, it is desirable that such stabilizers are not only effective in particle stabilization, but also environmentally benign and cost-effective. He and Zhao (He and Zhao, 2005; 2007) developed a technique for preparing stabilized zero valent iron (ZVI) nanoparticles by applying low concentrations of starch or carboxymethyl cellulose (CMC) as a stabilizer. Given that typical ZVI nanoparticles are covered with a shell of iron oxides, i.e. the stabilizers are actually functioning through interacting with iron oxides, we postulated that the particle stabilization strategy would also work for stabilizing magnetite nanoparticles. Furthermore, based on work by He and Zhao (He and Zhao, 2005;

2007), the particle size and surface chemistry may be manipulated by employing various types and concentrations of starch and/or CMC stabilizers.

When used for water treatment, two features of the nanoparticles are desired: 1) the particles should offer high As removal capacity, and 2) the spent particles should be amenable to easy separation from water and must not cause any harmful effect on the treated water. While stabilized nanoscale magnetite particles may offer the unique advantage of greater sorption capacity for As, a weak magnetic field would be required to separate the highly dispersed nanoparticles from water. Yavuz et al. (2006) showed that magnetite nanoparticles of 20 nm (high temperature decomposition of Fe(O)OH in oleic acid using 1-octadecene as a solvent) could be separated under very low magnetic gradients (<100 T/m).

Yean et al.(2005) studied the effect of particle size and pH of magnetite stabilized with oleic acid (synthesized by the same method as by Yavuz et al. (2006) on the adsorption and desorption behavior of arsenite and arsenate, and investigated the effect of natural organic matter (NOM) on arsenic sorption. An et al.(2005) observed that starch-bridged magnetite nanoparticles were able to highly effectively remove arsenate from ion exchange brine. Yet, our knowledge remains lacking pertaining to the effect of stabilizers on particle characteristics, long-term stability and As sorption behaviors.

The overall goal of this study was to prepare and test a new class of polysaccharide-stabilized magnetite nanoparticles for enhanced arsenate removal. The specific objectives were to: 1) synthesize stabilized magnetite nanoparticles through the aqueous co-precipitation approach in the presence of various concentrations of starch or CMC; 2) characterize the stabilized magnetite nanoparticles; 3) determine the effects of the type and concentration of the stabilizers, solution pH and dissolved organic matter (DOM) on As(V) sorption capacity and

kinetics by the stabilized nanoparticles; and 4) test the long term leachability and stability of the nanoparticles and arsenate associated therewith.

2.2 Materials and Methods

2.2.1 Chemicals

CMC (sodium salt, M.W. = 90000), a water soluble potato starch (hydrolyzed for electrophoresis), and ferrous sulfate heptahydrate ($FeSO_4 \cdot 7H_2O$) were obtained from Acros Organics (Pittsburgh, PA, USA). Sodium arsenate heptahydrate ($Na_2HAsO_4 \cdot 7H_2O$) was purchased from Sigma-Aldrich (St. Louis, MO, USA). Ferric chloride ($FeCl_3$) and sodium hydroxide (NaOH) were obtained from Fisher Scientific (Pittsburgh, PA, USA). Hydrochloric acid and nitric acid were purchased from Mallinckrodt Chemical (St. Louis, MO, USA). A commercial magnetite powder was purchased from Nanostructured & Amorphous Materials, Inc. (Houston, TX, USA).

2.2.2 Preparation of stabilized magnetite nanoparticles

The stabilized magnetite nanoparticles were prepared in 250 mL flasks in the presence of the starch or CMC. First, a 1 wt.% starch stock solution was prepared, heated to boiling point for 15 min under magnetic stirring, and then cooled down to room temperature. In parallel, a 1 wt.% of CMC stock solution was prepared at room temperature. In the meantime, a ferrous-ferric stock solution was prepared at an Fe^{2+}:Fe^{3+} molar ratio of 1:2 by dissolving $FeSO_4 \cdot 7H_2O$ and $FeCl_3$ in deoxygenated DI water. In a typical preparation, an aliquot of the Fe^{2+}-Fe^{3+} stock solution was mixed with a fraction of a stabilizer stock solution to yield a mixture of 188 mL containing 0.1 g/L Fe and a stabilizer (starch or CMC) ranging from 0.002 to 0.1wt. %. Then, 12 mL of a 0.5 M NaOH solution was injected in one shot into the mixture to raise the pH of the solution to ~11 under N_2 purging. The clear solution then turned to a black suspension, indicating that the

magnetite nanoparticles were formed. The nanoparticles were allowed to grow for 24 hours under N_2 purging at room temperature. Then, the suspension pH was lowered to 6.8±0.4 by adding < 1 mL of 1M hydrochloric acid. Based on the preliminary results, this study focused on fully stabilized magnetite nanoparticle suspensions, which were prepared at a final concentration of 0.1 g/L as Fe and 0.1 wt.% of CMC (or starch).

2.2.3 Physical characterization of polysaccharide stabilized magnetite nanoparticles

Suspensions of magnetite nanoparticles were prepared at 0.1g/L as Fe and with various concentrations of starch or CMC. Upon proper dilution, one drop of the samples was placed on 300 mesh formvar-carbon coated copper grids (Electron Microscopy Sciences, Hatfield, PA, USA) and then overnight dried in a glove box purged with nitrogen gas. Then, Transmission Electron Microscope (TEM) micrographs of the dried magnetite nanoparticles were obtained using a ZEISS EM10 TEM operated at 60 kv. The TEM images were analyzed using an image processing software known as Image J. The original TEM images were first converted to 8 bit format and then segmented by adjusting the threshold value to obtain segmentations of the sharpest particle images. Based on TEM images, a total of 311 representative particles were measured to obtain the particle size distributions.

The magnetite particles prepared at 0.1g/L as Fe and 0.1 wt.% of a stabilizer (starch or CMC) were also subjected to powder X-ray diffraction (XRD) analysis. The samples were first freeze-dried using a VirTis freeze mobile freeze dryer (Gardiner, NY, USA) at -50℃ for 24-48 hours. The samples were then scanned at defracted angles (2θ) from 20.000° to 79.990° with a constant step width of 0.010° and step time of 500s at room temperature (25℃). The XRD was operated with a Bruker D8 Discover X-ray diffractometer (Bruker Corp., Madison, WI, USA) with a GADDS (General Area Detector Diffraction Solution) area detector, with a Cu target

(λ=1.54060 Å) and a 4-bounce monochromator Ge (022). The resultant spectra were further processed by means of a semi-quantitative phase analysis software EVA to subtract background, smooth the data and search for peaks.

The zeta (ζ) potential of the magnetite nanoparticles was measured using a Zetasizer Nano ZS (Malvern Instruments Corp., Malvern, Worcestershire, UK) at a 173 degree scattering angle. About 1 mL of each sample suspension was measured in a special light scattering cuvette. The measurement was performed at 25 °C and was started 2 min after the cuvette was placed in the apparatus to allow for temperature equilibration. Suspensions of magnetite nanoparticles prepared in duplicate at 0.1 g/L as Fe with 0.1wt.% starch or 0.1wt.% CMC were directly used for the analysis. For comparison, bare magnetite particles were prepared following the same procedure but without any stabilizer and analyzed in parallel. Note that for the bare particles, a 10 minutes sonication (1 minute pulse off time with every 2 minutes pulse on) was performed at amplitude of 50 using a Branson Ultrasonic Processor S-4000 (Danbury, CT, USA) right before the analysis to break the aggregates. ζ was measured from pH 2 to 11. The resultant ζ values were corrected with the viscosity of the suspension, which was measured using a Gilmont viscometer (Barnant Company, Barrington, IL, USA). The viscosity was 1.086 cP for 0.1wt.% starch-stabilized magnetite suspension and 2.318 cP for 0.1wt.% CMC-stabilized suspension.

The hydrodynamic diameter of the particles was measured using the same Malvern's Zetasizer instrument with the sonicated suspension. This size was based on measurement of dynamic light scattering (DLS) and was calculated with the Stokes-Einstein equation. The results were corrected using the corresponding viscosity values of the suspensions.

The transmittance curve of magnetite suspension samples in the UV and visible range (380-760 nm) were measured by a Hewlett-Packard/Agilent 8453 UV-Visible

Spectrophotometer. In each measurement, a 1-cm quartz cell containing 3 mL of a magnetite suspension was subjected to the UV-Vis measurements over a wavelength range of 190 nm to 1100 nm.

2.2.4 Effects of starch and CMC concentration on stability of magnetite nanoparticles and arsenic sorption capacity

To test the effects of the stabilizers, magnetite particles were prepared at a fixed magnetite concentration of 0.1 g/L as Fe but with 0.02, 0.04, 0.06, 0.08 and 0.1% (w/w) of starch, or 0.002, 0.005, 0.01, 0.02, 0.04, 0.06 and 0.1% (w/w) of CMC. The particle stability was then compared by comparing the visual transparency, UV-Vis absorbance, DLS-based hydrodynamic size, ζ potential and particle concentrations in the supernatants. The particle concentration was determined by dissolving the magnetite particles with concentrated hydrochloric acid (the volume of HCl needed is 4 mL for every 1 mL 0.1 g Fe/L) and measuring the total dissolved iron concentration. Equilibrium As(V) sorption capacities of these samples were examined in the same way as in the isotherm tests as described below.

2.2.5 Sorption kinetics and isotherms

Arsenate sorption kinetics and isotherms were tested in batch experiments using bare or stabilized (with 0.1 wt.% CMC or starch) magnetite nanoparticles. For kinetic tests, the initial arsenate concentration was set at 8.0 mg/L as As and the concentration of magnetite nanoparticles was fixed at 0.1 g/L as Fe in all cases. The pH of the magnetite suspension was kept at 6.8±0.4 during the course of the tests through intermittent adjustment using 0.1M hydrochloric acid and 0.1M sodium hydroxide. The experiments were initiated by mixing 12 mL of a suspension of nanoparticles with 3 mL of an arsenate solution in 15 mL centrifuge tubes. The mixtures were continuously mixed on an end-to-end rotator operated at 50 rpm at room

temperature (21±1°C). At predetermined times, duplicate tubes were sacrificially sampled. The samples were then filtered through a 25 nm membrane of mixed cellulose esters (Millipore Corp., Billerica, MA, USA). The membrane was able to completely remove the particles, but did not remove any soluble arsenate. The filtrates (3 mL) were acidified to pH < 2.0 with 1N HNO_3 and then analyzed for total As and Fe using a Perkin Elmer Graphite Atomic Absorption Spectrometer 3110 (connected with an HGA 600 and EDL system 2) and a VARIAN 220FS Flame Atomic Absorption Spectrometer, respectively. The detection limits for arsenic and iron were 5 ppb and 50 ppb, respectively. The amount of arsenate adsorbed to magnetite nanoparticles was calculated from the difference in the initial and final concentrations of As in the aqueous phase.

Batch isotherm tests were conducted in the same centrifuge tubes at a fixed magnetite concentration of 0.1g/L as Fe and at initial As concentrations ranging from 0.030 to 8.24 mg/L. The suspension pH was kept at 6.8±0.4. The magnetite-arsenate mixtures were equilibrated on an end-to-end rotator (50 rpm) for 144 hrs, which was sufficient for the system to reach equilibrium based on prior kinetic tests. Upon equilibrium, samples were processed in the same manner as in the kinetic tests and then analyzed for As and Fe. The arsenate uptake was determined by mass balance calculation.

To test the chemical stability of the nanoparticles and As that is associated therewith, the isotherm tests were extended to two months, and then 18 months. The concentrations of arsenic and iron in the aqueous phase were measured upon nano-filtration at these extended times.

2.2.6 Effect of pH on arsenate sorption

Equilibrium arsenate uptake by bare and stabilized magnetite nanoparticles was measured in the pH range of 2 to 11. The tests were carried out following the same procedures as in the

isotherm tests but at a fixed initial As concentration of 8.0 mg/L and a magnetite concentration of 0.1 g/L as Fe.

2.2.7 Effect of DOM on arsenate uptake

Sorption isotherms were also constructed in the presence of DOM at 10 mg/L and 20 mg/L as total organic carbon (TOC). DOM was prepared using the Suwannee River Humic Acid obtained from the International Humic Substances Society (IHSS, Georgia Tech, Atlanta, GA, USA). According to the supplier, the organic matter contains water (8.15%), ash (7.0%), C (52.47%), H (4.19%), O (42.69%), N (1.10%), S (0.65%) and P (0.02%) (all by weight). The initial and final concentration of DOM was determined by a Tekmar Dohrmann Phoenix 8000 UV- Persulfate TOC Analyzer (Mason, OH, USA).

2.2.8 Arsenate leachability

The leachability of magnetite-sorbed arsenate was determined following the EPA TCLP (Toxicity Characteristic Leaching Procedure) (EPA Method 1311). In the TCLP tests, the extracant known as Fluid No. 1 was prepared by diluting a mixture of 5.7 mL of glacial acetic acid, 500 mL of reagent water, and 64.3 mL of 1N NaOH to 1 L, which gave a mixture pH of 4.93 ± 0.05. Spent magnetite nanoparticles were collected through centrifuging the suspensions from the equilibrium tests carried out at an Fe/As molar ratio of 15.9 to 1. The spent particles were nitrogen-dried for 48 hrs, and then mixed with the TCLP fluid at a solid-to-solution ratio of 1g to 20 ml. The mixtures were then rotated for 18 hrs at 50 rpm and at room temperature, and then centrifuged at 5000 g-force for 20 min to separate the particles. The supernatant was then filtered with the 25 nm membrane, and the filtrate was then acidified to pH<2.0 with 1M HNO_3 and analyzed for As.

2.3 Results and Discussion

2.3.1 Characterization of stabilized magnetite nanoparticles and role of stabilizers

Figure 2-1 shows TEM images of bare and stabilized magnetite particles. Because of CMC's negatively charged functional groups (pKa=4.3) at the experimental pH, CMC stabilizes the nanoparticles through concurrent electrostatic and steric stabilization mechanisms (He and Zhao, 2007). In contrast, starch is a neutral polysaccharide, and thus, it works through steric stabilization. **Figure 2-1** indicates that both starch and CMC can serve as effective stabilizers to yield well dispersed discrete magnetite nanoparticles. The presence of 0.1 wt.% starch resulted in well defined, fully dispersed stable magnetite nanoparticles with a mean diameter of 75±17 (standard deviation) nm (**Figure 2-1a**). The particles prepared with 0.04 wt.% starch (**Figure 2-1b**) appeared as incompletely developed and inter-bridged nanoparticles. However, the suspension was still well stabilized as no difference in total iron concentration in the suspension was detected between the 0.04 wt.% and 0.1 wt.% starch stabilized particles after 24 hours of preparation. In the presence of 0.1% of CMC, the particle size was determined to be 2.9±2.0 nm (**Figure 2-1c**). In contrast to these stabilized particles, the bare magnetite existed in the form of aggregated flocs (**Figure 2-1d**).

The DLS-based hydrodynamic diameter was 172 nm and 129 nm, respectively, for particles stabilized with 0.04 and 0.1 wt.% starch. For the sonicated non-stabilized particles, the hydrodynamic diameter was ~4.4 μm. Continued DLS monitoring indicated that the 0.04 wt.% starch stabilized particles continued to grow from 172 nm at 1hr to 203 nm after 22 days (see effects of starch and CMC concentration on nanoparticle stability and arsenate sorption capacity for more details), which agrees with the seemingly immature particle structure in **Figure 2-1b**. **Figure 2-2** displays the size distribution of stabilized magnetite nanoparticles.

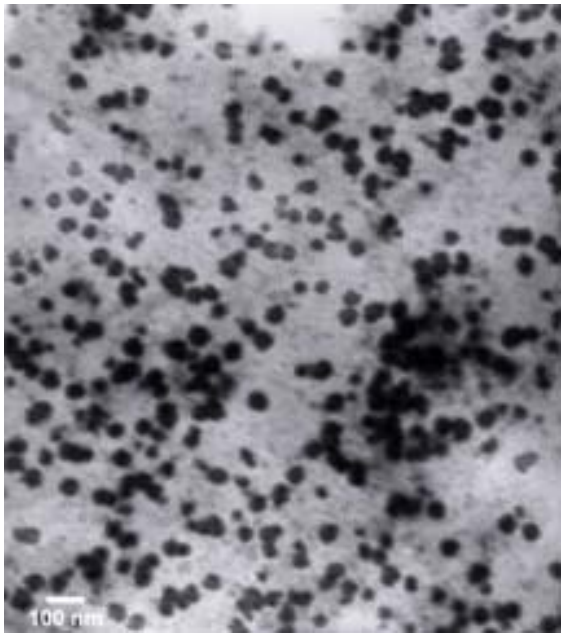

(a) 0.1g/L as Fe with 0.1 wt.% starch

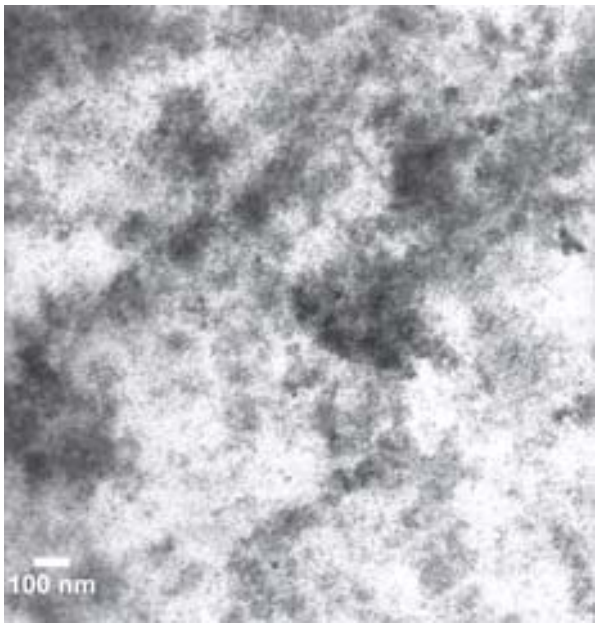

(b) 0.1g/L as Fe with 0.04 wt.% starch

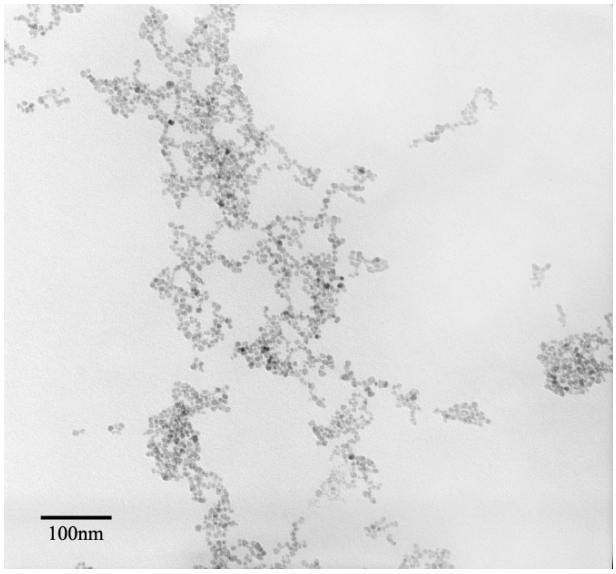

(c) 0.1g/L as Fe with 0.1 wt.% CMC

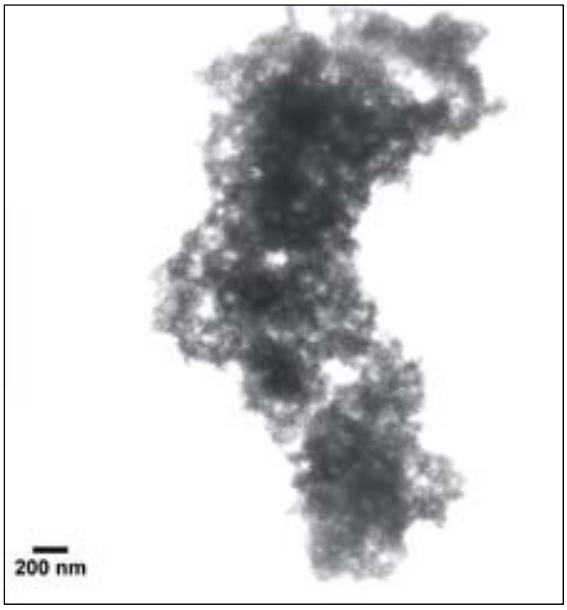

(d) 0.1g/L as Fe without a stabilizer

Figure 2-1. TEM images of magnetite nanoparticles prepared at 0.1g/L as Fe with: (a) 0.1 wt.% starch, (b) 0.04 wt.% starch, (c) 0.1 wt.% CMC, and (d) no stabilizer.

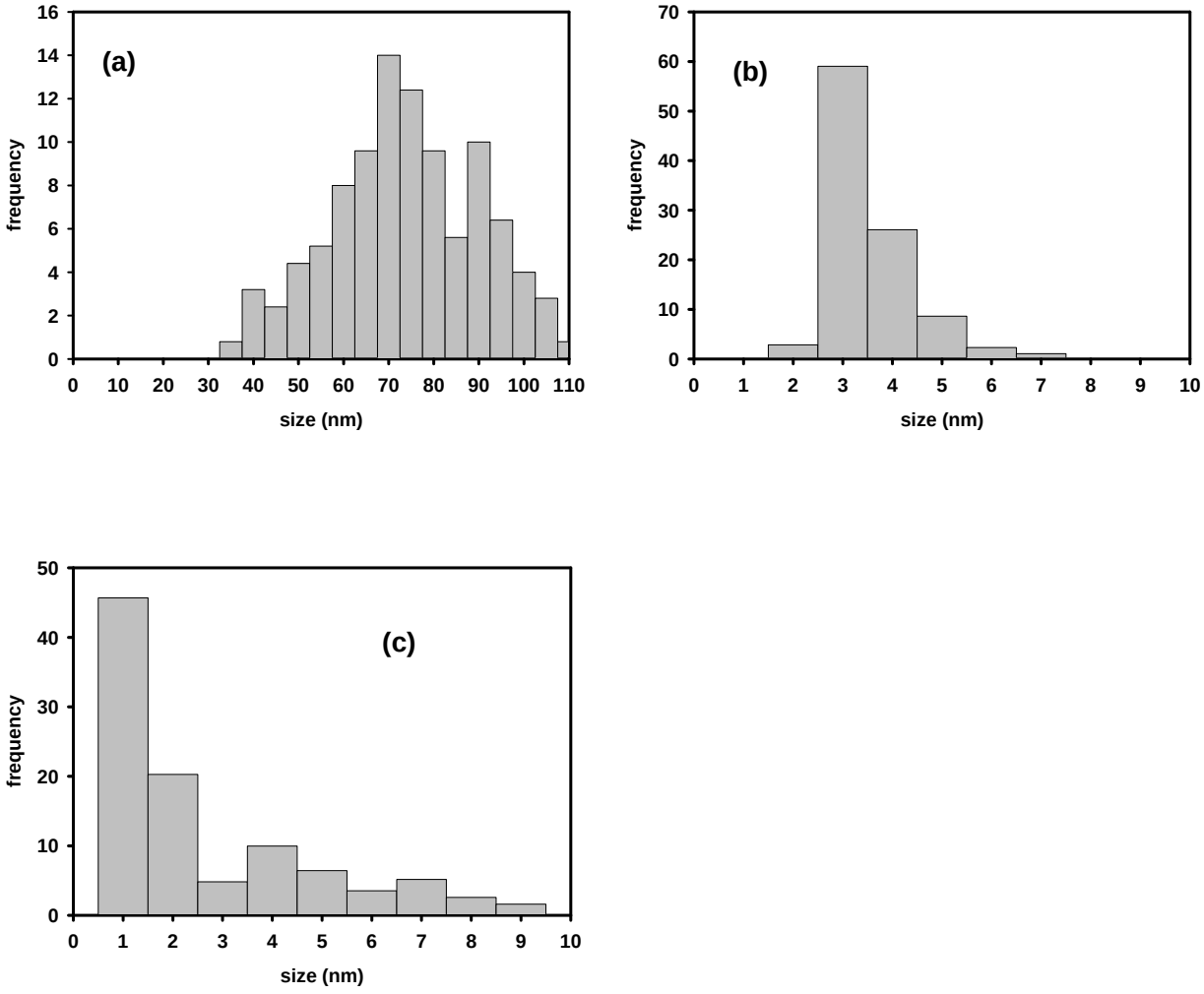

Figure 2-2. Histograms showing the size distribution of magnetite nanoparticles (0.1g/L as Fe) synthesized with (a) 0.1wt.% of starch, (b) 0.04 wt.% of starch and (c) 0.1 wt.% CMC as a stabilizer. The number of particles counted: (a) 250; (b) 952; (c) 311.

For the stabilized nanoparticles, the strong 'gelling effect" of the polysaccharide stabilizers prevents direct measurement of the specific surface area. Consequently, the specific surface area *S* was estimated per **Eq. 2-1**, assuming the nanoparticles are discrete and nonporous,

$$S = \frac{\text{Area}}{\text{Mass}} = \frac{6}{\rho d} \qquad \textbf{(Eq. 2-1)}$$

where ρ is the density of magnetite (4890 kg/m^3) and d is the mean diameter of the particles. Based on a mean diameter of 2.9 and 75 nm, the specific surface area was calculated to be 423 and 16 m^2/g, respectively, for the nanoparticles stabilized with 0.1 wt.% CMC and 0.1 wt.% starch. For non-stabilized magnetite aggregates, the BET surface area was measured to be 3.98 m^2/g, which is comparable to the literature reported value of 3.7 m^2/g (Yean et al., 2005).

Non-stabilized magnetite nanoparticles agglomerated and settled within a few minutes while the stabilized magnetite nanoparticles remained suspended in the water for more than 12 months with ~60% settled based on Fe in the supernatant.

Figure 2-3 shows XRD spectra of various magnetite particles. The XRD analyses confirmed that the peaks of stabilized magnetite particles resemble those of the non-stabilized magnetite and the commercial Fe_3O_4 powder. The characteristic peaks of magnetite are 30.00 (220), 35.5 (311), 43.1 (400), 53.4 (422), 57 (511) and 63 (440), which are consistent with reported crystallographic information for magnetite (Lee et al., 1996; Si et al., 2004). Peaks other than the characteristic peaks of magnetite were barely conspicuous, suggesting that the impurity content was quite low. For example, the characteristic peaks of (110), (210) and (211) for maghemite (Fe_2O_3) were not observed (Gnanaprakash et al., 2007; Santra et al., 2001).

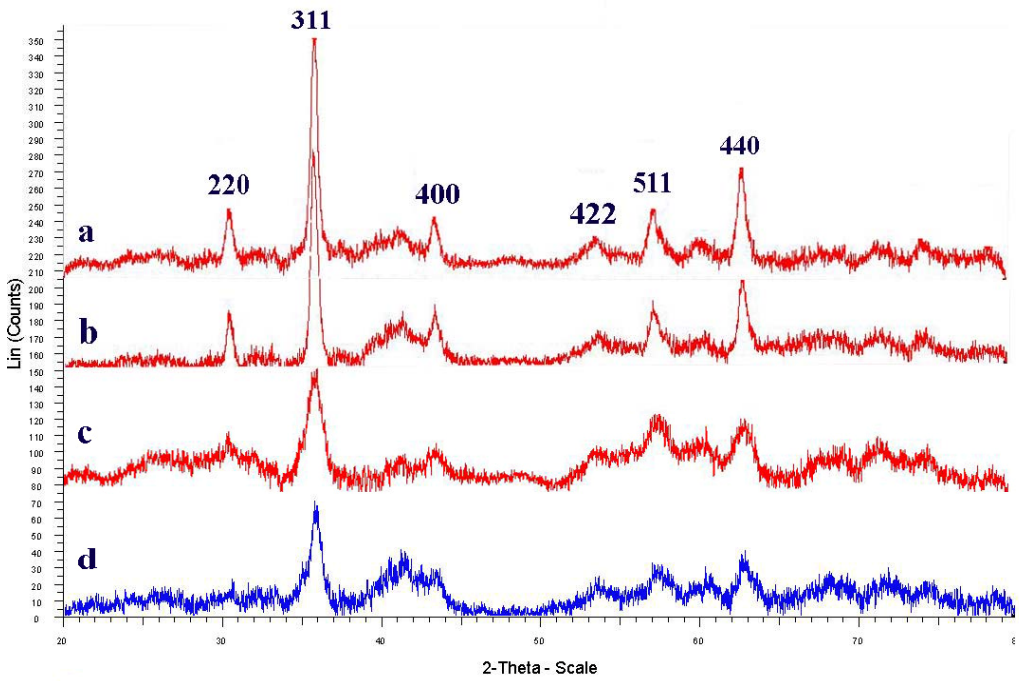

Figure 2-3. XRD patterns of various types of magnetite particles: (a) a commercial magnetite powder; (b) lab-prepared non-stabilized magnetite particles; (c) CMC-stabilized magnetite; and (d) starch-stabilized magnetite. (Lab samples prepared at 1.5 g/L as Fe with 0, or 0.5 wt.% of starch or CMC)

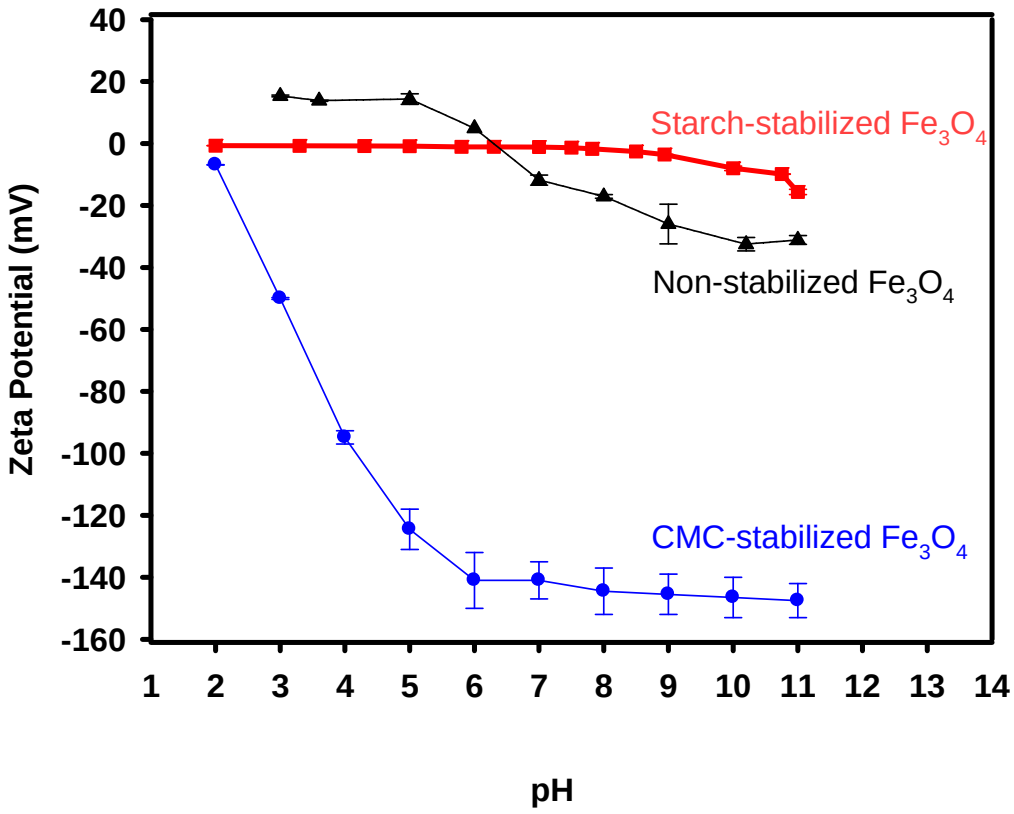

Figure 2-4. ζ potential for bare and 0.1 wt.% starch-, or CMC-stabilized magnetite nanoparticles as a function of pH. All particle suspensions were prepared at 0.1 g/L (as Fe). All measurements were carried out in duplicate. Error bars refer to standard deviation from the mean.

ζ potential is an important parameter that governs the inter-particle electrostatic interactions and stability of nanoparticles in water. In addition, ζ potential also affects sorption/desorption behavior of the nanoparticles for arsenate. **Figure 2-4** shows measured ζ potential as a function of pH for bare and stabilized magnetite nanoparticles. Due to the starch coating, a nearly neutral surface was evident over a pH range of 2-9 for starch-stabilized particles. It turned gradually more negative (> -0.9 mV) at pH above 9, and reached a ζ value of -16 mV at pH 11. In contrast, CMC-stabilized nanoparticles displayed a much more negative surface with a ζ value ranging from -120 mV to -150 mV at pH above the pK_a value of CMC. Based on **Figure 2-4**, the pH of the point of zero charge (PZC) is estimated to be <pH 2 for CMC-stabilized particles. For bare magnetite particles, the ζ potential turned from +15 mV at pH 3 to -31 mV at pH 11, resulting in a pH_{pzc} value of 6.1. The PZC value for the stabilized nanoparticles differed greatly from that for bare magnetite particles either measured here or reported by others, e.g. 7.9 ~ 8.0 by Illés and Tombácz (Illes and Tombacz, 2003) or 6.3 ~ 6.8 by Yean et al. (Yean et al., 2005) and Marmier et al. (Marmier et al., 1999). Evidently, adsorption of starch or CMC macromolecules to the particle surface can greatly alter the particle surface characteristics and inter-particle interactions. Given the anionic nature of the target arsenate, it would be expected that the nearly neutral starch-stabilized nanoparticles would offer a more favorable surface condition for arsenate uptake than the negatively charged CMC-stabilized counterparts.

2.3.2 Effects of starch and CMC concentration on nanoparticle stability and arsenate sorption capacity

Figure 2-5 demonstrates the physical stability of magnetite particles prepared at a fixed particle concentration of 0.1g/L as Fe but with various concentrations of starch ranging from 0 to 0.1 wt.%. Complete particle stabilization was achieved at a starch concentration of 0.04 wt.% or

higher. Thus, 0.04 wt.% of starch can be regarded as the critical stabilization concentration (CSC) for 0.1g/L as Fe magnetite particles. On the other hand, at a starch concentration of 0.02 wt.% or lower, rapid flocculation and settling of the particles were observed. This observation indicates that starch can play a dual role in regulating stability of the magnetite particles depending on the concentration. At a starch dosage at or above CSC, the starch coating acts as stabilizer facilitating effective particle stabilization; in contrast, at a concentration below CSC, starch serves as a flocculating or bridging agent promoting particle flocculation or destabilization. Such starch-bridged flocculation was indicated by the fact that the starch-bridged particles settled faster, and resulted in more flockulation, larger volume of settled aggregates and "clearer" supernatants than non-stabilized particles (**Figure 2-5**). The role of starch in regulating the particle stability was further revealed by measuring the concentration of suspended magnetite particles after 1 h of settling. The suspended particle concentration (measured as Fe) in the supernatants was 0.19, 0.25 and 33 mg/L, respectively, for starch concentrations of 0.002, 0.005 and 0.02 wt.%, compared to 100 mg/L for the fully stabilized suspension and 5.6 mg/L for non-stabilized particles.

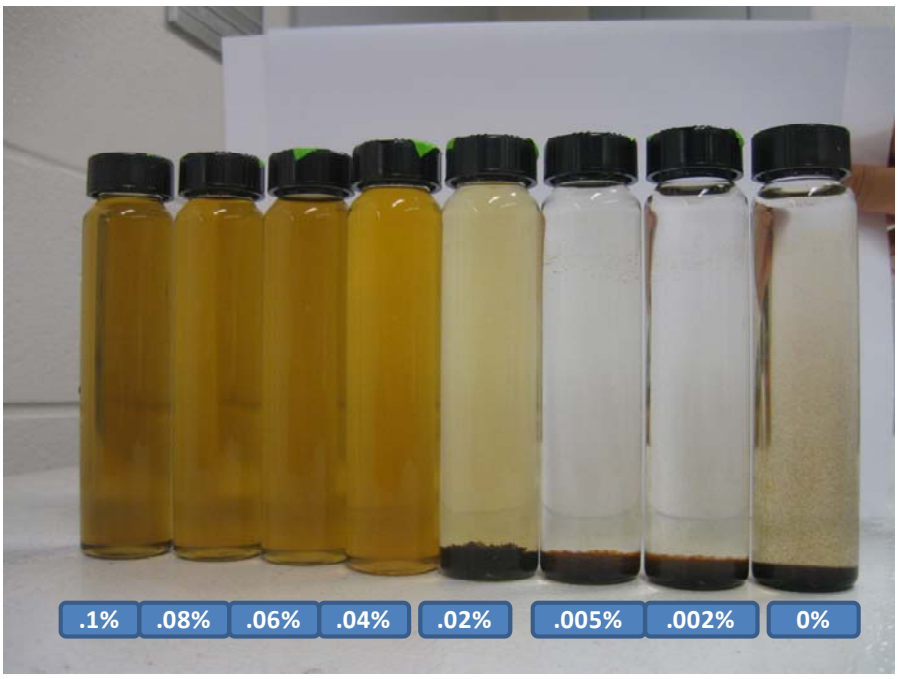

(a)

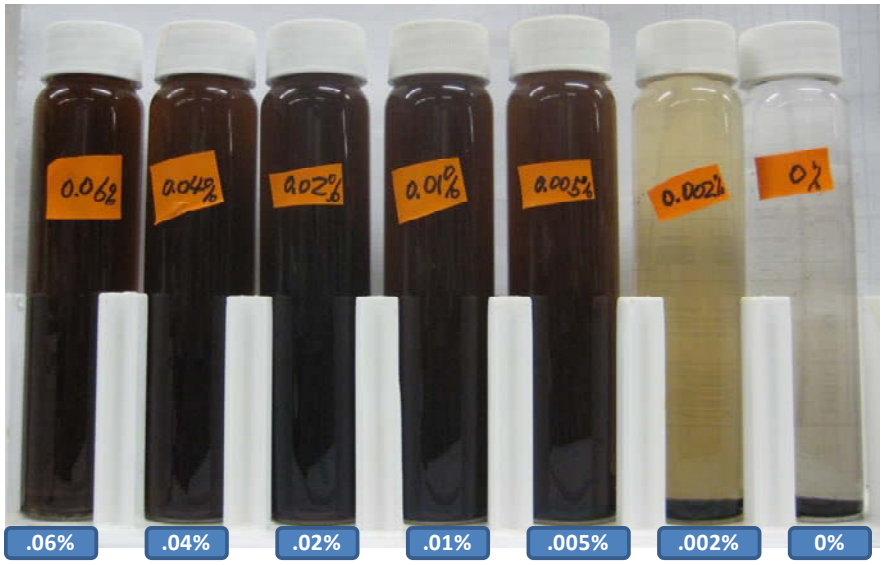

(b)

Figure 2-5. Magnetite (0.1g/L as Fe) nanoparticles synthesized in the presence of: (a) 0.1, 0.08, 0.06, 0.04, 0.02, 0.005, 0.002, and 0 wt.% starch (picture taken 1 h after preparation); and (b) 0.06, 0.04, 0.02, 0.005, 0.002 and 0 wt.% CMC (picture taken 2 h after preparation).

Like starch, CMC can also serve as a flocculating or bridging agent as well as a particle stabilizer. **Figure 2-5b** displays the visual difference of magnetite nanoparticles synthesized in the presence of various CMC concentrations. The ζ potential profile (**Figure 2-4**) predicts that CMC is a stronger stabilizer than starch. **Figure 2-5** reveals a much lower CSC value of 0.005 wt.% for stabilizing 0.1g/L as Fe of the nanoparticles. At a CMC concentration of 0.002 wt.%, only 37% of the nanoparticles remained in the supernatant. The UV-Vis results (**Figure 2-6**) agree with the visual observations as well as the measured Fe concentration in the supernatants.

Figure 2-7a shows the evolution of the DLS-based particle size of the nanoparticles stabilized with various concentrations of starch. First of all, it is noteworthy that higher starch concentrations result in smaller nanoparticles. For example, at 1 h of particle aging, the hydrodynamic diameter was measured to be 172, 157, 147 and 129 nm, respectively, for particles stabilized with 0.04, 0.06, 0.08 and 0.1 wt.% of starch. After 22 days of growth time, the DLS-based size for the 0.04 wt.% starch stabilized particles grew from 172 to 203 nm (by 18%), whereas the size for the particles prepared at higher starch concentrations remained about the same. **Figure 2-7b** shows that the difference of ζ potential for all cases was statistically insignificant, and remained unchanged over the 22 days of aging. These observations indicate that the particle stabilization by starch was governed by steric stabilization effect, i.e. the overlap of two interacting coated starch layers result in great repulsive osmotic force. The higher starch concentration, the greater the osmotic force, the smaller and more stable nanoparticles are formed.

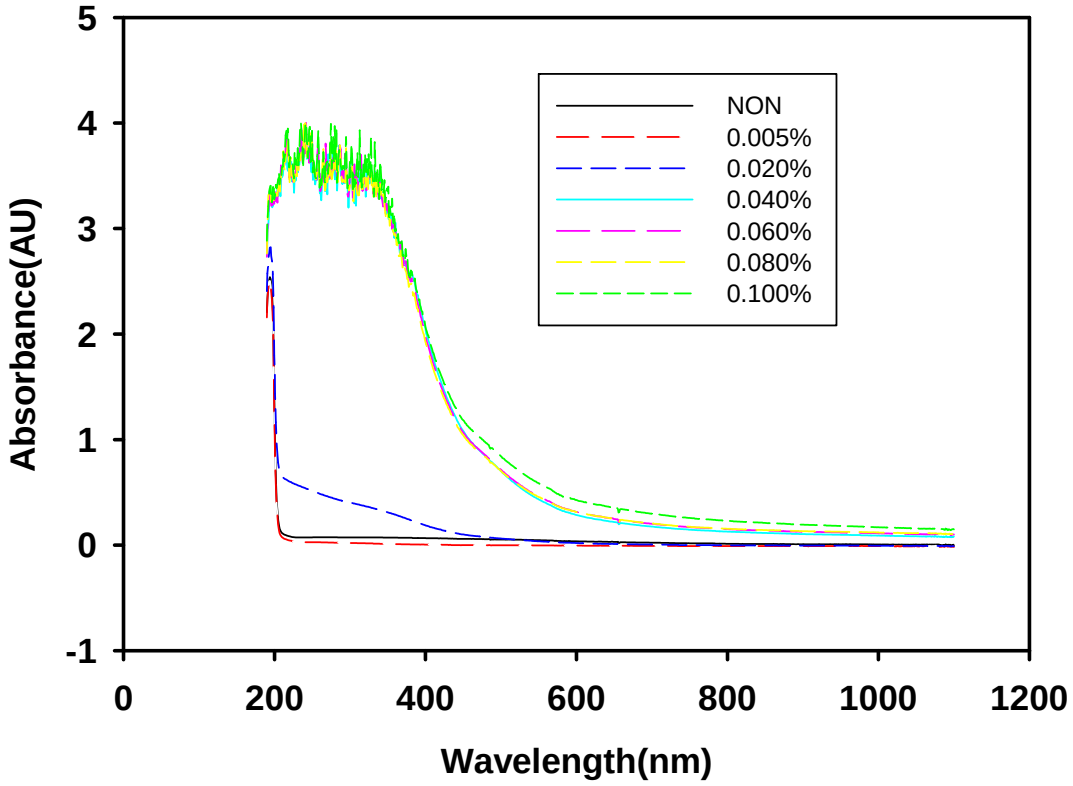

Figure 2-6. UV-Vis absorbance profiles for magnetite nanoparticle suspensions at various concentrations of starch. The UV-Vis absorbance profile was taken 60 minutes after preparation.

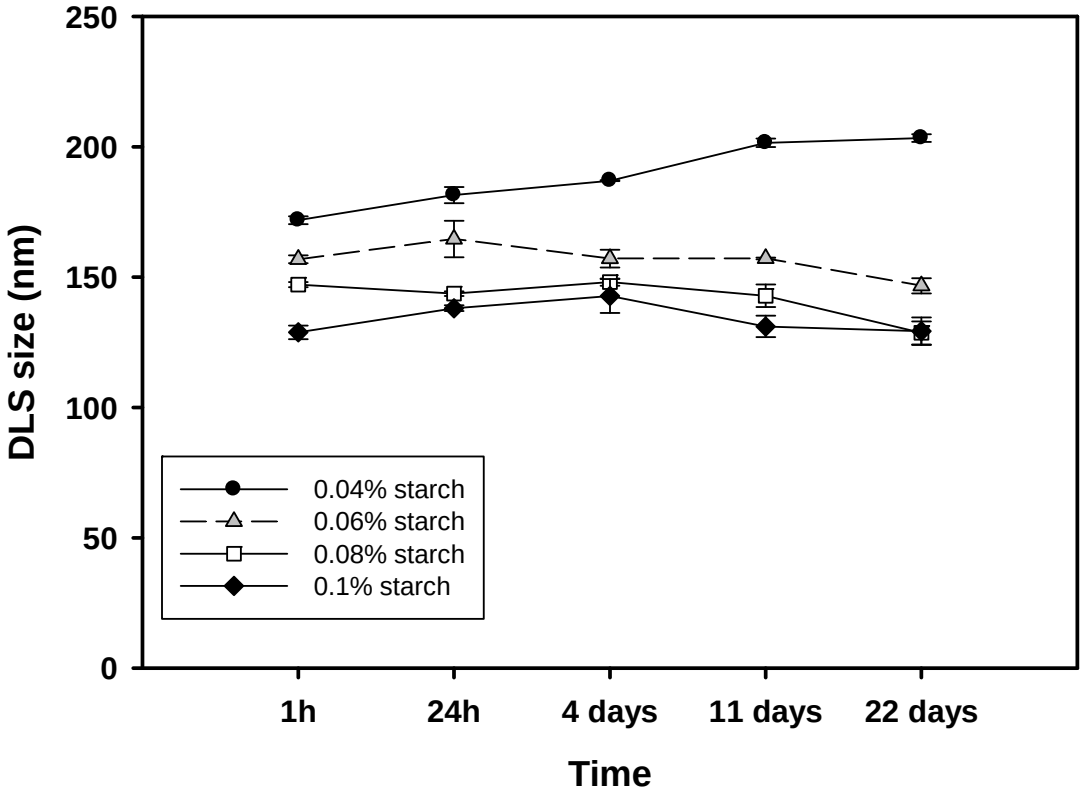
250
200
150
100
50
0
DLS size (nm)
0.04% starch
0.06% starch
0.08% starch
0.1% starch
1h
24h
4 days
11 days
22 days
Time

(a)

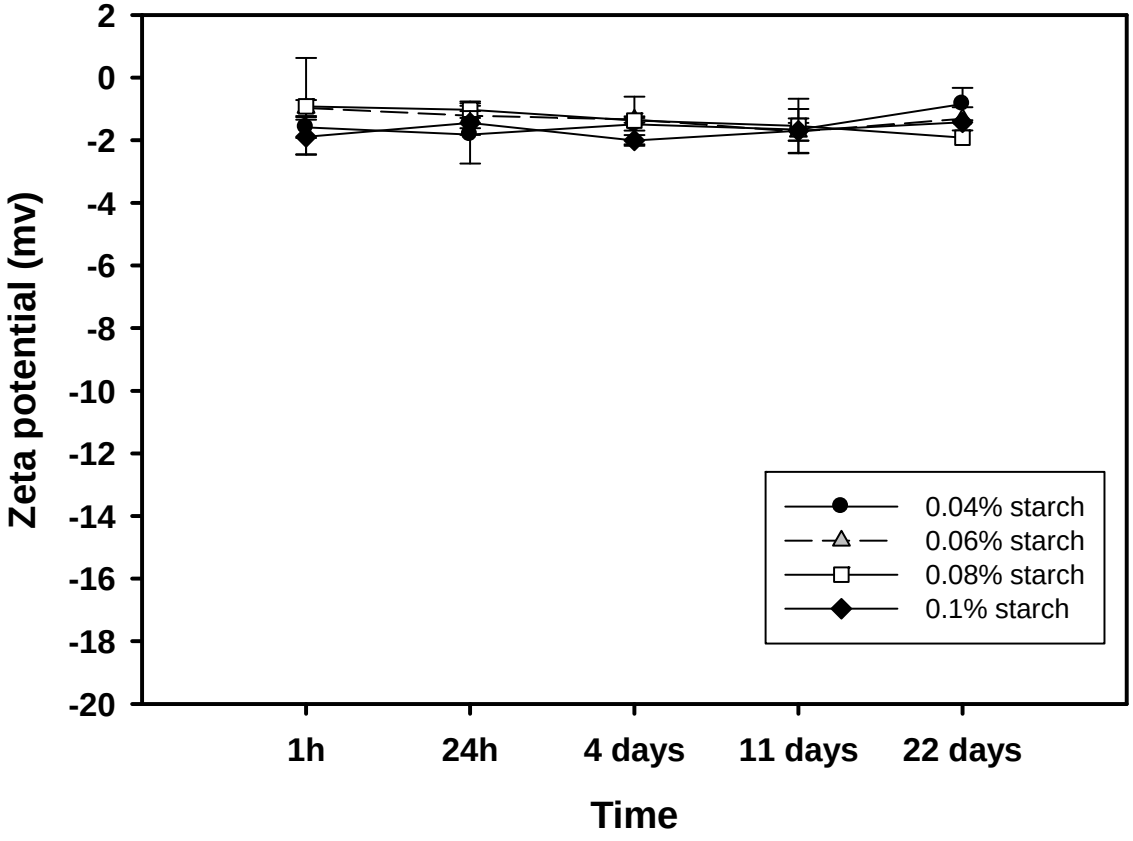

(b)

Figure 2-7. Evolution of DLS-based hydrodynamic diameter and ζ potential for 0.1 g-Fe/L magnetite particles prepared in the presence of various concentrations of starch. The DLS-based hydrodynamic size is volume-based.

Figure 2-8 shows equilibrium uptake of As(V) with magnetite particles prepared in the presence of various starch concentrations. Overall, the arsenic uptake increased with increasing stabilizer concentration, i.e. with decreasing particle size. In accord with the observed physical stability (**Figure 2-5**), at the CSC of 0.04% or higher, a sorption plateau was evident. Compared to bare magnetite particles, the 0.04 wt.% starch stabilized particles offered a 2.2 times greater As(V) uptake. However, when the stabilizer concentration was further increased from 0.04 to 0.1 wt.%, the capacity gain was only 14%. In fact, the sorption for 0.08 and 0.1 wt.% starch stabilized particles was about the same. The capacity enhancement for stabilized magnetite particles can be attributed to the smaller size, and thus, greater specific surface area for more stable particles. On the flip side, however, accumulation of starch on the particles can inhibit the sorption of As(V) both kinetically and thermodynamically (An et al., 2011b). Kinetically, a denser layer of starch results in elevated mass transfer resistance and increase the energy barrier for some of the sorption sites. Thermodynamically, the pre-sorbed starch molecules diminish the effective sorption sites of the particles.

While CMC is a more effective stabilizer than starch, and thus, results in smaller particles, **Figure 2-8b** shows that CMC stabilization does not offer any significant capacity enhancement for As(V) removal. The pK_a values of arsenic acid (H_3AsO_4) are as follows: pK_{a1} = 2.20, pK_{a2} = 6.97 and pK_{a3} = 11.53. At the experimental pH of 6.8, both $H_2AsO_4^-$ and $HAsO_4^{2-}$ are predominant arsenate species. As CMC stabilized magnetite particles carry a highly negative surface, sorption of these anions would have to overcome a substantial energy barrier due to the electrostatic repulsion between like charges. Consequently, although CMC stabilization gives smaller particle size and greater specific surface, arsenate uptake by CMC-stabilized magnetite was much lower than that by the starch-stabilized counterpart.

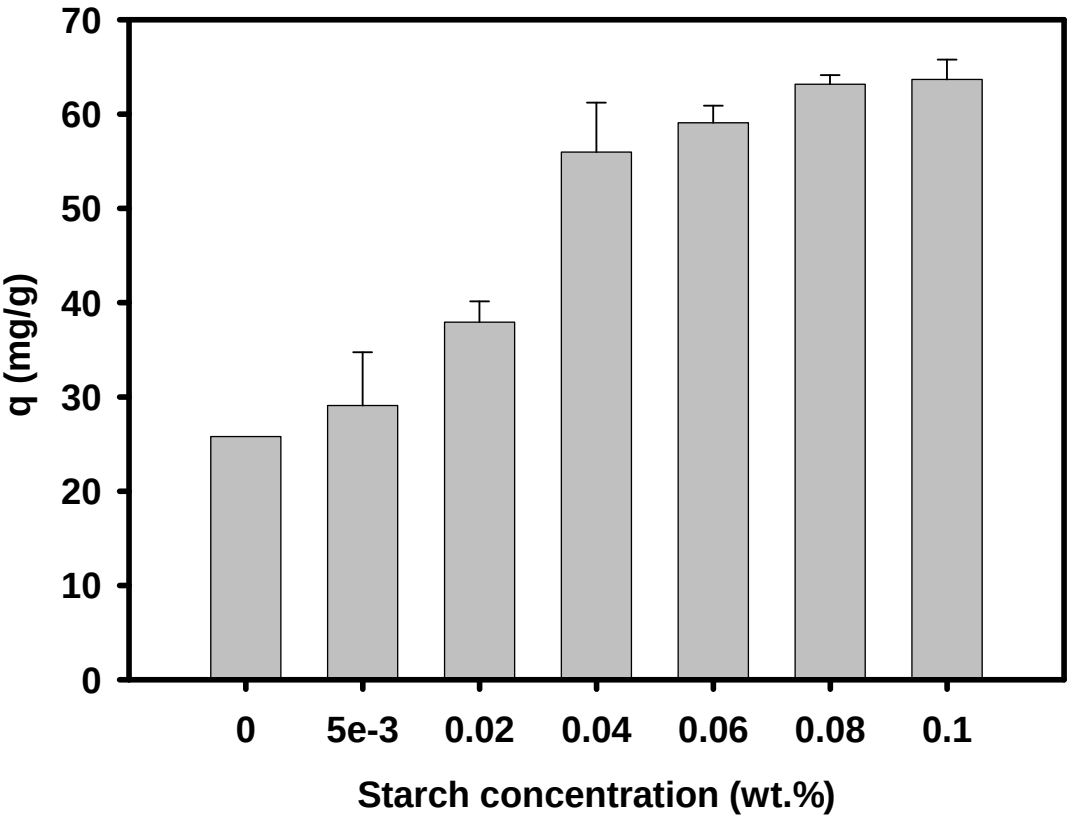
70
60
50
40
30
20
10
0
q (mg/g)
0
5e-3
0.02
0.04
0.06
0.08
0.1
Starch concentration (wt.%)

(a)

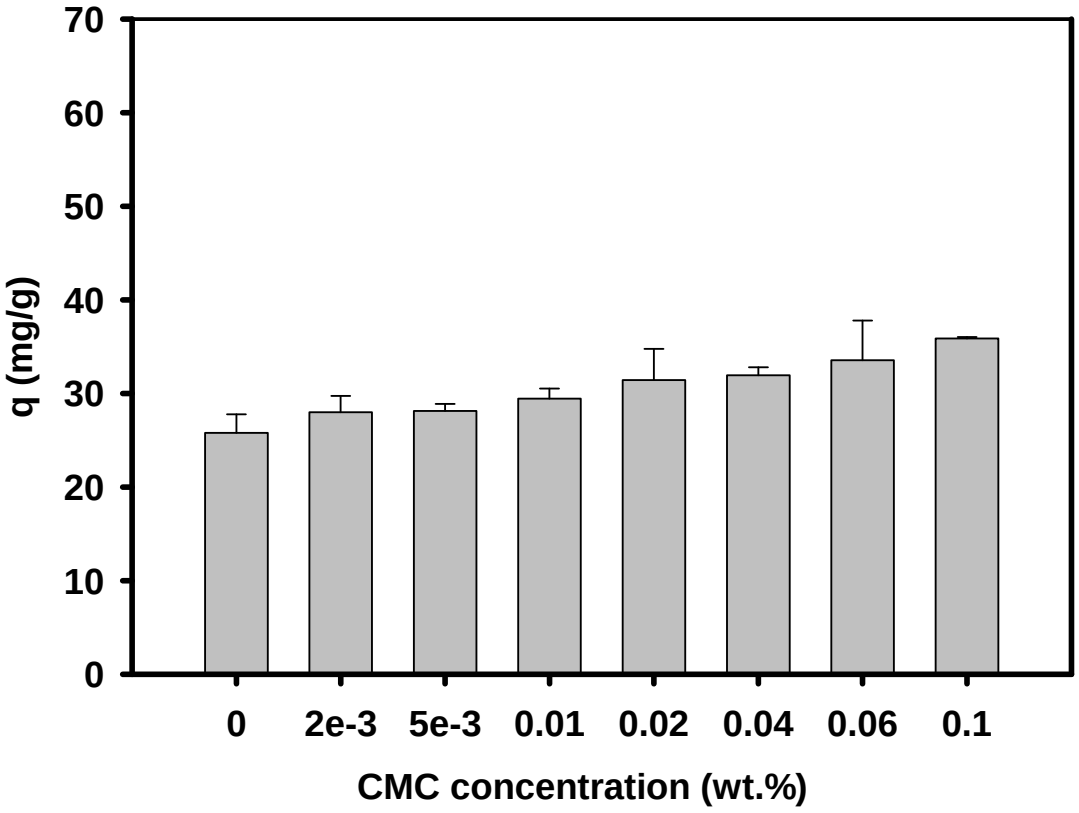

(b)

Figure 2-8. Effect of starch (a) or CMC (b) concentration on As(V) uptake (q). Nanoparticle dosage = 0.1g/L as Fe, initial As(V) = 8.24 mg/L, equilibrium pH = 6.8±0.4, equilibration time = 144 hrs. Data given as mean of duplicates and errors refer to standard deviation from the mean.

2.3.3 Arsenate removal kinetics

Figure 2-9 shows arsenic removal kinetic data for bare and stabilized magnetite particles under otherwise identical conditions. Three control tests with DI water, 0.1 wt.% starch or CMC solution indicated no As removal by the test apparatuses and during the filtration and analytical procedures. In accord with the ζ profile (**Figure 2-4**), starch-stabilized magnetite particles displayed the most effective removal of arsenate in terms of both extent and rate. In all cases, the arsenic concentration profile showed a rapid initial (<10 min) drop followed by a slow decreasing stage. For starch-stabilized magnetite, equilibrium was reached in ~96 h, while arsenate uptake appeared to slowly continue after 160 h for the bare or CMC-stabilized particles. After 96 h, the fractional approach to equilibrium (i.e. M_t/M_∞) of starch-stabilized particles reached 99.8%, compared to 87.2% and 91.9% for CMC-stabilized and bare magnetite, respectively. After 1 h, the fractional approach to equilibrium amounted to 52% for starch-stabilized magnetite nanoparticles, compared to less than 28% and 19% for CMC- stabilized and bare magnetite, respectively. The greater uptake rate and extent of both starch- and CMC-stabilized nanoparticles can be attributed to the larger specific surface area and smaller size of the nanoparticles. Of the two types of stabilized particles, although CMC resulted in smaller particles than starch, the highly negative surface (**Figure 2-4**) of CMC-stabilized particles inhibited sorption of the target arsenic oxyanions.

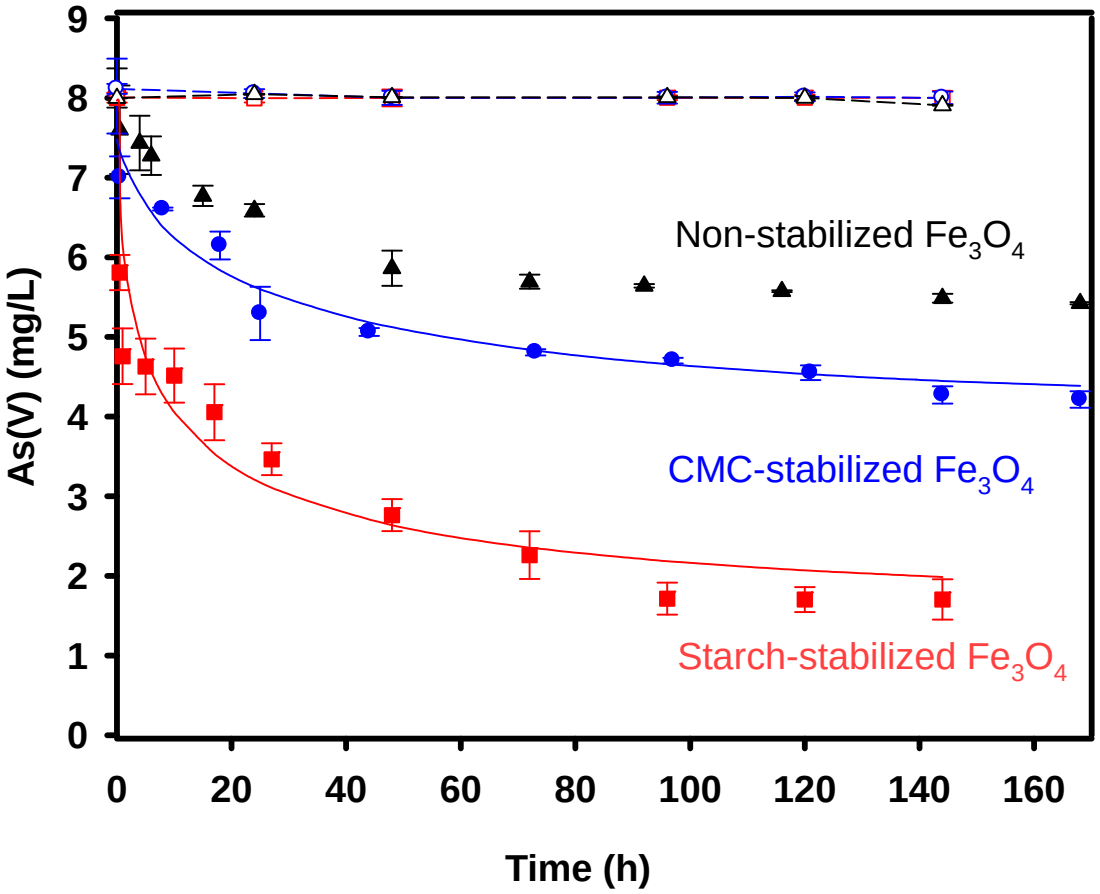

Figure 2-9. As(V) sorption kinetics using bare and stabilized magnetite particles. Experimental conditions: magnetite = 0.1 g/L as Fe, CMC or starch = 0.1 wt.% for stabilized particles. Control tests were carried out without nanoparticles but with DI water, 0.1 wt.% CMC or starch. Solution pH was kept constant at 6.8±0.4. Symbols: experimental data given as mean of duplicates (errors refer to deviation from the mean); Lines: model simulations.

To our knowledge, kinetic modeling of contaminant sorption to nanoparticles has not been well studied, partially owing to the uncertain particle structure and related mass transfer mechanisms. To simulate the kinetic data, we test-fitted a number of commonly used empirical and semi-physical kinetic models to the experimental data in **Figure 2-9**, including the first order, second order, power function, Elovich, and parabolic diffusion (Sparks, 1989). **Table 2-1** summarizes the models and fitting quality as indicated by the coefficient of determination (R^2). The results indicate that the parabolic diffusion model provides the best fitting quality, which is consistent with the findings by Raven et al (Raven et al., 1998), who modeled arsenic uptake kinetics on ferrihydrite. However, the parabolic equation assumes that the kinetics is controlled by intraparticle radial diffusion in a long cylinder (Crank, 1975), which does not appear to conform to the geometry and morphology of the nanoparticles.

Table 2-1. Various empirical models used for fitting arsenate sorption kinetic data and the resultant fitting coefficients of determination (R^2) .

Kinetic models	Governing Equation	Transformed Linear Equation	Coefficients of determination, R^2		
			Non-stabilized	CMC-stabilized	Starch-stabilized
First order	$As_t = As_\infty \cdot e^{-kt}$	$\ln[1-(As_t/As_\infty)]$ vs t	0.948	0.785	0.940
Second order	$1/As_t . 1/As_\infty = kt$	$1/[1-(As_t/As_\infty)]$ vs t	0.437	0.336	0.727
Power function	$\ln As_t = \ln k + v \ln(t)$	$\ln(As_t)$ vs $\ln(t)$	0.960	0.933	0.933
Simple Elovich	$As_t = (1/\beta)\ln(\alpha\beta)+(1/\beta)\ln t$	As_t vs $\ln(t)$	0.918	0.887	0.904
Parabolic diffusion	$(As_t/As_\infty)/t = \frac{4}{\pi^{\frac{1}{2}}}(\frac{D}{r^2})^{1/2}\frac{1}{t^{1/2}} - \frac{D}{r^2}$	$(As_t/As_\infty)/t$ vs $t^{-0.5}$	0.964	0.982	0.979

Note: As_t: sorbed As at time t; As_∞: sorbed As at equilibrium; t: reaction time; α and β are constants during any one experiment. The constant α can be regarded as the initial rate since $dAs_t/dt \rightarrow \alpha$ as $As_t \rightarrow 0$. r is the average radius of particle, D is the diffusion coefficient.

In search for a more mechanistically sound model, the classical intraparticle diffusion model was probed. The model formulation was based on the following postulations: 1) nanoparticles are clusters of smaller nucleated magnetite atoms, leaving the particles a porous structure with significant interior and exterior surface sorption sites for As sorption; 2) intraparticle diffusion is the rate limiting step, and 3) nanoparticles can be approximated as spherical beads with the particle size represented by the TEM measurements. The intraparticle diffusion is then described by the following equation:

$$F = \frac{q(t)}{q_\infty} = 1 - \sum_{n=1}^{\infty} \frac{6\alpha(\alpha+1)\exp\left(-\frac{Dq_n^2 t}{a^2}\right)}{9+9\alpha+q_n^2\alpha^2} \qquad \textbf{(Eq. 2-2)}$$

where F is the factional attainment of equilibrium; $q(t)$ and q_∞ are the arsenate uptake at time t and at infinite time (i.e., at equilibrium), respectively; a is the mean radius of the magnetite particles, α is expressed in terms of the final fractional uptake of arsenate as

$$\frac{Mq_\infty}{V_0 C_0} = \frac{1}{1+\alpha} \qquad \textbf{(Eq. 2-3)}$$

where V_0 and C_0 are initial solution volume and initial As concentration in solution, respectively. The q_n's are the non-zero roots of a tan function related to α (An et al., 2005). The mean radius of CMC- and starch-stabilized particles was 1.45 nm and 37.5 nm, respectively. No attempt was made to model the kinetic data for the bare particles as the particle size of the aggregates was hardly discernible based on the TEM images.

The model was then employed to simulate the experimental kinetic data in **Figure 2-9**. The best fit was achieved by adjusting the diffusivity value (D) until the sum of the squared errors was minimized. **Figure 2-9** shows that the model was able to adequately simulate the kinetic data for both cases (the goodness of fitting exceeded that of the parabolic model, R^2 = 0.989, 0.984, 0.980 for non-, CMC-, starch-stabilized particles). The resultant diffusivity values

were 3.0×10^{-7} cm^2/s and 8.0×10^{-10} cm^2/s for starch- and CMC-stabilized nanoparticles, respectively. The diffusivity for CMC-stabilized nanoparticles was more than two orders of magnitude smaller, confirming the formidable inhibition of the negatively charged CMC molecules of the nanoparticle surface on the sorption of arsenate.

2.3.4 Arsenic sorption isotherms

Figure 2-10 shows arsenic sorption isotherms at a fixed pH of 6.8±0.4 for the bare and stabilized nanoparticles. The Langmuir isotherm model was used to interpret the equilibrium data:

$$q = \frac{b*Q*C_e}{1+b*C_e} \qquad \textbf{(Eq. 2-4)}$$

where b is the Langmuir affinity coefficient related to sorption energy (L/mg), C_e is the aqueous-phase concentration of As (mg/L), q is the solid-phase concentration of As (mg/g), and Q (mg/g) is the Langmuir capacity.

Table 2-2. Best-fitted Langmuir sorption isotherm parameters at pH = 6.8±0.4.

	Stabilizer conc. by weight	Magnetite conc. as Fe (g/L)	*Q* (mg/g)	*b* (L/mg)
Starch-stabilized magnetite	0.1%	0.1	62.1	30.2
CMC-stabilized magnetite	0.1%	0.1	36.0	8.13
Bare magnetite	0	0.1	26.8	3.06

Table 2-2 provides the best-fitted Langmuir parameters *b* and *Q*. For starch-stabilized nanoparticles, a very favorale, nearly rectangular isotherm was evident with a *Q* value of 62.1mg/g. For the CMC-stabilized counterparts, the unfavorable surface potential greatly diminished the sorption capacity. As a result, a 42% lower *Q* value of 36.0 mg/g was observed despite the much smaller particle size. Both stabilized nanoparticles offered much greater sorption capacity than the bare magnetite (Q = 26.8 mg/g). For comparison, the isotherm data for the commercial magnetite powder is also superimposed in **Figure 2-10**, and the results indicate that this commercial counterpart offered even lower As sorption capacity than the lab-prepared bare magnetite.

Yean et al. (Yean et al., 2005) synthesized and tested a class of magnetite nanoparticles (11.72 nm) by dissolving FeO(OH) in 90% oleic acid followed by heating at 320 °C in 1-octadecene. They observed a comparable Langmuir Q of 64 mg-As/g-Fe at pH=8 at *As*(V) concentration <3.7 mg/L. However, compared to the particle preparation method, starch-stabilized magnetite nanoparticles are not only much more straightforward to prepare, but also likely to be more cost-effective and more environmental-friendly as it eliminates the needs of the organic solvent and heating.

Based on our previous FTIR analyses of As(V) adsorption on bare and starch-bridged magnetite particles (An et al., 2011b), surface complexation (i.e., formation of inner-sphere complexes Fe-O-As) was the predominant mechanism for arsenate sorption on starch coated magnetite particles.

Our preliminary isotherm data (not shown) also revealed that the nanoparticles can effectively remove arsenite. However, the stabilizers displayed quite different effects on As(III) removal. For example, at an equilibrium pH=6.8±0.4 and at the aqueous concentration of <2

mg/L as As(III), the Langmuir capacity (Q) for As(III) followed the sequence: bare magnetite (90.7 mg/g) > 0.1% CMC stabilized (88.8 mg/g) > 0.1% starch stabilized (32.6 mg/g).

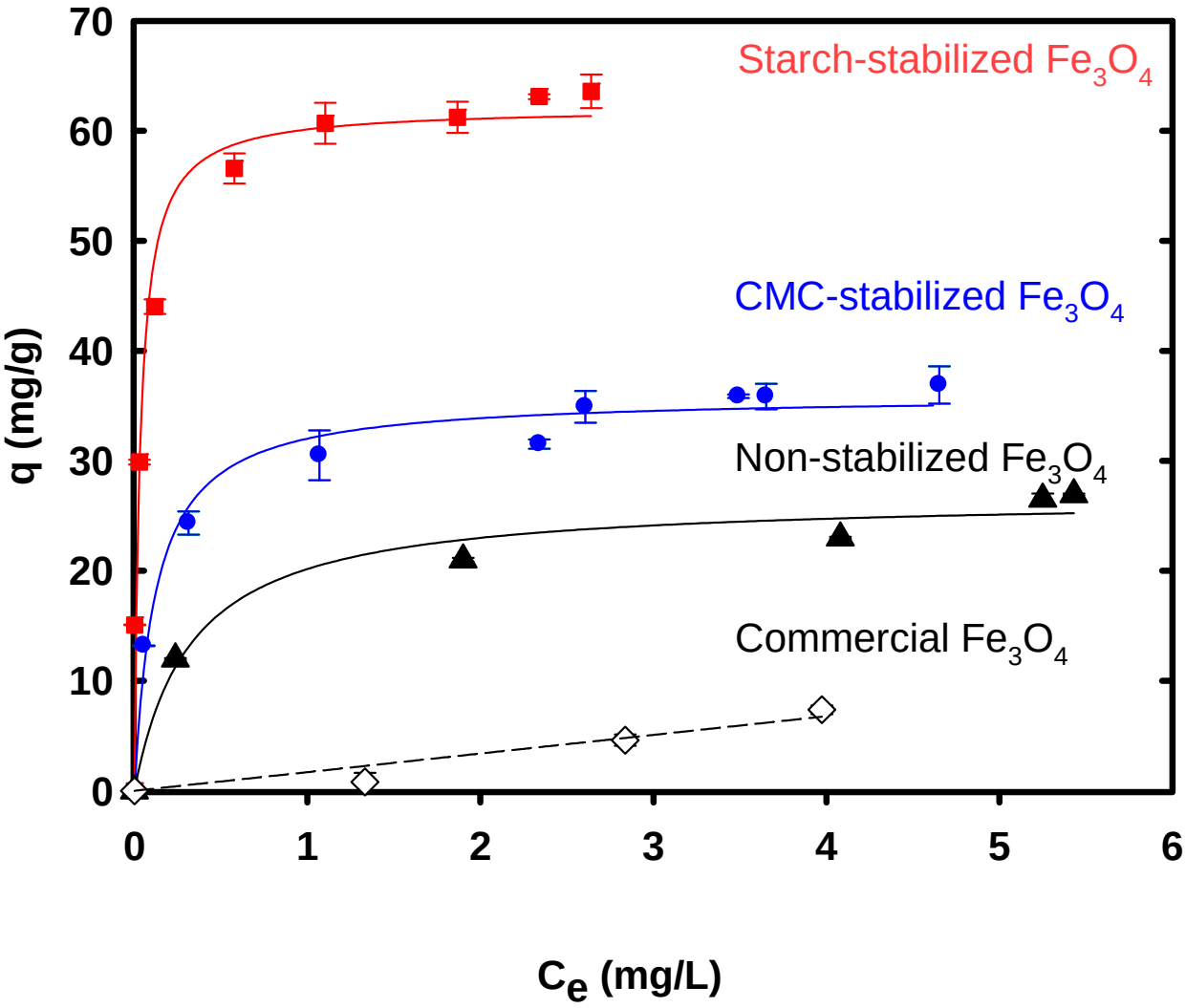

Figure 2-10. Arsenate sorption isotherms for various types of magnetite particles. Magnetite dosage = 0.1 g/L as Fe, starch or CMC = 0.1wt.% for stabilized particles, initial As = 0.03 to 8.24 mg/L, final pH = 6.8±0.4, equilibration time = 144 hrs. Data given as mean of duplicates and errors refer to deviation from the mean.

2.3.5 Effect of pH on arsenate sorption

Solution pH can affect both surface potential of the nanoparticles and the speciation of arsenate in the aqueous phase, both being important factors for arsenic removal. **Figure 2-11** shows arsenate uptake as a function of final solution pH for the bare, starch- and CMC-stabilized magnetite particles. Again, starch-stabilized nanoparticles displayed a much greater arsenic uptake capacity than CMC-stabilized nanoparticles; and the stabilized particles outperformed bare particles over the broad pH range tested. In general, the lower pH, the greater sorption capacity, which is consistent with the literature data on arsenate sorption with other types of magnetite particles (Dixit and Hering, 2003; Gimenez et al., 2007; Raven et al., 1998; Yean et al., 2005). This is not surprising given that the surface of the core magnetite particle is less negatively charged at lower pH, and the surface turns to positively charged at pH < pH_{PZC} (**Figure 2-4**). Although the ζ potential for starch-stabilized particles appeared to be nearly the same below pH 7 (**Figure 2-4**) due to the starch coating, the more positive core surface becomes more favorable for arsenate anions at lower pH. At the extremely low pH of 2, however, the arsenic uptake was lowered, which can be attributed to 1) partial dissolution of the nanoparticles, 2) partial decomposition of starch (An et al., 2011b), and 3) reduced fraction of the anionic arsenate species. Arsenate uptake diminished with increasing pH due to elevated electrostatic repulsion and more fierce competition of hydroxyl anions.

At pH 5 or lower, >10% of the nanoparticles became dissolved (**Figure 2-12a**), suggesting that the particles may not be suitable under very acidic conditions. The DLS-based hydrodynamic size decreased from 209 nm to 141 nm as pH increased from 6 to 10 (**Figure 2-12b**), whereas it remained about the same at ~225 nm in the pH range of 3 to 6.

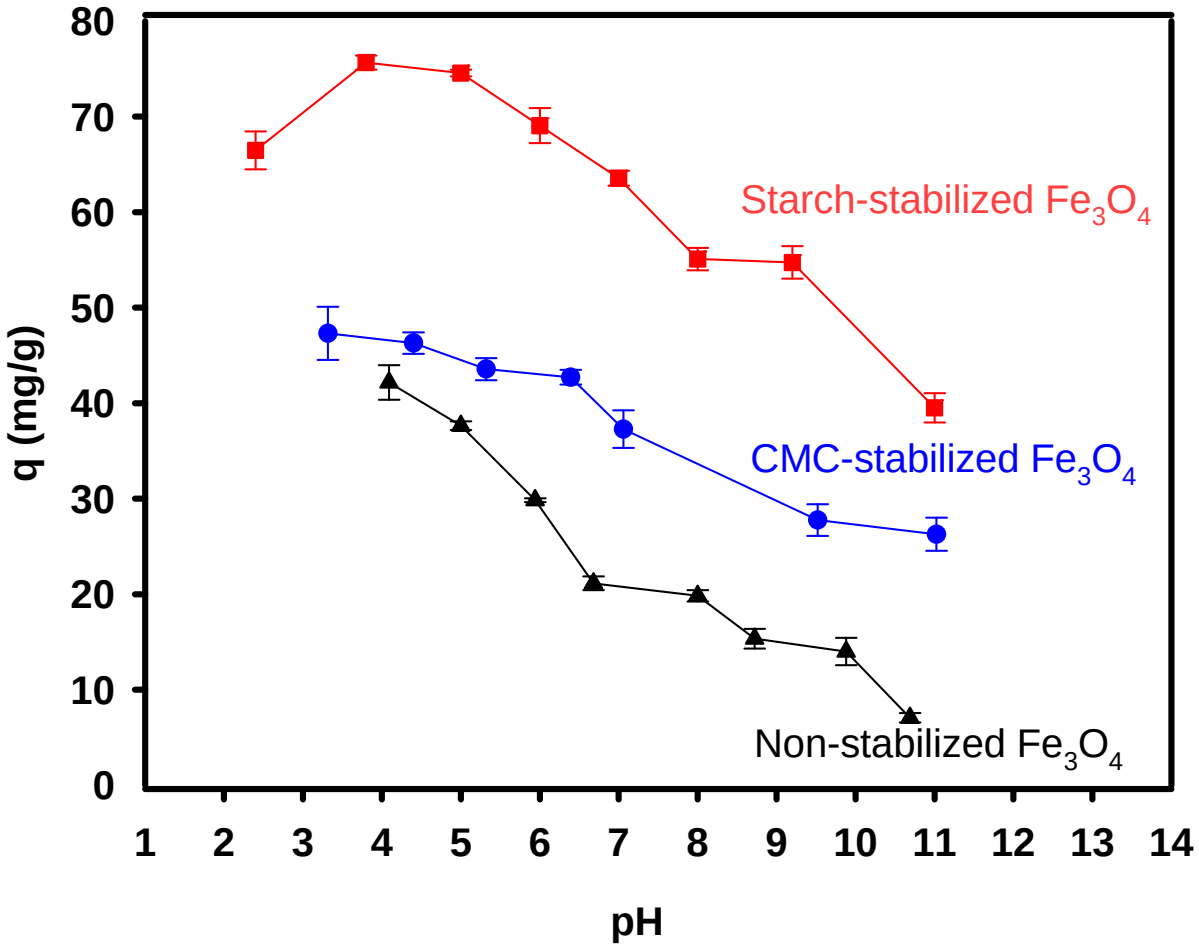

Figure 2-11. Equilibrium arsenate uptake as a function of final solution pH. Experimental conditions: initial As = 8.0 mg/L, nanoparticle = 0.1 g/L (as Fe), CMC or starch = 0.1 wt.%, Equilibration time = 144 hrs. Data given as mean of duplicates and errors refer to deviation from the mean.

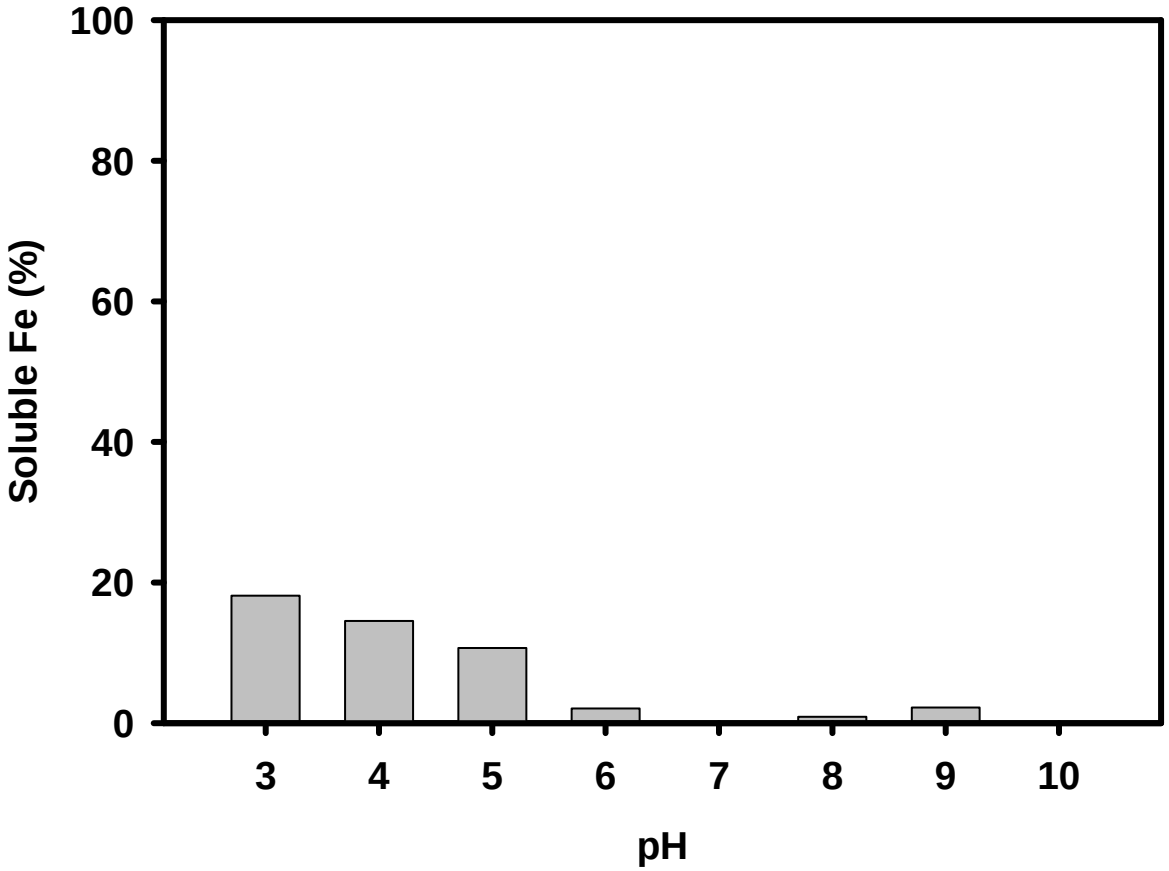

(a)

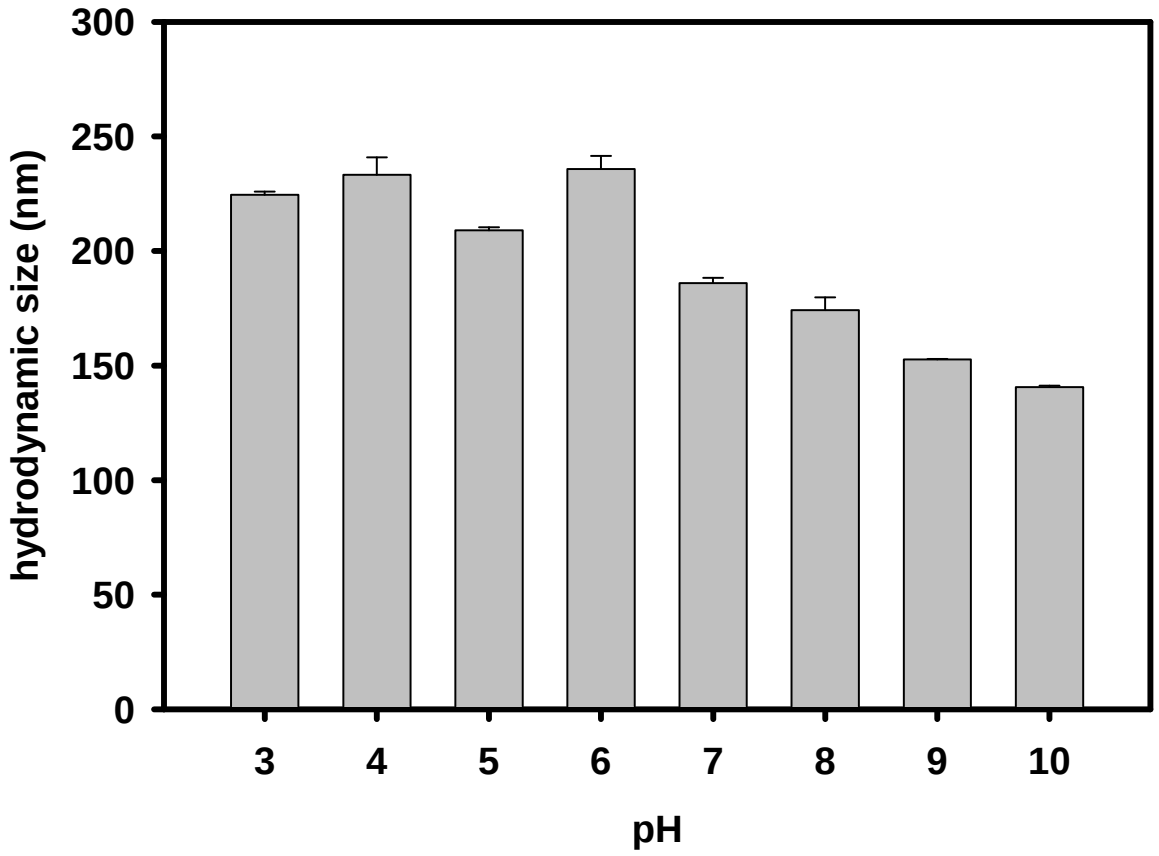

(b)

Figure 2-12. Dissolved iron concentration (a) and hydrodynamic size (b) as a function of pH in starch-stabilized magnetite nanoparticle suspensions. Experimental conditions: nanoparticles = 0.1 g/L as Fe, starch = 0.1 wt.%, equilibration time = 144 hrs. Data given as mean of duplicates and errors refer to deviation from the mean.

2.3.6 Effects of DOM and sulfate on arsenate sorption

Previous work (Grafe et al., 2001; Liu et al., 2008; Redman et al., 2002; Shipley et al., 2010) demonstrated that DOM plays an important role in regulating arsenic sorption on metal oxides. **Figure 2-13** compares arsenate sorption isotherms for starch-stabilized magnetite nanoparticles in the presence of 0, 10 and 20 mg/L as TOC of DOM. The presence of high concentrations of DOM can markedly inhibit arsenate sorption capacity. Similar results were reported by others, who studied As uptake by amorphous iron oxides (Bauer and Blodau, 2006; Yean et al., 2005). The reduced As uptake is attributed to: 1) the anionic ligands of DOM can strongly interact with the core iron oxides, and compete with arsenate for the sorption sites (Chen et al., 2006; Grafe et al., 2001; Gu et al., 1995); 2) DOM can also compete with the stabilizer molecules, altering the stabilizing effectiveness of starch and ζ potential of the nanoparticles. However, our observation did not indicate any significant change of ζ potential as well as the hydrodynamic size in the presence or absence of DOM (**Figure 2-14**).

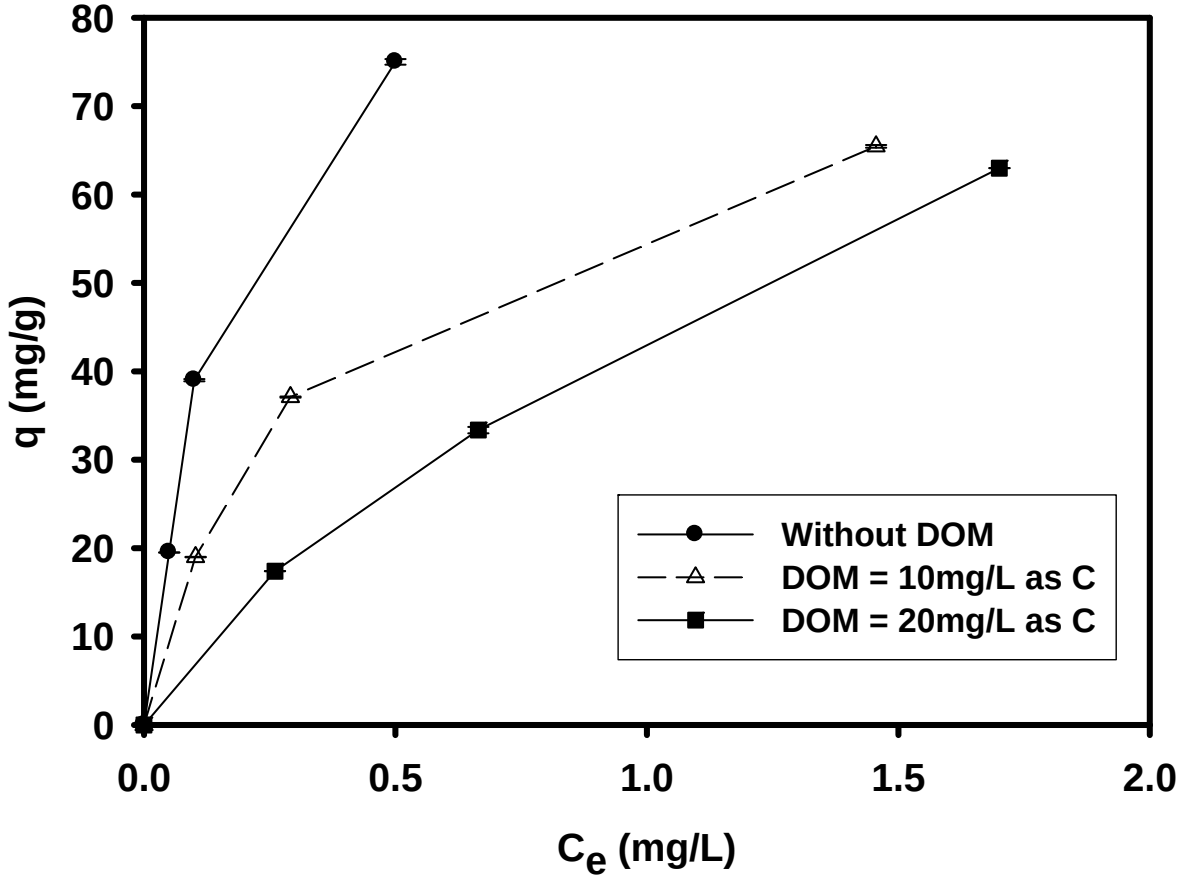

Figure 2-13. NOM effect on arsenate sorption isotherms for starch-stabilized magnetite nanoparticles. Experimental conditions: magnetite = 0.1 g/L as Fe, starch = 0.1 wt.%, equilibration time = 144 hrs. Data given as mean of duplicates and errors refer to deviation from the mean.

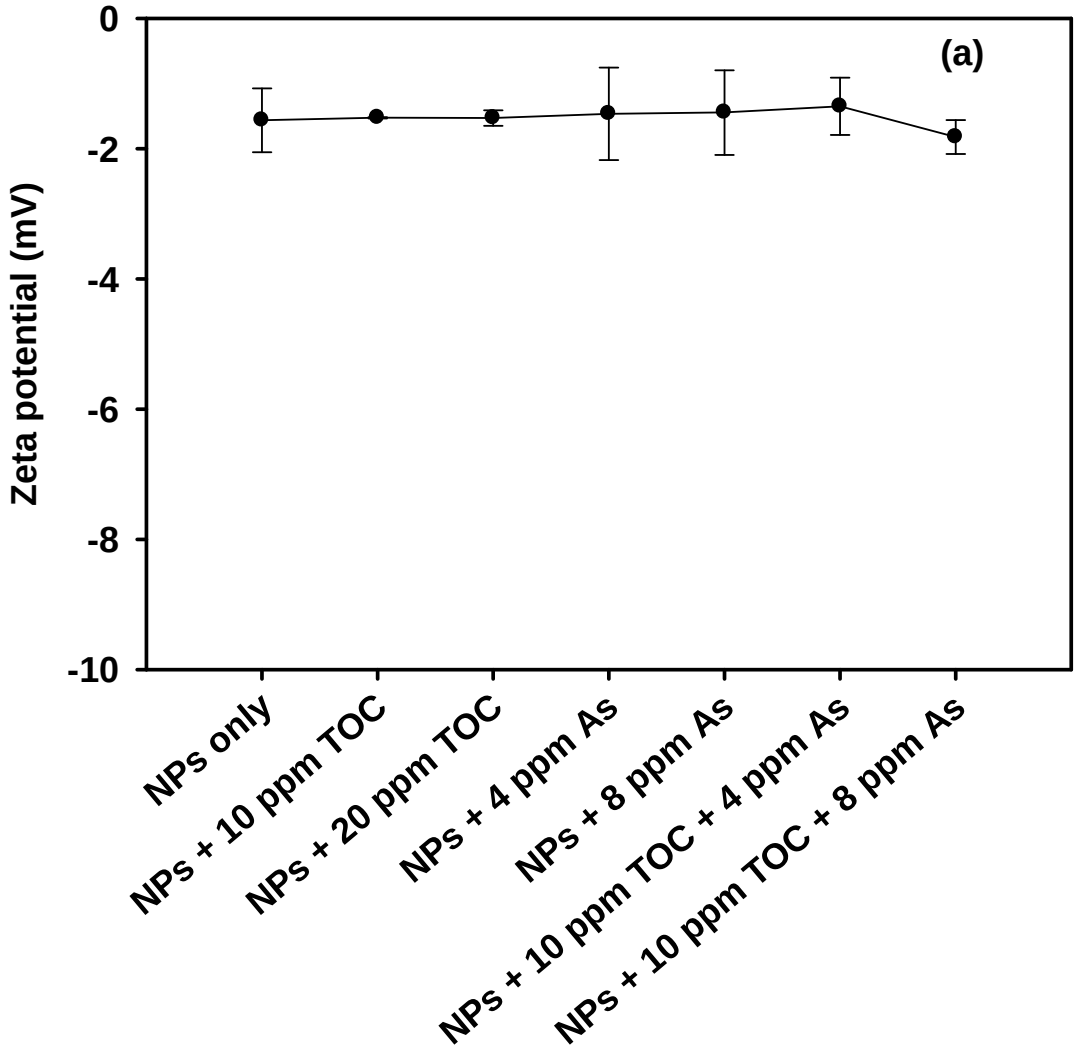
(a)
Zeta potential (mV)
0
-2
-4
-6
-8
-10
NPs only
NPs + 10 ppm TOC
NPs + 20 ppm TOC
NPs + 4 ppm As
NPs + 8 ppm As
NPs + 10 ppm TOC + 4 ppm As
NPs + 10 ppm TOC + 8 ppm As

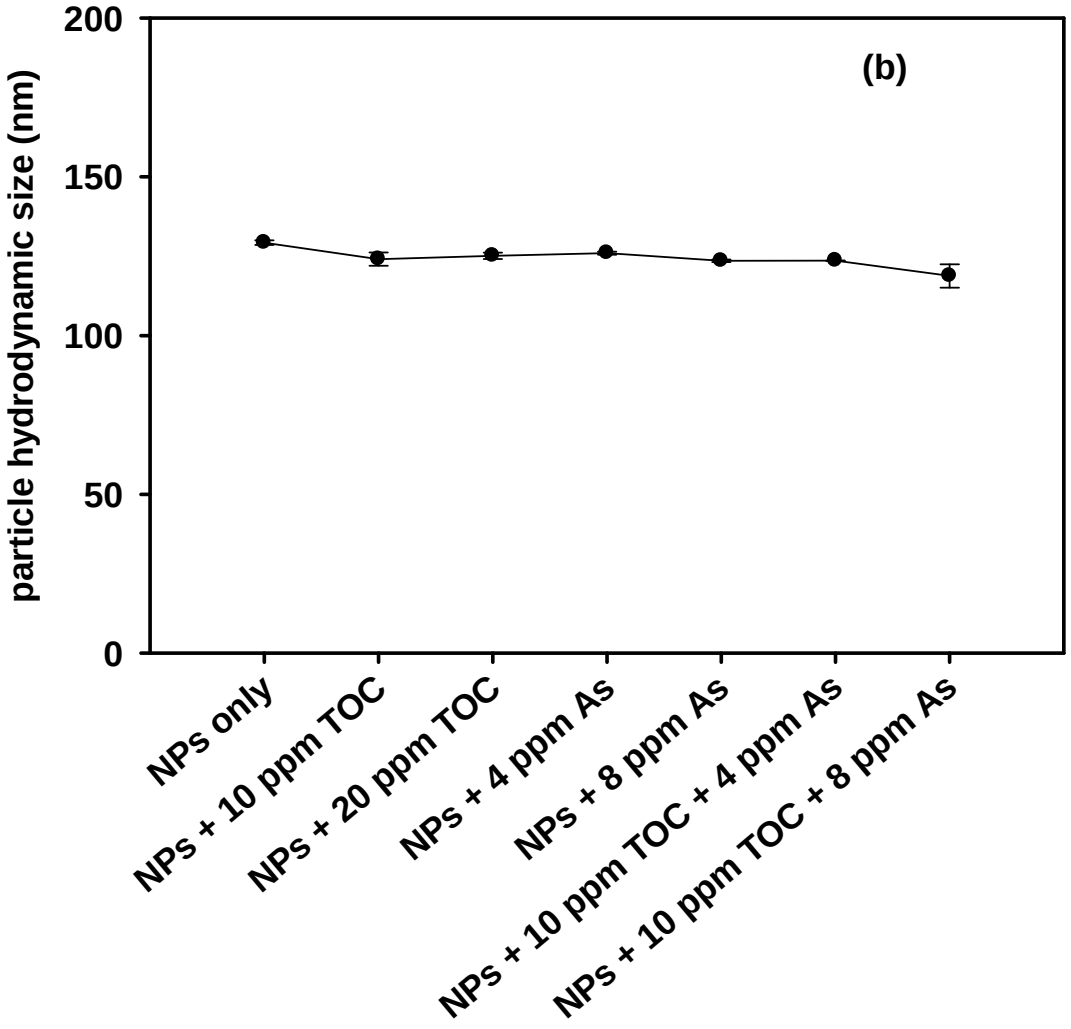

Figure 2-14. Effect of DOM on ζ potential (a) and hydrodynamic sizes (b) of starch stabilized magnetite. Experimental conditions: magnetite = 0.1 g/L as Fe, starch = 0.1 wt.%, the measurements were taken after the equilibration time (144 hrs).

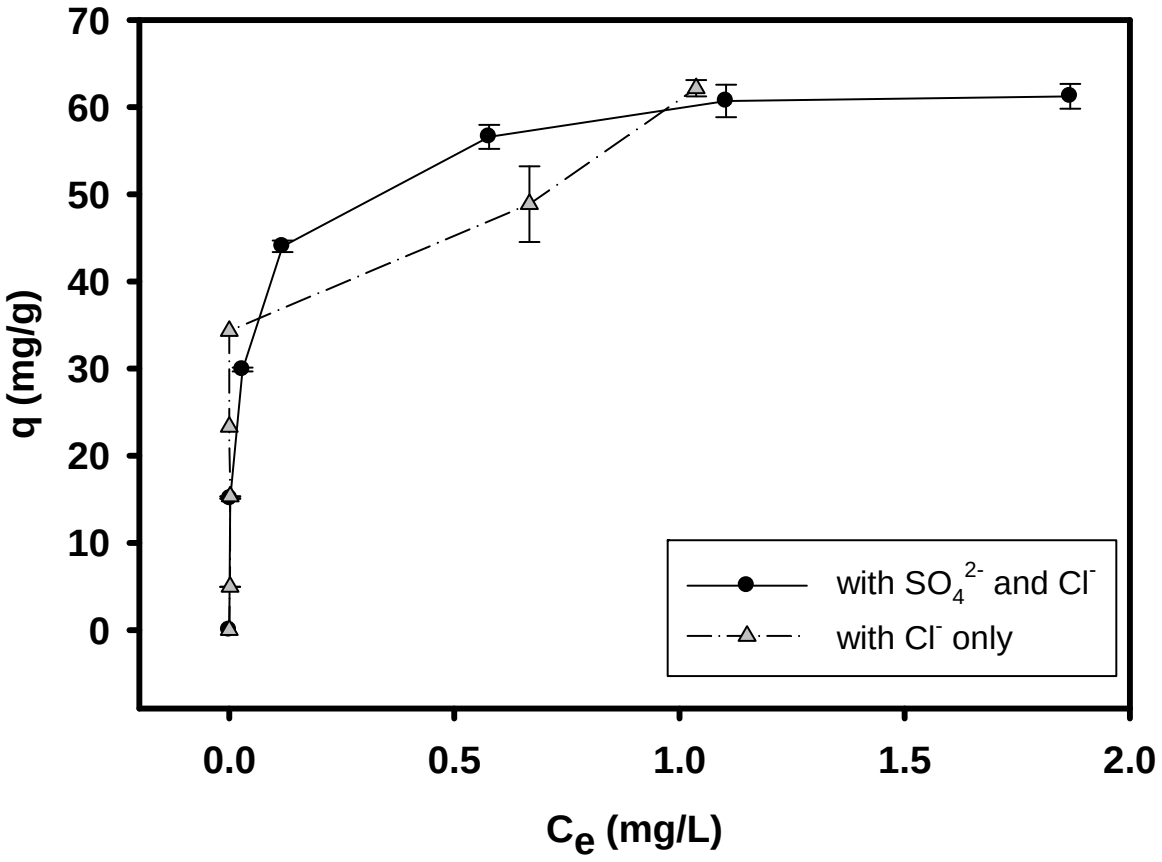

Figure 2-15. Effects of sulfate and chloride on arsenate uptake by starch-stabilized magnetite nanoparticles. Experimental conditions: magnetite = 0.1 g/L as Fe, starch = 0.1 wt.%, equilibration time = 144 hrs, SO_4^{2-} = 1.19 meq/L and Cl^- = 3.58 meq/L for $FeSO_4/FeCl_3$ based magnetite, and Cl^- = 4.77 meq/L for $FeSO_4/FeCl_3$ based magnetite. Data given as mean of duplicates and errors refer to deviation from the mean.

Sulfate has been well known to inhibit arsenate and arsenite (Su and Puls, 2001; Vaishya and Gupta, 2003) uptake by ion exchange resins, whereas chloride has little effect (An et al., 2005). **Figure 2-15** compares As(V) sorption isotherms for starch-stabilized magnetite in the presence of sulfate and the same equivalent amount of chloride. The results show that the isotherms nearly coincided for the two cases, indicating that the inhibitive effect of sulfate is minimal. An et al.(An et al., 2011b) pointed out that sorption of arsenate to starch-bridged magnetite was primarily due to specific surface complexation based on Lewis acid-base interaction (i.e. formation of surface Fe-O-As complexes). Because sulfate and chloride are much weaker ligands compared to arsenate, these omnipresent anions would not pose significant effect on the surface complexation of arsenate.

2.3.7 Leachability and stability of nanoparticle-sorbed arsenate

To compare the physico-chemical stability of arsenate sorbed on the stabilized magnetite nanoparticles, the spent arsenate-laden nanoparticles following the equilibrium tests were subjected to the standard TCLP tests. The results indicated that at an Fe/As molar ratio of 15.9 to 1, the TCLP leachable arsenic was less than 0.1%, and the arsenic concentration in the TCLP fluid phase was 1.11 mg/L, which is 4.5 times lower than the TCLP threshold of 5 mg/L.

After 1.5 years of aging at room temperature (~20^{o}C), the As-laden nanoparticles remained visually suspended in water, whereas the suspension pH dropped from pH=6.8 to pH=6.0. When the As(V) sorption isotherm was re-measured at this prolonged contact time , the sorption capacity remained about the same in the lower concentration range (C_e<0.5 mg/L), and displayed a marked increase at C_e>0.5 mg/L (**Figure 2-12**). Based on the pH effect results (**Figure 2-9**), the increase in arsenic uptake can be attributed to the observed pH drop. In addition, long-term slow diffusion of arsenic species into the nanopores of the nanoparticles can also increase the

equilibrium uptake (Fuller et al., 1993). Moreover, the aging of amorphous iron oxides to energetically more stable phases may also contribute to the elevated arsenic sorption capacities (Melitas et al., 2002).

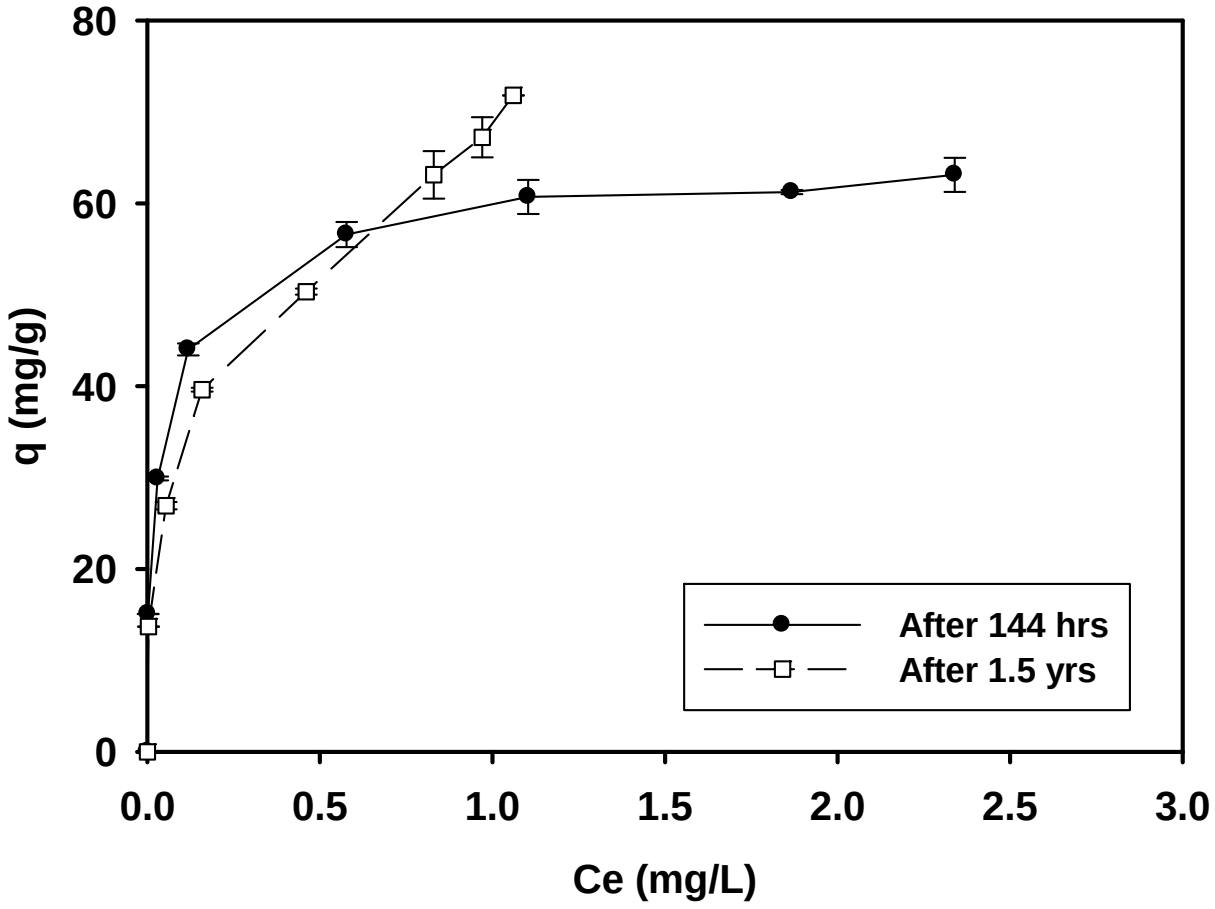

Figure 2-16. Comparing arsenate sorption isotherms for starch-stabilized magnetite nanoparticles when equilibrated for 144 hrs and 1.5 years. Magnetite = 0.1 g/L as Fe, initial *As* = 0.03 to 8.24 mg/L, pH at 144 h = 6.8±0.4, pH at 1.5 years = 6.0±0.4. Data given as mean of duplicates and errors refer to deviation from the mean.

Based on total Fe analysis, Fe concentration in the top layer of the 1.5 year aged magnetite suspension dropped from its initial 100 mg/L to 43 mg/L, indicating that slow aggregation and settling were occurring over prolonged times. Complete re-dispersion was established upon handshaking or gentle sonication of the suspensions. Less than 1% of iron was detected as dissolved Fe in the 1.5 year aged suspensions, indicating very little dissolution of the stabilized nanoparticles.

2.3.8 Separation of the stabilized magnetite nanoparticles

Compared to aggregated particles, the stabilized nanoparticles not only offer greater sorption capacity, but also offer the convenience that the particles can be used for water treatment or delivered into contaminated porous media such as soil and solid waste to facilitate in situ immobilization of arsenic. When used for water treatment, it is desired that the spent As-laden nanoparticles be easily separable from water. Magnetite particles are known to be amenable to easy separation from aqueous solution under weak low magnetic fields (Yavuz et al., 2006). Our preliminary experiments indicated that the spent starch-stabilized magnetite nanoparticles can be easily and completely separated (**Figure 2-17**) using a weak magnetic separator (Dexter Magnetic LifeSep 50SX, Elk Grove Village, IL, USA). Alternatively, the stabilized magnetite nanoparticles could be separated by gravity through manipulating the Fe-to-stabilizer ratio (An et al., 2011b).

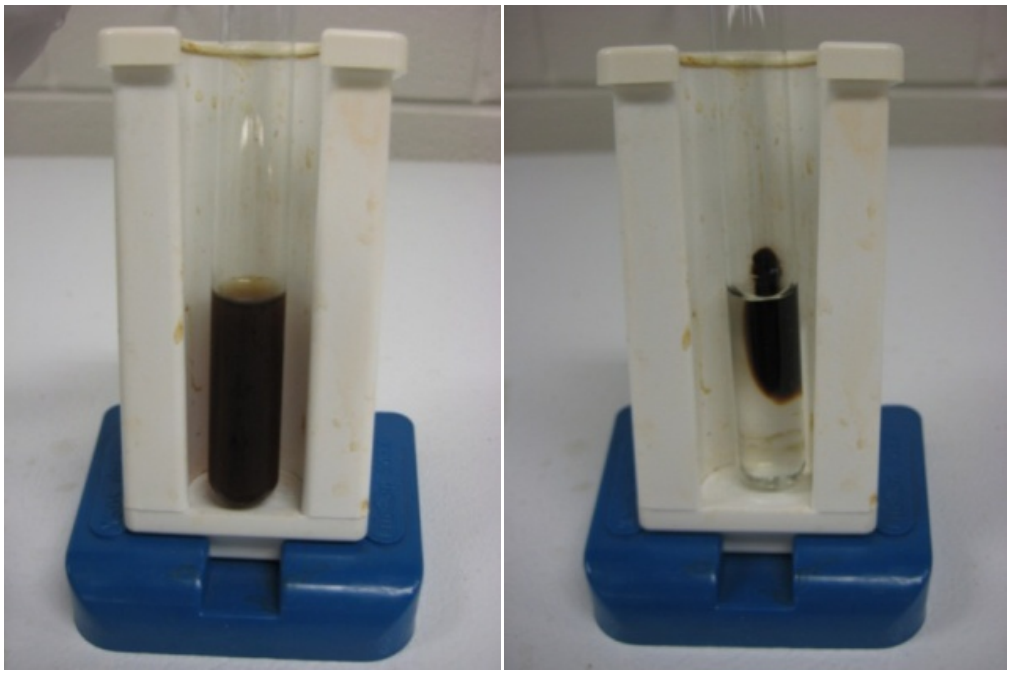

(a) **(b)**

Figure 2-17. Separation of stabilized magnetite nanoparticles: (a) Suspension of CMC-stabilized magnetite nanoparticles before magnetic separation, and (b) the concentrated nanoparticles after separation with a portable weak magnetic separator (Dexter Magnetic LifeSep 50SX, the magnetic field gradient = 23.3 T/m).

2.4 Conclusions

Our results demonstrated great potential of starch-stabilized magnetite nanoparticles for enhanced removal of arsenate from contaminated water, and possibly for soil remediation. The primary findings and conclusions are summarized as follows:

Both starch and CMC can act as effective stabilizers for preparing highly stable magnetite nanoparticles of much greater arsenic sorption capacity than conventional magnetite particles. The particle stability, degree of aggregation and size may be controlled by manipulating the type and concentration of the stabilizer.

The starch coating renders the ζ potential of the magnetite particles nearly neutral over a broad pH range, while the use of CMC results in a highly negative surface. Consequently, CMC acts as a more effective stabilizer than starch, while starch-stabilized magnetite particles offer a much greater arsenate uptake capacity. Based on the maximum Langmuir capacity, starch stabilized-stabilized magnetite particles offer, respectively, 1.7 and 2.3 times greater arsenic sorption capacity than CMC- and non-stabilized counterparts.

Starch-stabilized magnetite nanoparticles offer a greater and more aggressive arsenate removal rate than CMC-stabilized and non-stabilized magnetite. Removal rates can be adequately modeled using the intraparticle-diffusion model, which results in a diffusivity value of 3.0×10^{-7} cm^2/s and 8.0×10^{-10} cm^2/s for starch-stabilized and CMC-stabilized magnetite particles, respectively.

In the pH range of 3-11, the arsenate sorption capacity follows the sequence of: starch-stabilized magnetite >> CMC-stabilized magnetite > non-stabilized magnetite. The sorption capacity increases with decreasing pH and very high sorption capacity was observed at pH<7 for the starch-stabilized nanoparticles.

The presence of unusually high concentrations (10 and 20 mg/L as TOC) DOM can inhibit arsenate uptake by 15% and 19%, respectively.

The spent starch-stabilized nanoparticles can be separated via a weak magnetic separator. The As-laden sludge can easily pass the TCLP test, and thus, the spent particles can be either reused upon proper regeneration or disposed of as a non-hazardous material. When subjected to 1.5 years of aging, no arsenic leaching was observed, and <1% of the nanoparticles were dissolved.

Chapter 3. In Situ Immobilization of Arsenate in a Sandy Soil Using Starch Stabilized Magnetite Nanoparticles

Presented in this chapter is an innovative in-situ arsenate (As(V)) immobilization technology using starch-stabilized magnetite (Fe_3O_4) nanoparticles that were evaluated through a series of batch and column experiments. TCLP (Toxicity Characteristic Leaching Procedure) based As leachability of As-laden soil after the treatment was measured to validate the performance of nano-sized magnetite nanoparticles. Though Fe_3O_4 nanoparticles are highly mobile and deliverable in sandy soil, the effective travel distance of Fe_3O_4 nanoparticles can be manipulated by controlling the injection flow rate.

3.1 Introduction

Arsenic (As) has been widely detected in soil and groundwater all over the world, particularly in the Bengal Delta (Bangladesh and West Bengal, India) (Berg et al., 2001) and western United States (Berg et al., 2001). Based on analysis of 30,000 of groundwater samples in the United States, about 10% exceeded 10 μg/L (Welch et al., 2000). More than one third of the National Priorities List sites have excessive arsenic levels (deLemos et al., 2006). The growing knowledge in the health effects of arsenic has rendered more stringent environmental regulations on As in drinking water. For example, effective in 2006, the US EPA lowered the maximum contaminant level (MCL) of As in drinking water from 50 to 10 μg/L (Kapaj et al., 2006).

Exposure to As in drinking water has been associated with the development of skin and internal cancers and non-carcinogenic effects such as diabetes, peripheral neuropathy, and cardiovascular diseases (Kapaj et al., 2006). In addition, As has been reported to impede verbal IQ and long term memory and to suppress hormone regulations and hormone mediated gene transcription (Kapaj et al., 2006). Chronic exposure to As even at <10 µg/L has been associated with increased fetal loss, premature delivery, and decreased birth weights of infants (Kapaj et al., 2006). Of the various arsenic species, based on acute lethality data, the inorganic arsenicals are more acutely toxic than the most organic species (Abernathy et al., 1999).

The predominant species of As in groundwater are As(III) and As(V), depending on redox conditions, pH and microbial activity (Dixit and Hering, 2003; Smedley and Kinniburgh, 2002). Although both species can be adsorbed on soil, they also undergo slow desorption/dissolution into groundwater, posing long-term threat to the groundwater quality. Depending on the groundwater biogeochemical conditions, three principal mechanisms of arsenic mobilization have been identified: desorption in alkaline conditions, competitive sorption of co-ions, and reductive release, especially reductive As dissolution associated with the dissolution of iron oxides (deLemos et al., 2006). Changes in the redox potential and pH can greatly affect As speciation in soil and groundwater. At higher redox potential (200-500 mV), As(V) is the predominant species in solution and it is subject to strong sorption to the solid phase. Increasing pH or reducing As(V) to As(III) increases the concentration of As species in the solution phase (Masscheleyn et al., 1991). In addition, phosphate has been reported to displace adsorbed As from soils. For example, Woolson et al. (1973) reported that addition of 0.05 M KH_2PO4 desorbed approximately 77% of the total As in As-contaminated soils (Woolson et al., 1973). Deuel and Swoboda (Deuel and Swoboda, 1972) found that there was an increase of As in

soil solution over time under flooded soil conditions, which they attributed to the release of As(V) during dissolution of iron oxyhydroxide minerals that have a strong affinity of As(V) under aerobic conditions.

Su and Puls (2003) reported that zero valent iron (ZVI) particles may serve as an effective reducing agent and adsorbent for immobilization of As in groundwater. It was believed that the key mechanism for As removal from water was due to adsorption of As(III) and/or As(V) on the incoherent and porous iron oxide layers on the ZVI cores.

Iron oxides have been known to offer high adsorption affinity for both As(V) and As(III) (Gimenez et al., 2007; Jang et al., 2006; Raven et al., 1998; Yavuz et al., 2006; Yean et al., 2005). Investigations using extended X-ray absorption fine structure (EXAFS) (Guo et al., 2007; Manning et al., 2002), energy dispersive X-ray analysis: EDS or EDX (Kanel et al., 2005), and Fourier Transform Infrared Spectroscopy (FTIR) (An et al., 2011b) have shown that As(V) forms strong inner-sphere Fe-O-As surface complexes. Over the past decade, the uses of nanoscale adsorbents have gained momentum in water treatment and soil remediation engineering (He et al., 2007; Hristovski et al., 2007; Liang et al., 2012b; Shipley et al., 2009; Su and Puls, 2003). Compared to the bulk counterparts, nanoparticles offer much greater specific surface area, and thus, greater adsorption capacity. For example, studies have demonstrated that iron and iron oxide nanoparticles can offer 10 times greater sorption capacity than the micro-scale counterparts based on the Langmuir capacity coefficient (An et al., 2011b; Yean et al., 2005).

In addition, well dispersed nanoparticles offer another unique feature that these nanoscale adsorbent materials may be delivered into contaminated soil or deep aquifers to facilitate in situ immobilization of the contaminants. For example, Xiong et al. (Xiong et al., 2009) developed a

class of CMC (carboxymethyl cellulose) stabilized FeS nanoparticles and found that the nanoparticles are transportable through a clay loam sediment and effectively immobilize Hg^{2+} in the sediment. (Xu and Zhao, 2007) observed that CMC-stabilized ZVI nanoparticles were deliverable in sandy loam soil and facilitate in situ reductive immobilization of Cr(VI) in the soil column.

Limited work has been reported on transport of aggregated iron oxides (Fe_3O_4, Fe_2O_3) nanoparticles in porous media and application to As remediation (Hristovski et al., 2007; Kanel et al., 2007; Shipley et al., 2009). Hristovski et al. (Hristovski et al., 2007) compared 16 commercial metal oxide nano-powders in four water matrices and demonstrated that TiO_2 nanoparticles can be aggregated using an inert binder and amply remove arsenate in a fixed bed adsorber setting. Shipley et al. (Shipley et al., 2011) examined the effectiveness of iron oxide (magnetite and hematite) nanoparticles for arsenate and arsenite removal from water by mixing nanoparticles with a sandy soil through column studies and observed that the flow rate (1.5 or 6 mL/h) and the portion of iron oxide (1.5 or 15 wt%) in the soil column influenced the occurring time and the percentage of As release. However, the aggregated/bare magnetite nanoparticles are not deliverable into typical soil, and thus, cannot be used for *in situ* remediation of contaminated aquifiers. Kanel et al. (Kanel et al., 2007) synthesized and tested a class of surface-modified ZVI nanoparticles (S-INP) for removing arsenite from influent solutions through S-INP pretreated sand-packed columns. S-INP breakthroughs were observed in different porous media (glass beads, unbaked sand and baked sand), while un-modified INP was immobile and aggregated on porous media surfaces in the column inlet area. Yet their studies did not touch the subject about the fate and transport of the spent nanoparticles nor the particle-associated As mobility.

Previously, we successfully synthesized a class of starch stabilized magnetite nanoparticles, and tested the effectiveness of the nanoparticles for arsenate removal in simulated groundwater water (Liang et al., 2012b). The 0.04 wt% starch stabilized magnetite nanoparticles offered a 2.2 times greater As(V) uptake than non-stabilized particles (based on the Langmuir capacity coefficient), yet the particles remained settleable in water by gravity. Further increasing the starch concentration resulted in fully stabilized/dispersed nanoparticles, which can be potentially used for *in situ* immobilization of As in contaminated soil and sediment.

Given the great potential of the starch stabilized nanoparticles for environmental cleanup applications as well as the concern of environmental impacts of spent nanoparticles, this study aimed to test the feasibility of using these starch-stabilized magnetite nanoparticles for *in situ* immobilization of As(V) in soil and groundwater. The specific objectives of this work were to: 1) test the soil deliverability and transport behavior of the starch-stabilized magnetite nanoparticles; 2) probe the effectiveness of the stabilized nanoparticles for in situ immobilizing As(V) in soil and simulated groundwater through batch and column experiments; and 3) examine the effect of the nanoparticle treatment on As leachability in contaminated soil.

3.2 Materials and Methods

3.2.1. Chemicals

A water soluble potato starch (hydrolyzed for electrophoresis) and ferrous sulfate heptahydrate ($FeSO_4 \cdot 7H_2O$) were obtained from Acros Organics (Pittsburgh, PA, USA). Sodium arsenate heptahydrate ($Na_2HAsO_4 \cdot 7H_2O$) was purchased from Sigma-Aldrich (St. Louis, MO, USA). Ferric chloride ($FeCl_3$) and sodium hydroxide (NaOH) were obtained from Fisher Scientific (Pittsburgh, PA, USA). Hydrochloric acid and nitric acid were purchased from Mallinckrodt Chemical (St. Louis, MO, USA).

3.2.2 Preparation of stabilized magnetite nanoparticles

Starch-stabilized magnetite nanoparticles were prepared following the co-precipitation approach described in our prior work (Liang et al., 2012b). In brief, a 1.0 wt.% stock solution of starch was prepared with deionized (DI) water and heated to the boiling point under magnetic stirring, kept boiling for 15 min and then cooled to room temperature. Another stock solution of $FeCl_2 \cdot 4H_2O$ and $FeCl_3$ at a Fe^{2+}:Fe^{3+} molar ratio of 1:2 ([Fe^{2+}] = 0.033 g/L, [Fe^{3+}] = 0.067 g/L) was freshly prepared for immediate use. Then, 100 mL of the Fe^{2+}-Fe^{3+} stock solution was mixed with 7-20 mL of the starch stock solution and DI water to yield a mixture of 188 mL containing 0.1 g/L total Fe and a starch concentration ranging from 0.035 to 0.1 wt.%. Then 12 mL of 0.5 M NaOH solution was injected in one shot into the mixture to raise the pH of the solution to ~11 under nitrogen purging. Based on our prior experience (Liang et al., 2012b) in preparing stabilized magnetite nanoparticles, the stabilizer-to-iron ratio can be varied to yield nanoparticles of various size and stability. Our previous study indicated that the TEM size and DLS-based hydrodynamic diameter were 75±17 nm and 129 nm, respectively, for the nanoparticles stabilized with 0.1 wt% starch (Liang et al., 2012b). Due to the starch coating, a nearly neutral surface (as indicated by zeta potential) was observed over a pH range of 2-9 for the starch stabilized nanoparticles; it turned gradually more negative (ζ value >-0.9 mV) at pH above 9, and reached a ζ potential value of -16 mV at pH 11 (Liang et al., 2012b).

3.2.3 Preparation of As(V)-spiked soil and soil analysis

A sandy soil was obtained from the E.V. Smith Research Center (EVSRC) in Shorter, AL, USA. According to the information provided by EVSRC, the soil is designated as fine sandy loam. Before use, the soil was sieved through a standard sieve of 2 mm opening, and then washed with tap water to remove suspended colloids and water soluble compositions. The

washed soil can be completely separated from water through centrifugation at 400 g-force. The soil was then air-dried at room temperature and stored in a sealed glass bottle. Soil analyses were performed by the Soil Testing Laboratory at Auburn University. **Table 3-1** provides salient physical and chemical properties of the soil. Elemental analysis of the soils was conducted following EPA method 3050B and using an inductively coupled plasma optical emission spectrometer (Vista-MPX, Varian Inc., Palo Alto, CA, USA). The content of sand, silt and clay was determined following the pipette method (Gee, 2002). Soil organic matter (SOM) was measured per the Dumas method with a LECO CN-2000 combustion unit (LECO Corp., Joseph, MI, USA) at 1050 ºC after the soils were treated with 4N H_2SO_4 to dissolve free carbonates before the dry combustion.

Table 3-1. Physicochemical characteristics of E.V. Smith Research Center soil.

Textural Class	pH	H_2O	O.M. %	Ca ppm	K ppm	Mg ppm	P ppm	Al ppm	As ppm	B ppm	Ba ppm	Cd ppm	Cr ppm	Cu ppm	Fe ppm	Mn ppm	Mo ppm	Na ppm	Ni ppm	Pb ppm	Zn ppm
Sand	6.0	0.0	0.2	45	9	28	3	22	<0.1	<0.1	2	<0.1	<0.1	1	5	8	<0.1	6	<0.1	<0.1	2

The pH corresponding to the point of zero salt effect (PZSE) for the soil was determined following the potentiometric titration method (Marcano-Martinez and McBride, 1989). In brief, soil samples of 1.5 g each were mixed in 15 mL of 0.1, 0.01 and 0.01 M KCl solutions, and the pH's were adjusted to a range between 3 and 8 with measured amounts of HCl or KOH. The suspensions were kept at room temperature (22.0 ± 0.1 °C) in capped 20-mL polyethylene vials and shaken twice daily over a 3-d period. Then, the equilibrium pH values of the supernatants were recorded, and the amounts of H^+ and OH^- adsorbed by the soil samples were calculated based on the amounts of acid or base applied to the samples as compared to those to a control solution (KCl solution without soil) to achieve the same final pH. **Figure 3-SM-1** (in Supplementary Material) shows the titration curves, describing the net adsorption and desorption of H^+ as a function of pH and ionic strength From **Figure 3-SM-1**, the point of PZSE was determined to be 6.0.

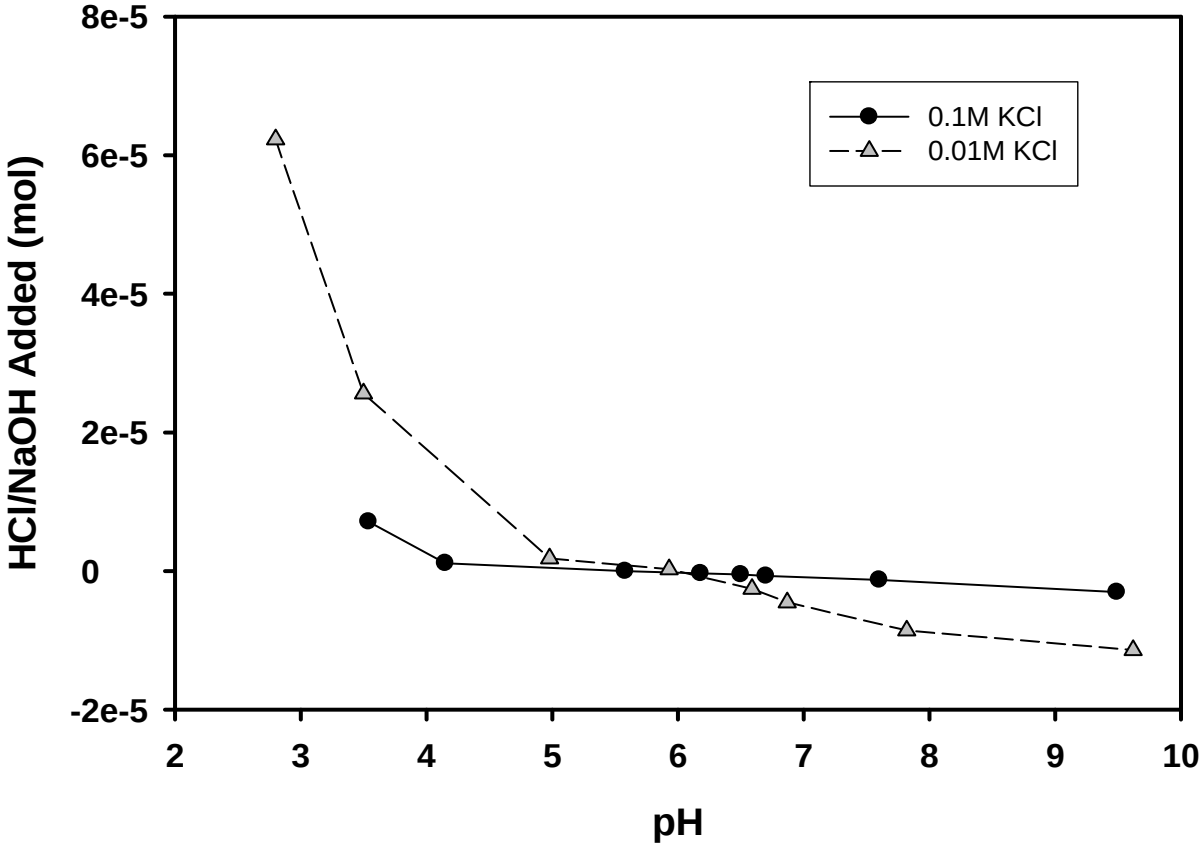

Figure 3-SM-1 – Estimation of surface charge in sandy soil from EVSRC by potentionmetric titrations at two electrolyte concentratons (0.1M and 0.01 M KCl).

A known concentration of As(V) was pre-spiked in the soil following the procedure by Yang et al. (Yang et al., 2002). In brief, 200 g of the air-dried soil was mixed with 2000 mL of an As(V) solution containing 10 mg/L As(V). The solution pH was adjusted to the original soil pH of 6.0, which was maintained through intermittent pH adjustment with 0.1 N NaOH and 0.1 N HNO_3. After one month's equilibration, the soil suspension was centrifuged at 400 g-force. The supernatant was filtered through a 25 nm membrane of mixed cellulose esters (Millipore Corp., Billerica, MA, USA), and the filtrate was analyzed for total As remaining. The As loading on the soil was then determined to be 31.45 mg/kg by measuring the difference between the initial and final As(V) concentrations in the aqueous phase. The adsorbed As was further verified via acid digestion of the soil per USEPA Method 3050B (USEPA, 1996) and the difference was <5%. The As(V) spiked soil was then air-dried for subsequent experimental uses.

3.2.4 Immobilization of As(V) in soil: batch kinetic tests

Batch kinetic tests of As(V) leaching from the As(V) spiked soil were carried out in the presence and absence of the starch-stabilized Fe_3O_4 nanoparticles. The Corning plastic (polyethylene tetraphthalate or PET) centrifuge tubes of 53 mL were used in the batch tests. Typically, 5.3 g and 21.2 g of the As(V) spiked soil were added to centrifuge tubes each containing 53 mL of the nanoparticle suspension containing 0.5 g/L (as Fe) of the Fe_3O_4 nanoparticles (stabilized with 0.4 wt.% starch). The soil to liquid ratio (SLR) was set at 0.1 and 0.4 (g/mL). The tubes were then capped and rotated on an end-to-end rotator operated at 50 rpm at room temperature (22.0 ± 0.1 ºC). The solution pH was kept at 6.8 ± 0.4 through intermittent adjustment with 0.1 N NaOH and 0.1 N HNO_3. The arsenic leaching rate was then followed for one week by measuring the As concentration in the aqueous phase. At pre-determined times, the tubes were sacrificially sampled by centrifuging the mixtures at 400 g-force for 20 min. The

supernatants were then passed through the 25 nm Millipore membrane filters, and the filtrates acidified to pH < 2.0 with 0.1 N HNO_3 and then analyzed for total As. The membrane was able to completely remove the nanoparticles, but did not remove any soluble As. All tests were conducted in duplicate.

The arsenate distribution coefficient (K_d) was obtained from arsenate sorption isotherms through batch equilibrium experiments to probe the absorbability of arsenic on the EVSRC soil. The initial As(V) concentration ranged from 0.8 mg/L to 100 mg/L. The adsorption tests were initiated by mixing 3 g of an air-dried clean soil sample with 30 mL of arsenate solutions in 30 mL polyethylene vials. The solution pH was maintained at 6.8 ± 0.4 through intermittent adjustment with 0.1 N HNO_3 or NaOH solution. The mixtures were equilibrated on a rotator at 50 rpm for 12 days at room temperature (22.0 ± 0.1 ºC). The mixtures were centrifuged at 400g-force for 20 min and then filtered through 25 nm Millipore membrane filters. The filtrates were acidified to pH < 2.0 with 0.1 N HNO_3 and then analyzed for total As. All tests were conducted in duplicate.

3.2.5 Toxicity characteristic leaching procedure (TCLP) tests

TCLP tests were performed following the U.S. EPA Method 1311 (USEPA, 1992) to determine the leachability of As(V) in the soil. TCLP fluid #1 (pH = 4.93) was prepared with dilute acetic acid. The extraction tests were carried out by mixing 1.0 g of a freeze-dried As-laden soil sample with 20 mL of the TCLP fluid in 20 mL glass vials. The mixtures were rotated at 30 rpm for 18 h. Then, the vials were centrifuged at 400 g-force for 20 minutes, and the supernatants were filtered through the 25 nm membrane filters, and the filtrates were acidified and analyzed for As in the same manner described before. The soil samples were prepared as follows. First, 20 g of the As-spiked soil was amended with 200 mL of the starch-stabilized

Fe_3O_4 nanoparticles (0.1 g Fe/L with 0.04 wt.% starch) in a glass flask. The mixtures were shaken at 200 rpm at room temperature for 1 week, and then freeze-dried using a VirTis FreezeMobile freeze dryer (Gardiner, NY, USA) at -50℃ for 4 days. Lastly, the resultant As-laden soil sample was mixed thoroughly for even distribution and then subjected to the TCLP tests. For comparison, control tests were carried out with the same As-laden soil that was only amended with DI water (i.e., no nanoparticle treatment) at the same SLR. All tests were conducted in duplicate.

3.2.6 Soil sorption and mobility of stabilized Fe_3O_4 nanoparticles in soil

Sorption of starch-stabilized magnetite nanoparticles on the soil was investigated through batch kinetic experiments to examine the soil uptake rate and extent of the nanoparticles. Fully stabilized magnetite nanoparticle suspensions were prepared at 0.1 g/L as Fe with 0.04 wt% of starch. The sorption tests were initiated by mixing 5.3 g of an air-dried clean soil sample with 53 mL of the magnetite suspensions in 53 mL polyethylene vials. The solution pH was maintained at 6.8±0.4 through intermittent adjustment with 0.1 N HNO_3 and NaOH solution. The vials were rotated at 50 rpm at room temperature (22.0 ± 0.1 ºC) and sacrificially sampled at pre-determined times. The upper portion of suspension in each vial was sampled and particle concentration was determined by dissolving the magnetite particles with concentrated hydrochloric acid (the volume of HCl needed is 4 mL for every 1 mL of 0.1 g/L Fe), followed by measuring the total dissolved iron. Control tests with only starch-stabilized magnetite but without the soil were carried out under otherwise identical conditions. All tests were conducted in duplicate.

For *in situ* remediation, the nanoparticles must be deliverable in the target soil. To test the particle deliverability, column breakthrough tests were carried out with the sandy soil. The experimental setup (**Figure 3-1**) includes a Harvard Apparatus PHD 2000 syringe pump (Plymouth Meeting, PA, USA), a Plexiglas column (inner diameter = 10 mm, length = 100 mm, Omnifit, Cambridge, UK), and a fraction collector (Eldex Laboratories, Napa, CA, USA). To facilitate a uniform soil packing and avoid air entrapment, a nitrogen-sparged background solution (0.84 mM NaCl + 0.16 mM $NaHCO_3$, pH 7.5) was pre-introduced into the column in the down-flow mode, and then 12 g of the sandy soil was added from the top into the solution while the column was constantly patted with a plastic rod, yielding a porosity of 0.36 and a bulk bed volume of 7.23 mL. Then, a stabilized Fe_3O_4 nanoparticle suspension (Fe = 0.1 g/L, starch =

0.04 wt.%) was pumped through the column in the same down-flow mode at an EBCT (Empty Bed Contact Time) of 118 min. The flow rate was set to be 0.06 mL/min, which translates into a pore water velocity of 3.5×10^{-3} cm/s. The effluent was collected by the fraction collector, and the samples were then acidified by concentrated hydrochloric acid (4 mL acid for each mL of the sample) to dissolve the nanoparticles. The concentration of the nanoparticles in the effluent was then determined by measuring the total iron content in the samples. To study the elution behavior of the starch-Fe_3O_4 nanoparticles that were retained in the soil bed after complete breakthrough, the influent was switched to the background solution, and then, the nanoparticle elution history was followed until the effluent Fe concentration became undetectable (<0.001 mg/L). For comparison, the breakthrough behavior of a tracer (50 mg/L Br^-) was also tested in parallel. The concentration of Br^- was followed to obtain a complete breakthrough curve of the tracer. A separate elution test using an eluent containing 0.04 wt% starch indicated that leaching of native iron of the sandy soil was negligible.

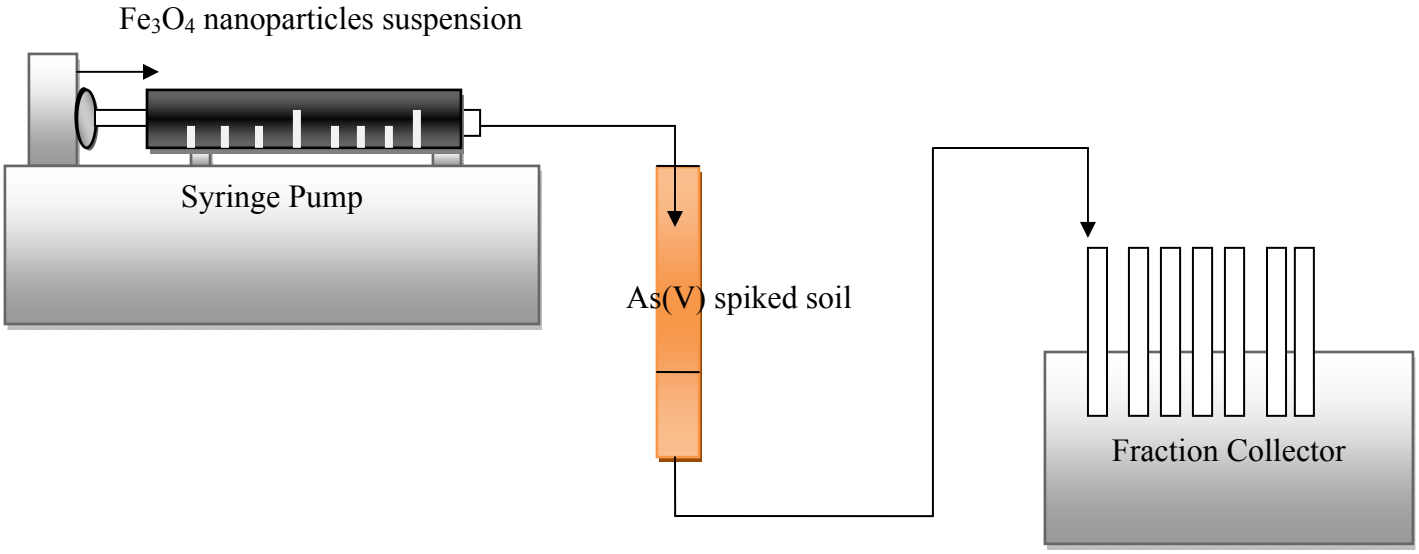

Figure 3-1. Schematic of column apparatus set-up

To determine the maximum transport distances of the nanoparticles as a function of injection pore velocity, the column breakthrough studies were carried out using the nanoparticles that escaped the first column run. Following a full column breakthrough run as described above, approximately 34 pore volumes (PVs) of the spent nanoparticle suspension was collected in a flask under nitrogen purging. The suspension was then pumped through a freshly packed column containing the same amount (12 g) of the sandy soil. Then the breakthrough curve of the nanoparticles through the soil bed was measured by following the total Fe concentration in the effluent. To examine the effect of the pore velocity on the filtration removal of the nanoparticles, the breakthrough experiments were conducted under four pore velocities (3.5×10^{-3}, 1.8×10^{-3}, 3.5×10^{-4}, and 2.2×10^{-4} cm/s, respectively) to simulate different groundwater flow conditions.

3.2.7 In situ immobilization of As(V): column tests

The effectiveness of the stabilized nanoparticles for in situ immobilization of As(V) pre-loaded in the sandy soil was tested with the same experimental column setup. Briefly, 12 g of the As-laden soil was wet-packed in the column with a porosity of 0.36. Then, an influent of 0.1 g/L of the starch-stabilized nanoparticle suspension was passed through the soil bed at an EBCT of 118 min. Then, the effluent As(V) concentration was followed in two ways. First, the effluent samples, which include both dissolved As and nanoparticle-sorbed As, were acidified at pH < 2.0 with 1 N HNO_3 and analyzed for total As; second, the effluent samples were filtered through the 25 nm membrane, and the filtrates were acidified at pH < 2.0 with 1 N HNO_3, and then analyzed for As, which gave the free or dissolved As. For comparison, As elution history was also determined by subjecting identical soil bed to a simulated groundwater (SGW) with a chemical composition of 7 mM NaCl + 0.86 mM $CaSO_4$ (pH 6.5) under identical hydrodynamic conditions.

To determine the spatial distribution of the retained nanoparticles along the soil bed following the nanoparticle treatment, the soil bed was sectioned into five layers. Each segment was then air-dried and subjected to the EPA 3050B method for total Fe content. The nanoparticle concentration in each section was then quantified by subtracting the native Fe content (1.11 µg-Fe/g-soil) in the soil from the measured total Fe.

3.2.8 Chemical analyses

Total As was analyzed using a Perkin Elmer Graphite Atomic Absorption Spectrometer 3110 (connected with an HGA 600 and EDL system 2). The detection limit was ~5 µg/L. Br^- was analyzed using a Dionex Ion Chromatography (DX-120) equipped with an AS14 column

(detection limit = 0.5 mg/L). Total iron concentration was analyzed with a VARIAN 220FS Flame Atomic Absorption Spectrometer (detection limit = 0.1 mg/L).

3.3 Results and Discussion

3.3.1 As(V) immobilization: batch tests

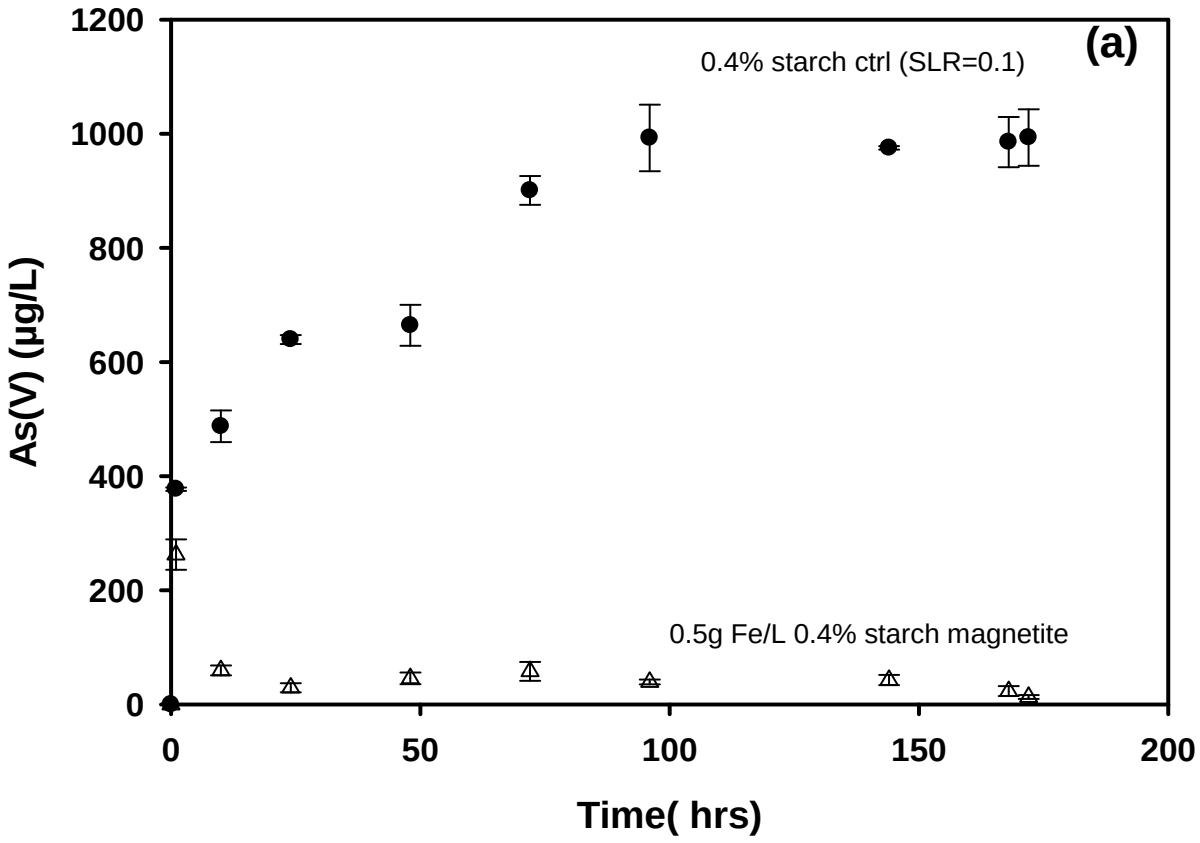

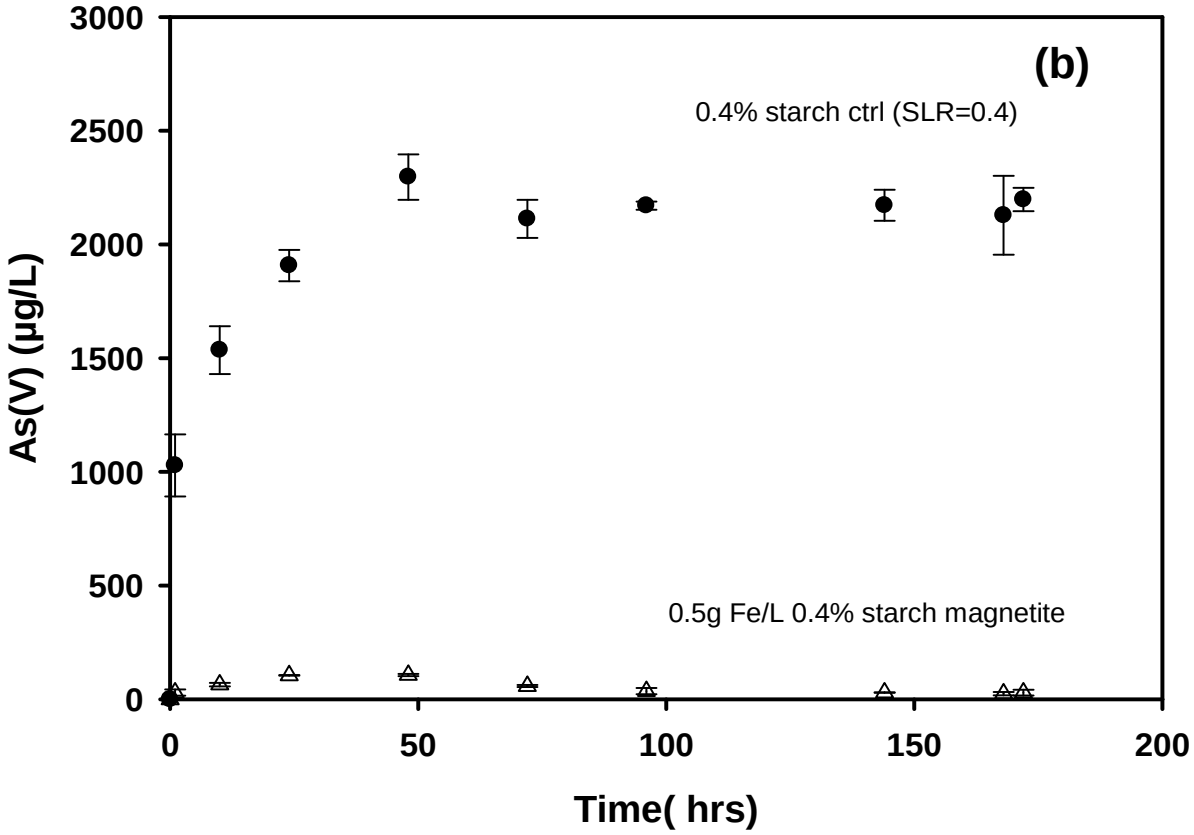

Figure 3-2. Desorption kinetics of arsenate from As-laden sandy loam in the absence and presence of starch stabilized magnetite nanoparticles (0.5 g-Fe/L with 0.4 wt% starch). The solid to liquid ratio was 0.1 in case (a) and 0.4 for case (b). Control tests were conducted with 0.4 wt% starch solution only. The pH was controlled at 6.8 ± 0.4. Data plotted as mean of duplicates, and errors refer to deviation from the mean.

The effectiveness of stabilized Fe_3O_4 nanoparticles for immobilizing As(V) in the sandy soil was tested in batch desorption experiments. **Figure 3-2** compares arsenate desorption kinetics from the As-laden sandy soil in the absence and presence of starch-stabilized magnetite nanoparticles under the two SLRs: 0.1 and 0.4. In the absence of the nanoparticles (i.e., when the soil was mixed with the 0.04 wt% starch solution), the equilibrium aqueous phase concentration of As reached ~1000 μg/L at SLR = 0.1 and ~2200 μg/L at SLR = 0.4, which accounted for ~31.8% and 17.5% of the total As in the soil, respectively. In contrast, in the presence of the nanoparticles, the water-soluble As (or free As) concentration was reduced by ~98% in both cases. The total solid (soil + Fe_3O_4) to water distribution coefficient (K_d) is calculated to be 50 and 121 L/g at SLR = 0.1 and SLR = 0.4, respectively. Separate sorption tests with the soil (**Figure 3-SM-2**) revealed a nearly linear sorption isotherm with a mean $K_{d(soil)}$ of 2.6 L/kg over an equilibrium concentration range of 0-40 μg/L As. Then, the sorption distribution coefficient of As to the nanoparticles, $K_{d(Fe_3O_4)}$, can be obtained via Eq. (1):

$$K_{d(Fe_3O_4)} = \frac{W_s}{W_{Fe_3O_4}}(K_d - K_{d(soil)}) \qquad \text{(Eq.1)}$$

where W_s and $W_{Fe_3O_4}$ are the weights of soil and the nanoparticles in the system, respectively. The resultant $K_{d(Fe_3O_4)}$ is 9999.5 L/g (SLR = 0.1) and 96798 L/g (SLR = 0.4), which is more than five orders of magnitude greater than $K_{d(soil)}$ for the sandy soil.

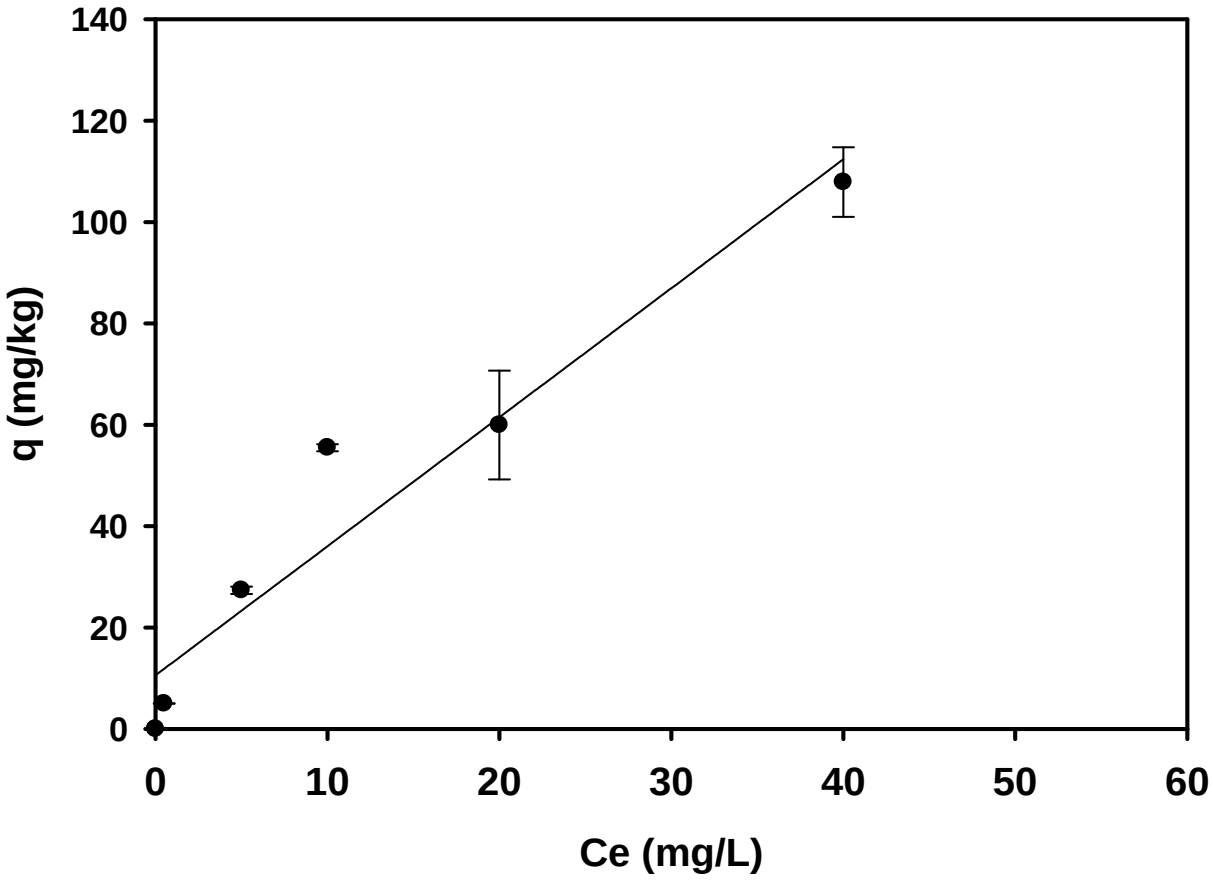

Figure 3-SM-2 – Arsenate sorption isotherm for the EVSRC soil. The initial arsenic concentration ranged from 0.8 mg/L to 100 mg/L. 5.3 g of an air-dried clean soil sample was mixed with 53 mL of arsenate solution. The solution pH was maintained at 6.8 ± 0.4. The mixtures were equilibrated on the rotator at 50 rpm for 12 days. Data reported as mean of duplicates and error bars indicate standard deviation from the mean.

Figure 3-SM-2 shows the arsenate sorption isotherm for EVSRC soil. Based on the isotherm data, the average arsenate distribution coefficient K_d for the soil was calculated to be 2.6 L/kg, which is in the range of 0.3 – 4.3 L/kg of EPA's estimated values from MINTEQA2 results (Allison and Allison, 2005). In our prior work (Liang et al., 2012b), the K_d value for the starch-stabilized magnetite nanoparticles was determined to be 55.2 L/g. The K_d value for the nanoparticles is nearly one order of magnitude greater than that for the soil. This observation indicates that adding a small fraction of the nanoparticles to the soil matrix can greatly enhance immobilization of As by transferring water leachable As from the soil onto the nanoparticles. The nanoparticle associated As will be immobilized as the nanoparticles are trapped/incorporated in the soil matrix through the well-known filtration effects. Based on prior spectroscopic studies (An et al., 2011b; Jain et al., 1999), the enhanced As immobilization by the nanoparticles is attributed to the formation of strong surface complexes Fe-O-As between As(V) and the nanoparticles.

The TCLP approach has been commonly used to quantify the leachability of As in solid wastes under simulated landfill conditions (Ghosh et al., 2004). The effect of the nanoparticle amendment on the TCLP-based leachability of As in the soil was determined through TCLP tests. **Figure 3-3** compares the soluble As concentration in the TCLP fluid for the untreated and nanoparticle-treated soil samples. The nanoparticle amendment was able to reduce soluble As from 240 μg/L for the untreated soil to 46 μg/L, a reduction of ~81%. Apparently, the nanoparticle treatment may also be applied to As-laden solid and hazardous waste to convert a hazardous waste to a non-hazardous waste.

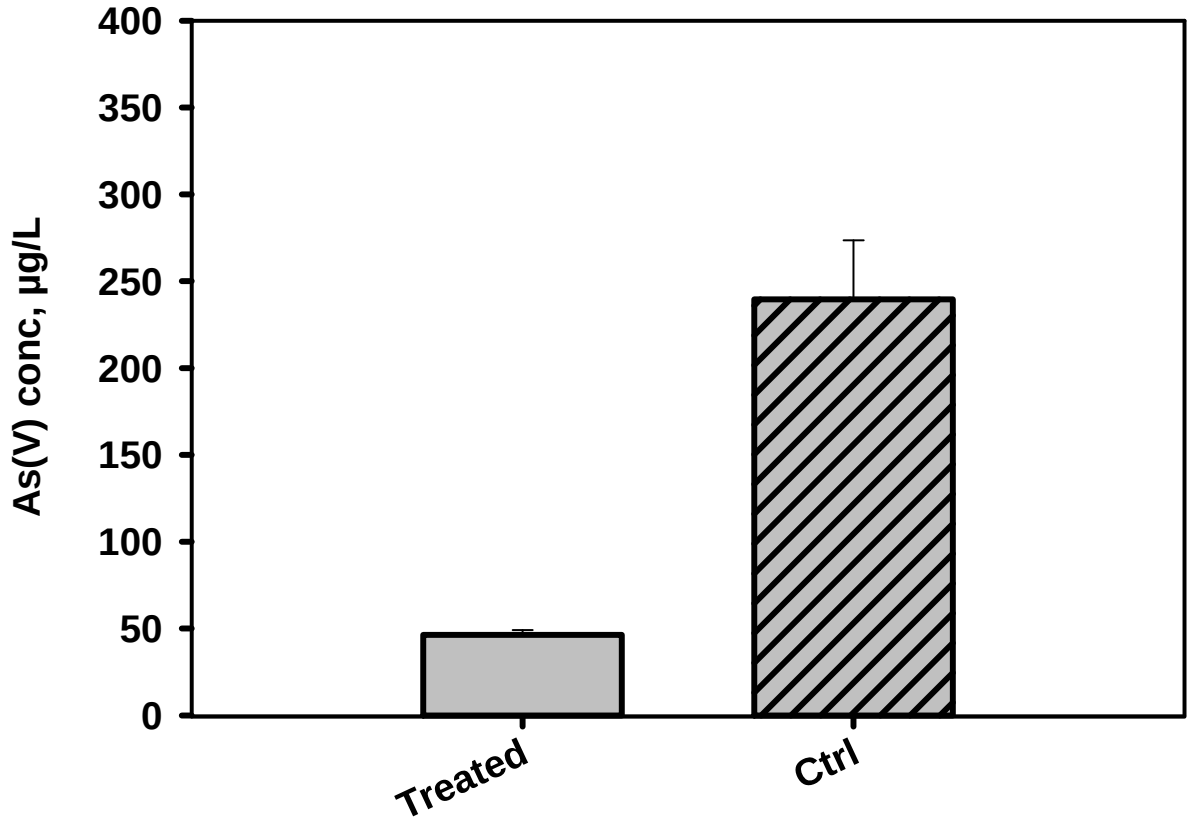

Figure 3-3. Arsenic concentrations in TCLP fluid #1 for As-laden sandy soil amended by stabilized Fe_3O_4 nanoparticles (0.1 g Fe/L with 0.04 wt. % starch) with comparison to that for As-laden soil without treatment.

3.3.2 Transport of starch-stabilized magnetite Fe_3O_4 nanoparticles in the sandy soil

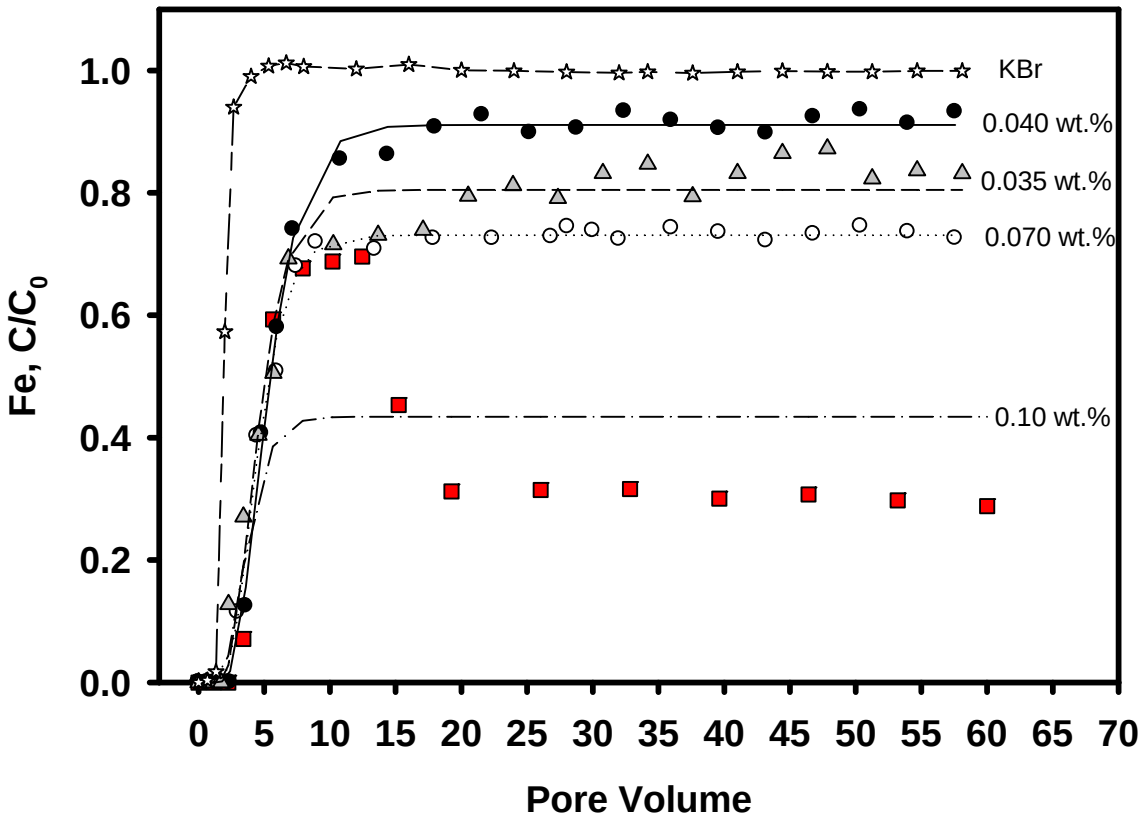

Figure 3-4. Breakthrough curves of a tracer (bromide) and Fe_3O_4 nanoparticles prepared at various concentrations of starch through a sandy loam soil bed. Experimental conditions: Influent Br^- = 50 mg/L, Fe_3O_4 = 0.1 g/L as Fe, empty bed contact time (EBCT) = 103 min, pore flow velocity = 0.001273 cm/s. Symbols: Experimental data; lines: CXTFIT model simulations.

For *in situ* immobilization of arsenic in soil and groundwater, the nanoparticles must meet some fundamental attributes: 1) they must be deliverable into the contaminated zones under external hydraulic gradient (i.e., must be mobile in soil under moderate external pressure), and 2) once the external pressure is removed, the delivered nanoparticles ought to remain within a confined domain (i.e., under natural groundwater conditions, the delivered nanoparticles will serve as a immobile sink for capturing soluble As).

Figure 3-4 shows the breakthrough curves of a tracer (bromide) and the starch-stabilized magnetite nanoparticles through a sandy soil bed. The hydrodynamic dispersion coefficient (D) was obtained by fitting the classic 1-D convection-dispersion equation to the experimental breakthrough data of the non-reactive tracer using the CXTFIT code (STANMOD software, USDA). The resultant D value was then applied to modeling the breakthrough curves of the nanoparticles at various starch concentrations. In all cases, the effluent Fe concentration reached a plateau after ~15 PVs, whereas full breakthrough occurred at ~3 PVs for the tracer ($C/C_0 = 0.5$ occurred at PVs = 1.5). Nanoparticles prepared at various starch concentrations displayed different levels of the breakthrough plateaus (C/C_0), with the nanoparticles stabilized at 0.04 wt% starch appearing most transportable (C/C_0=0.91). At a starch level of 0.035 wt%, more nanoparticles were removed by the soil bed ($C/C_0 = 0.80$). On the other hand, increasing the stabilizer concentration to 0.07 wt%, the level of C/C_0 was lowered to 0.73; Further increasing the starch concentration to 0.10 wt% resulted in a greatly distorted breakthrough profile. The full breakthrough C/C_0 rose to ~0.68 before 13 BVs, then dropped to a steady level of ~0.3 after 15 BVs.

Based on the classical filtration theory (Kretzschmar et al., 1999), filtration removal of fine particles in porous media involves two consecutive steps: (i) mass transfer of particles to the

matrix surfaces by Brownian diffusion, interception, and/or gravitational sedimentation, and (Ghosh et al., 2004) (ii) deposition of particles to the matrix surface (the collector). The physical properties of the particles and the collectors can affect the mass transfer of the particles. Particle size, liquid viscosity, media pore size and surface potential can affect mass transfer and particle-collector interactions. For examples, smaller particles tend to have faster diffusion, but slower sedimentation rate. Suspensions of higher viscosity tend to slow down the mass transfer process and may cause clogging of the soil pores, resulting in contrasting effects on the overall particle deposition. Although the particle prepared with 0.1 wt.% of starch resulted in smallest particle size, the gaining of faster mass transfer rate diminished by high viscosity and soil plugging.

Our previous study confirmed that higher starch concentrations resulted in smaller nanoparticles with larger specific surface area (Liang et al., 2012b). At 1 h of particle aging, the hydrodynamic diameter was measured to be 206, 172, 153, and 129 nm, respectively, for particles stabilized with 0.035, 0.04, 0.07, and 0.10 wt% of starch. The viscosity was measured to be 1.057, 1.063, 1.075 and 1.086 cP for the suspensions of 0.035, 0.04, 0.07 and 0.1 wt% of starch, respectively. It was also determined that the critical stabilization concentration (CSC, defined as the minimum concentration of starch for complete stabilization of the nanoparticles) for 0.1 g/L as Fe of the nanoparticles is 0.04 wt%. Because 0.035 wt% of starch was not enough to fully stabilize the nanoparticles, more of the particles were removed by the soil. The increased removal of the particles prepared at elevated starch concentrations (0.07 and 0.10 wt%) can be attributed to: 1) elevated starch concentrations tend to clog the soil pores, resulting in more straining of the particles; and 2) smaller particles can reach more collector surfaces, especially those not accessible by larger particles, favoring more deposition of the particles (He et al., 2009).

In addition, the surface potential can also affect transport of the nanoparticles. For bare magnetite particles, the pH at point of zero charge (PZC) was measured to be ~6.1 (Liang et al., 2012b). The starch coating greatly suppressed the sensitivity of the ζ potential to the potential-determining ions (H^+/OH^-). For instance, between pH 5 and 8, the ζ potential varied from +20 to -40 mV for the bare particles; when the nanoparticles were stabilized with 0.04 wt.% of the starch, the ζ-potential was narrowed down to a range of -0.69 to -15.7 mV. On the other hand, the PZC of the sandy soil was determined to be 6.1, and thus, the collector surfaces are negatively charged at the experimental pH of 6.8. Consequently, nanoparticles stabilized with lower starch would undergo greater electrostatic repulsive forces among the nanoparticles and between the nanoparticles and collector surfaces.

The software STANMOD, a Windows-based computer software package for evaluating solute transport in soils and groundwater, has been often employed to simulate solute transport in soil (Feinstein and Guo, 2004). The software package includes a modified and updated version of the **CXTFIT** code for estimating solute transport parameters using a nonlinear least-squares parameter optimization method. The one-dimensional equilibrium advection-dispersion equation is given by:

$$R\frac{\partial C}{\partial t} = D\frac{\partial^2 C}{\partial x^2} - v\frac{\partial C}{\partial x} \qquad \text{(Eq. 2)}$$

where C is the solution concentration, x is distance, t is time, D is the dispersion coefficient, v is the average pore water velocity, and R is the retardation factor, defined as:

$$R = 1 + \frac{\rho K}{\theta} \qquad \text{(Eq. 3)}$$

where ρ is the soil bulk density, K is an empirical distribution constant, θ is the volumetric water content.

The computer code was used to solve the governing transport equation and to simulate the breakthrough curves of starch-stabilized Fe_3O_4 nanoparticles at various starch concentrations.

Figure 3-5 shows the spatial distribution of the nanoparticles that were retained in the soil column following the As immobilization column run. The As distribution profile mimics that of colloids retention in a typical filtration process (Chen et al., 2001; Tufenkji and Elimelech, 2004). A concentration peak of the nanoparticles was observed on the top layer of the soil column, and nanoparticle retention was evident throughout the column. A gel-like layer was observed in all cases on top of the soil bed. Similar nanoparticles deposition phenomenon was also reported by other researchers (Adler et al., 2001; Liu et al., 2009). There is slight difference (~9%) between the concentration of nanoparticle in the effluent and influent. Such gel-like layer is postulated to be mostly nanoparticles, a result of increase in surface related attraction (Liu et al., 2009) and, which would then contribute to lower concentration of nanoparticles in the effluent, as compared to that in the influent (He et al., 2009).

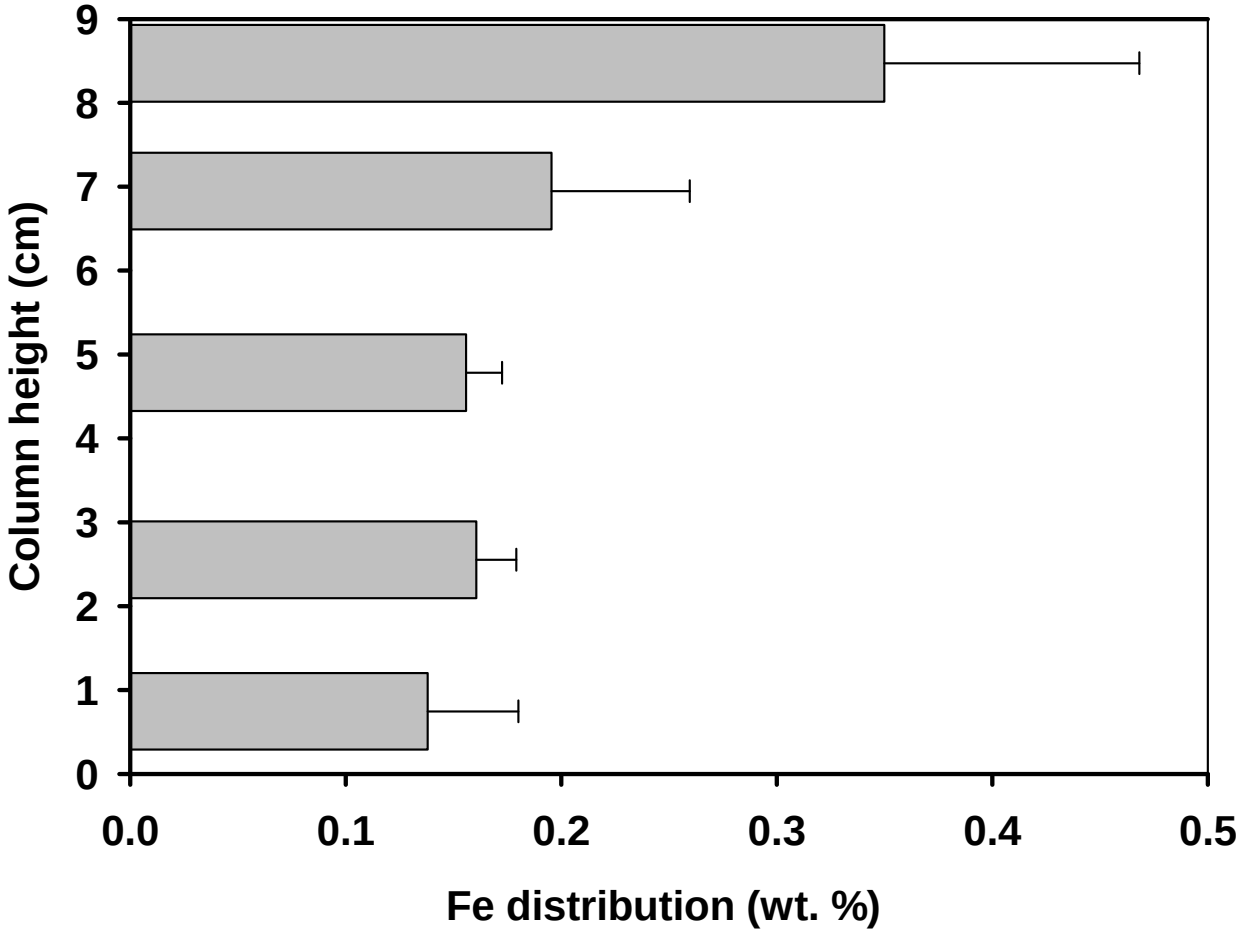

Figure 3-5. Spatial distribution of soil retained magnetite nanoparticles (measured as total Fe, wt.% of the total amount of Fe) that are retained as a function of column height (cm). The stabilized Fe_3O_4 nanoparticle suspension was introduced through the column in the down flow mode, i.e., from 9 cm to 0 cm in the plot. Data plotted as mean of duplicates, and error bars refer to deviation from the mean.

3.3.3 Immobilization of As(V) in soil: column tests

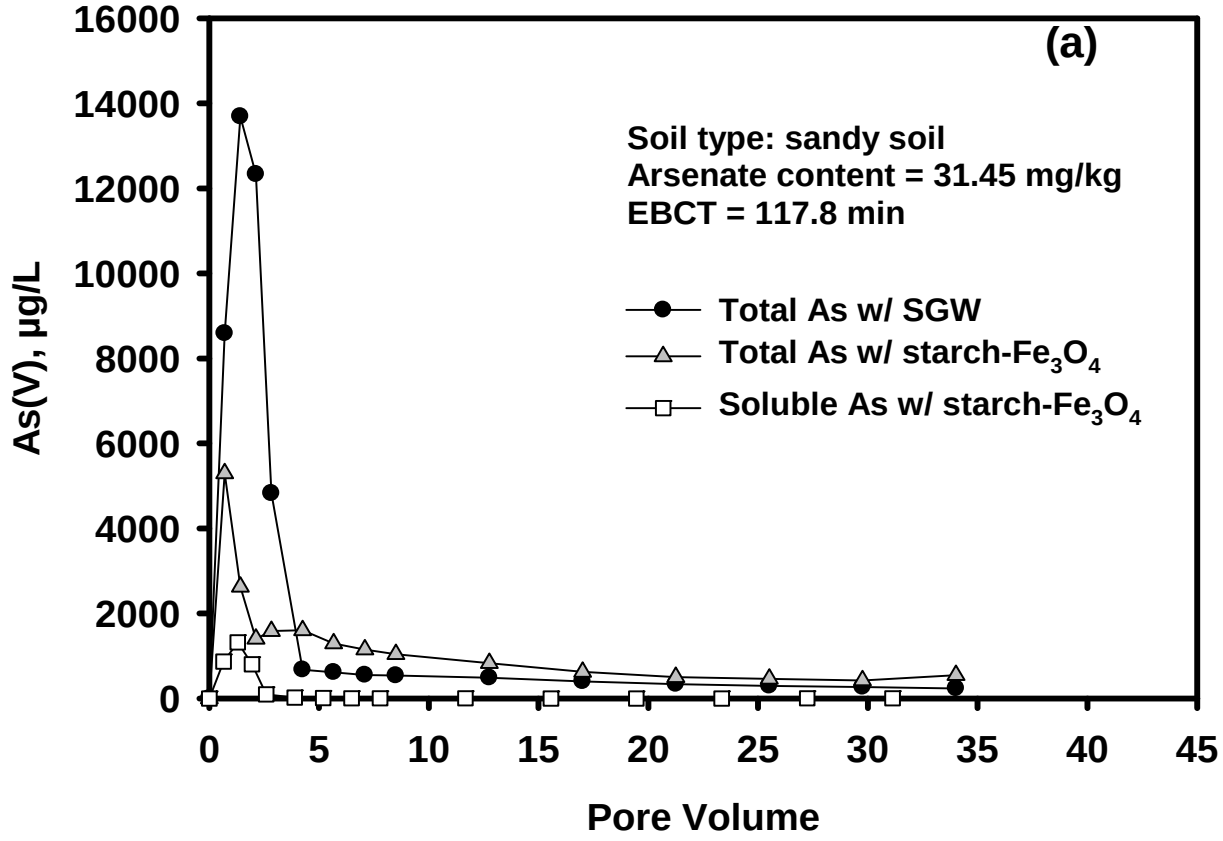

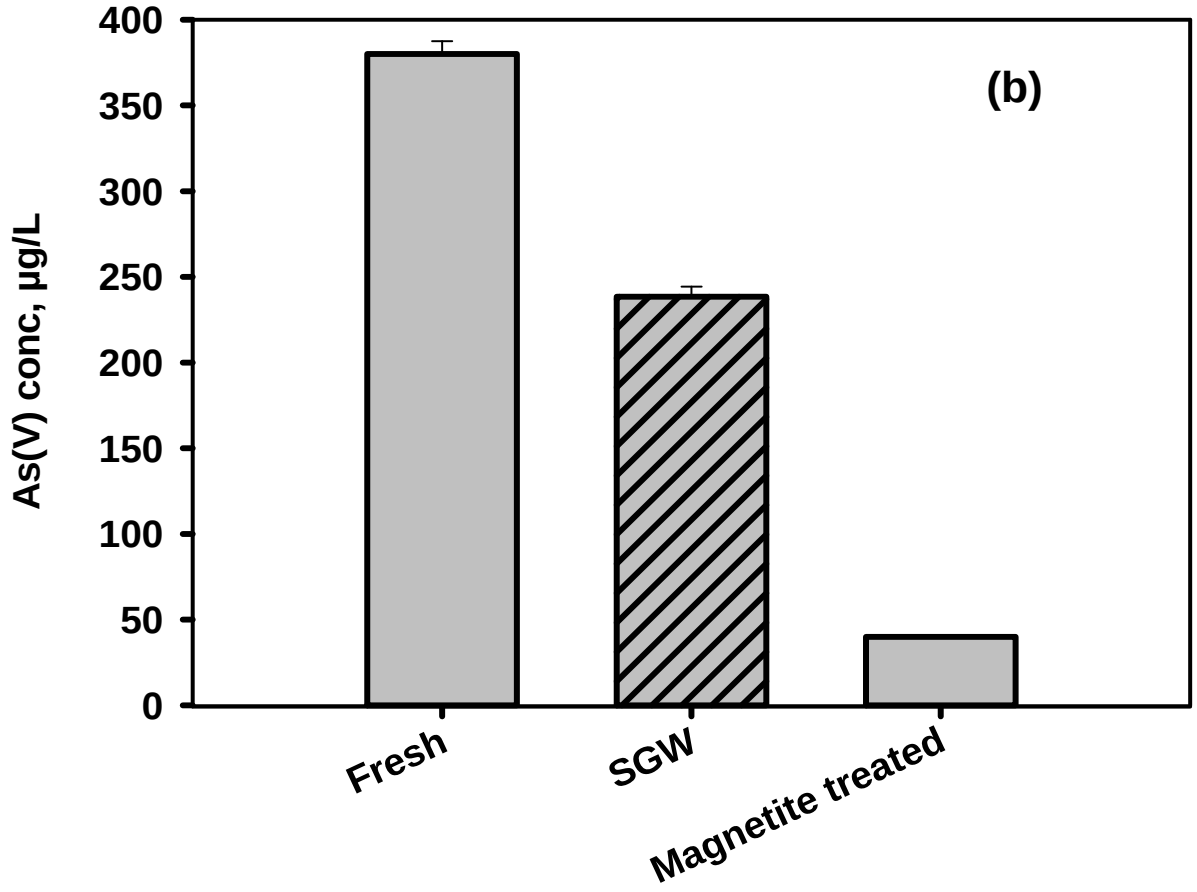

Figure 3-6. (a) Arsenic elution histories from an As(V)-laden sandy loam soil column when subjected to a starch stabilized Fe_3O_4 nanoparticle suspension or a simulated ground water (SGW). Nanoparticle suspension: Fe_3O_4 = 0.1 g/L as Fe, starch = 0.04 wt%. SGW: NaCl = 7 mM, $CaSO_4$ = 0.86 mM. And **(b)** arsenate concentrations in TCLP fluid #1 when virgin As-spiked soil and the nanoparticle amended soil samples from **(a)** were subjected to TCLP tests.

The effectiveness of the starch-stabilized Fe_3O_4 nanoparticles was tested for in-situ immobilization of As(V) in the sandy soil through fixed-bed column experiments. **Figure 3-6a** shows the arsenate elution histories during two parallel column runs: one with SGW (simulated groundwater) and the other with the starch-stabilized Fe_3O_4 nanoparticle suspension under otherwise identical conditions. In both cases, the elution curves displayed an immediate peaking during the first 5 PVs followed by a gradual tailing profile. Based on mass balance, SGW eluted 27% of As pre-loaded in the soil while the nanoparticle suspension leached 20% during the 34 PVs of elution. Further examination of the effluent nanoparticle suspension revealed that 93% of the eluted As was associated with the nanoparticles, while all As eluted by SGW was soluble. After ~5 PVs of the nanoparticle treatment, the soluble As(V) concentration reached a steady level of <5 μg/L, while As in the SGW effluent remained at ~450 μg/L. The nanoparticle treatment reduced the peak soluble As concentration by 90% from 13.7 mg/L to 1.32 mg/L, and the peak total As concentration by 61% from 13.7 mg/L to 5.3 mg/L.

It has been known that the key soil components that can bind with arsenate through specific interactions (e.g., Lewis acid-base interaction) are hydrous oxides of some transition metals such as Fe, Al and Cu (Wenzel et al., 2001). Based on the soil analysis data (**Table 3-1**), the soil contains 22 ppm of Al and 5 ppm of Fe, while other transition metals are ≤2 ppm. Noting that not all of the metal sites are necessarily accessible by arsenate, the relatively low contents of the transition metals in the soil may account for the fairly high water leachability (27%) of As. According to Wenzel et al. (2001), the most labile As sorbed in a soil refers to the so-called exchangeable fraction (i.e., As sorbed through non-specific Columbic forces or outer sphere complexation). Noting that the SGW contains 7 mM of NaCl and 0.86 mM of $CaSO_4$ and that SO_4^{2-} offers greater affinity than non-specifically sorbed $H_2AsO_4^-$ or $HAsO_4^{2-}$ (An et al., 2005),

the high elution peak of As by SGW can be attributed to sulfate exchange for the arsenate species.

During the 34 PVs of column run, ~9% of the nanoparticles were retained in the soil bed due to the filtration effect. The added Fe content to the soil increases the sorption capacity and affinity for arsenate, which can be easily revealed by the much greater K_d value for the nanoparticles (55.2 L/kg) than that for the soil (5.93 L/kg). It should be noted that while the exchangeable fraction of As in the soil was leached out in both cases, the leached As is firmly associated with the effluent nanoparticles when the nanoparticles were applied. As to be illustrated in Section 3.4, the nanoparticle associated As will be eventually immobilized as the nanoparticles become immobile in the soil upon relaxing of the injection pressure.

TCLP tests were performed to probe the leachability of the residual As in the soil beds following the column elution tests in **Figure 3-6a**. **Figure 3-6b** compares the leached As concentration in the TCLP solutions for the soil samples subjected to the SGW or nanoparticle elution tests. For comparison, untreated As-laden soil samples were also tested. To facilitate a fair comparison, the weight of the soil samples was adjusted to ensure that the As mass in the TCLP tests was the same in all cases while maintaining the solid to liquid ratio of 1g to 20 mL as prescribed by the test procedure. The results indicated that the TCLP leachability in the nanoparticle treated soil was more than 83% lower than that for the SGW eluted soil, and more than 90% lower than for the virgin As-laden soil. **Figures 3-6a** and **6b** indicate that the nanoparticle amendment can not only reduce the soluble As concentration in the downstream groundwater, but also reduce the leachability of the remaining As(V) in the soil phase.

3.3.4 Effective transport distance of Fe_3O_4 nanoparticle

It is evident from the nanoparticle breakthrough curves (**Figure 3-4**) and column soil treatment data (**Figure 3-6a**) that the starch stabilized nanoparticles can be delivered to the As contaminated soil under external pressure (i.e., at an elevated pore flow velocity). **Figure 3-6a** shows that under the experimental flow conditions, ~91% of the nanoparticles broke through the soil bed and 93% of As eluted was associated with the nanoparticles. From the standpoint of As immobilization, two critical questions must be addressed: 1) How far will the nanoparticles travel under the external injection hydraulic gradient (i.e., what is the effective distance of the nanoparticles?) And 2) Will the delivered nanoparticles be mobile after the external pressure is released, and if so, how far can the nanoparticles (and the associated arsenic) transport under natural groundwater flow conditions?

To address these issues, transport modeling based on the filtration theory and detailed experimental breakthrough studies of the starch stabilized nanoparticles under various pore flow velocities were carried out. **Figure 3-7** shows breakthrough histories of the nanoparticles that had broken through the sandy soil bed after one column run (tell which column run and under what conditions). To test the effects of pore velocity, which correspond to the pumping pressure, the breakthrough tests were performed at broad range of pore flow velocities from 3.5×10^{-3} cm/s to 2.2×10^{-4} cm/s. The pore velocities were chosen to simulate the pore velocities during injection/delivery of the nanoparticles and after the injection pressure is released (i.e., at representative natural groundwater flow velocity). **Figure 3-7** indicates that pore velocity strongly impacts the mobility, or soil retention, of the nanoparticles in the soil. At the injection pore velocity of 3.5×10^{-3} cm/s, the nanoparticles were readily deliverable with a full breakthrough C/C_0 of ~0.91. Halving the pore velocity from 3.5×10^{-3} to 1.8×10^{-3} cm/s decreased

the full breakthrough C/C_0 from 0.91 to 0.80. Further decreasing the pore velocity to 3.5×10^{-4} cm/s decreased the full breakthrough C/C_0 to 0.51. When the flow rate was reduced to a groundwater flow velocity (2.2×10^{-4} cm/s), the nanoparticles became virtually immobile ($C/C_0 \approx 0$). Similar velocity effects have been observed on CMC-stabilized ZVI nanoparticles (He et al., 2009) and fullerene and oxide nanoparticles (Lecoanet and Wiesner, 2004) in porous media.

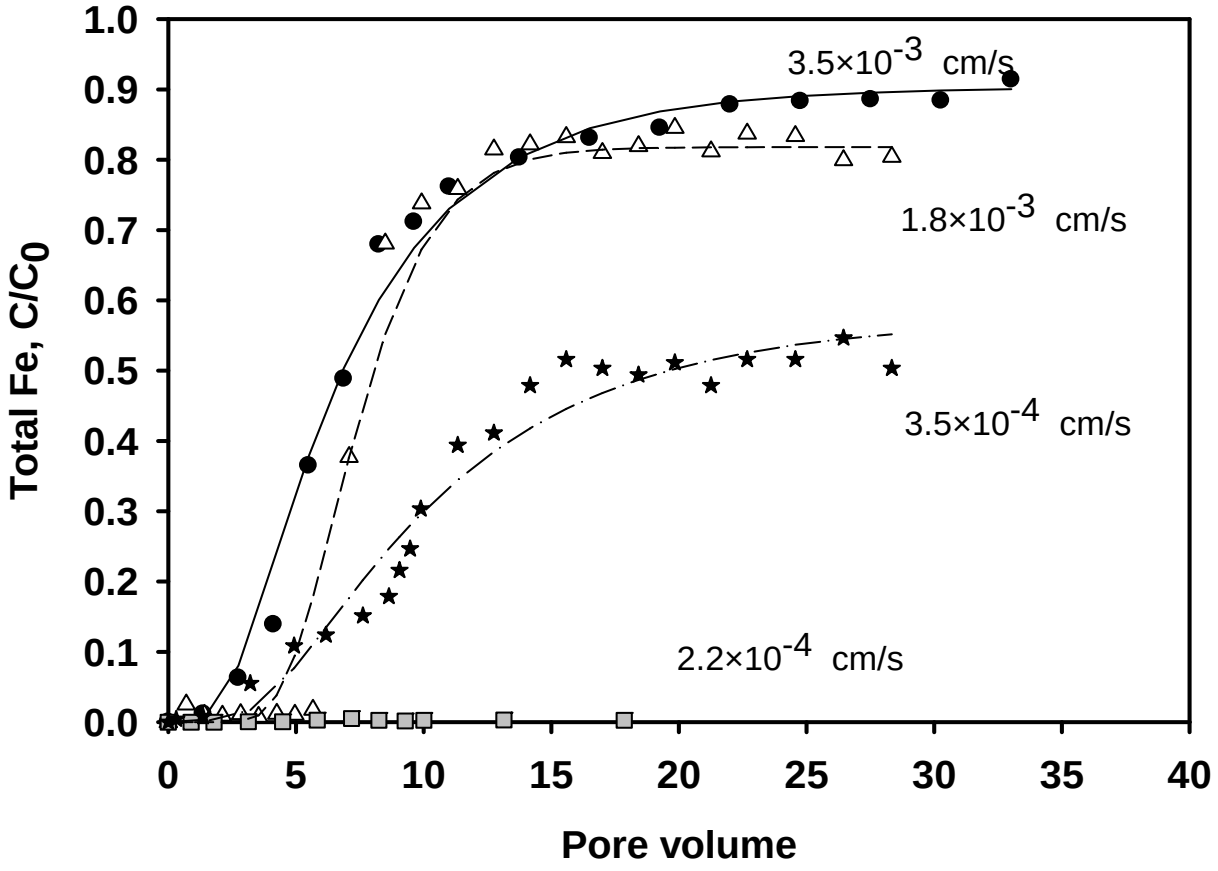

Figure 3-7. Breakthrough histories of starch stabilized magnetite nanoparticles through a clean sandy loam soil bed at various pore velocities (3.5×10^{-3}, 1.8×10^{-3}, 3.5×10^{-4}, and 2.2×10^{-4} cm/s). The influent Fe_3O_4 nanoparticle suspension was collected following parallel column runs as shown in Figure 3-6a, where Fe_3O_4 = 0.1 as g/L Fe, starch = 0.04 wt%.

The deposition and transport of the nanoparticles can be modeled in accord with the classical filtration theory. In this work, the modeling protocol by (He et al., 2009) was adopted to calculate the maximum travel distance of the nanoparticles as a function of the pore flow velocity:

$$L_{max} = -\frac{2}{3}\frac{d_c}{(1-f)\alpha\eta_0}\ln(0.01) \quad (4)$$

where L_{max} is defined as the maximum travel distance over which 99% removal of the nanoparticles occurs, d_c is the collector grain diameter, f is the bed porosity, α is the attachment efficiency representing the fraction of collisions between particles and collectors that result in attachment, η_0 is the overall single collector removal efficiency. The attachment efficiency α, representing the fraction of collisions between particles and collectors that result in attachment, is then calculated via

$$\alpha = \frac{\eta}{\eta_0} = -\frac{2}{3}\frac{d_c}{(1-f)L\eta_0}\ln\left(\frac{C}{C_0}\right) \quad (5)$$

where L is the length of the porous medium bed (m), $\frac{C}{C_0}$ is the column outlet normalized particle concentration at the initial stage of the particle breakthrough curve. The overall single collector removal efficiency can be expressed as a function of four dimensionless groups (Tufenkji and Elimelech, 2004).

$$\eta_0 = \eta_0(N_R, N_{Pe}, N_{vdW}, N_{gr})$$

where N_R is an aspect ratio, N_{Pe} is the Peclet number, N_{vdW} is the van de Waals number, and N_{gr} is the gravitational number. Based on the simulation, the maximum travel distance is plotted as a function of pore velocity. Considering a high groundwater flow velocity of 10 feet per day (v=3.5×10^{-3} cm/s) (i.e., in sandy or gravelly aquifers) and a low velocity of 0.62 foot per day (v=2.4×10^{-4} cm/s) (Alley, 1999), the estimated L_{max} ranges from 4.5 m to 6.1 cm (**Table 3-2**).

Table 3-2. Experimental conditions and model parameters for simulating the breakthrough curves of the starch stabilized magnetite nanoparticles.

Porous media	Flow rate (mL/min)	Pore velocity (cm/s)	C/C_0	η_D	$\eta_I \times 10^{-5}$	$\eta_G \times 10^{-5}$	η_0	α
Sandy soil	0.0038	2.24×10^{-4}	0	0.025	12.5	52.1	0.0259	6.46
	0.006	3.54×10^{-4}	0.51	0.018	11.9	31.4	0.0187	0.63
	0.03	1.77×10^{-3}	0.8	0.0058	9.69	5.26	0.0059	0.05
	0.06	3.54×10^{-3}	0.91	0.0035	8.89	2.44	0.0036	0.09

Note:

C/C_0 is the column outlet normalized particle concentration at the initial stage of the particle breakthrough curve.

η_D is single-collector contact efficiency for transport by diffusion.

η_I is single-collector contact efficiency for transport by interception.

η_0 is overall single-collector contact efficiency.

α is attachment efficiency.

Figure 3-7 indicates that for *in situ* remediation uses, the effective area or particle travel distance can be manipulated by controlling the injection flow rate. The delivered injected nanoparticles will remain within a confined soil domain under typical groundwater flow conditions.

3.4 Conclusions

To our knowledge, this has been the first study on the effectiveness of starch stabilized for in tiu immobilization of arsenic in soil and the transport behavior of the nanoparticles. The key findings are summarized as follows:

(1) Batch tests showed that the stabilized Fe_3O_4 nanoparticles were highly effective to immobilize As in a sandy loam. When the arsenic laden soil was treated with 0.1 g-Fe/L of starch-stabilized nanoparticles at a soil to suspension ratio of 0.1, the water soluble As concentration was reduced by ~98% and the TCLP leachability of As was reduced by 80%. The As distribution coefficients for nanoparticles was calculated to be 9999.5 L/g (SLR = 0.1) and 96798 L/g (SLR = 0.4), which are >5 orders of magnitude than for the sandy soil.

(2) Column breakthrough studies confirmed that the stabilized nanoparticles are deliverable in the model soil under moderate external pressure. However, the particle transport was found strongly affected by the concentration of the starch stabilizer. For the 0.1 g-Fe/L nanoparticle suspension, a starch concentration of 0.04 wt% gives the greatest mobility with a full breakthrough C/C_0 of 0.91. A lower starch concentration resulted in partial aggregation of the nanoparticles, whereas elevated concentrations of starch renders the suspension more viscous and partial clogging go the soil pores, all diminishing soil transportability of the nanoparticles.

(3) Column tests revealed that the stabilized nanoparticles were effective for in situ immobilization of As(V) in the model soil. When an As-laden soil bed was treated with 34 PVs

of the 0.1g-Fe/L nanoparticle suspension, 20% of the 31.45 mg/kg As(V) initially spiked on the soil containing was eluted, compared to 27% when the same soil was subjected to a simulated groundwater elution. In nanoparticle eluted effluent, 93% of the eluted As was associated with the nanoparticles, i.e., the nanoparticle treatment reduced the soluble As in the effluent by 93%. Upon the nanoparticle treatment, the peak soluble As concentration was decreased by 90% from 13.7 mg/L to 1.32 mg/L.

(4) The effective travel distance of the stabilized Fe_3O_4 nanoparticles can be manipulated by controlling the injection flow rate. Once delivered, the nanoparticles will remain within a confined distance under typical groundwater conditions, serving as a fixed sink for immobilizing of soluble arsenic in groundwater.

Chapter 4. Immobilization of Arsenic on Poultry Litter by Polysaccharide-Coated Magnetite and Fe-Mn Binary Nanoparticles

In the previous two chapters, it has been demonstrated that magnetite nanoparticles were effective in removal of As from water and contaminated sandy soil. In this study, a new class of Fe-Mn nanoparticles and magnetite nanoparticles would be tested to mitigate the environmental impacts of poultry litter, including the effectiveness of nanoparticles for reducing leachabilities of As, assessment of the environmental fate and impact of the nanoparticles and investigation of the effects of nanoparticles on the performances of poultry litter as a fertilizer.

4.1 Introduction

The U.S. broiler industry produces about 8.9 billion birds each year (USDA, 2007), resulting in tremendous amounts of poultry litter (PL). For example, Alabama is the third largest broiler producing state in the U.S., and produced 1 billion birds in 2007 (USDA, 2008a), generated more than 1 billion kg of litter annually, of which 90% is disposed of through land application (Jackson et al., 2003).

Since the 1970s, the poultry industry has been using As-based ingredients (typically roxarsone or 3-nitro-4-hydroxyphenylarsonic acid) as chicken feed additives to control intestinal parasites and promote growth (Garbarino et al., 2003). In the U.S., ~70% of broiler chickens are fed with roxarsone, totaling between 1.7 and 2.2 million pounds of the drug added to poultry feed per year (Wallinga, 2006), and resulting in about 900 metric tons of roxarsone released annually into the environment in the U.S. (Cortinas et al., 2006). Our preliminary data indicate

that poultry litter from various Alabama sources and a commercial product contained total As up to 26 mg/kg of litter with the presence of As (III), As (V), and roxarsone. Although the use of arsenical feed additives was banned in Europe in 1998, the arsenical feed additives are presently approved for use in United States poultry feeds with approved usage levels and indications (Nachman et al., 2005). The Institute of Agriculture and Trade Policy reported that detectable levels of arsenic were found in a variety of raw and prepared poultry products (Wallinga, 2006). While a fraction of the feed roxarsone remains in chicken tissue, the majority of the drug has been demonstrated to be excreted in the waste (Rutherford et al., 2003a).

Typically, PL as an effective fertilizer is repeatedly and intensely applied or disposed of on local farmland. The side effect, however, is that a substantial amount of As is introduced into the environment (up to 250 g/ha with every application) (Garbarino et al., 2003). Recently, Cortinas et al. (Cortinas et al., 2006) reported that upon land disposal of poultry litter, roxarsone can be bio-transformed to highly soluble carcinogenic arsenite, and leach into groundwater and surface waters, and taken up by crops (Bellows, 2005). Rutherford et al. (Rutherford et al., 2003b) claimed that 75% of As in poultry litter is water-soluble. Recent work also confirmed that the majority of arsenic in PL is rapidly converted into more leachable inorganic forms during composting or storage through both biotic and abiotic processes (Garbarino et al., 2003).

Arsenic in drinking water has become an extremely sensitive issue since EPA mandated water utilities to lower the maximum contaminant level (MCL) from 50 ppb to 10 ppb effective in January 2006. Since PL can be a significant source of carcinogenic As (Cortinas et al., 2006; Schaefer, 2007) and disposal of As-laden PL has been under close scrutinization. For instance, in Alabama, special permits are required for poultry farmers to dispose of waste PL, and as a result, many farmers yielded their PL to specialty companies that collect, process and sell the PL.

To mitigate the environmental impacts of land application of PL, various PL treatment practices have been studied, including amendment of PL with alum, sodium bisulfate (PLT), ferrous sulfate (Blake and Hess, 2001; Shah et al., 2006), and zeolite (Li et al., 2006). Because water soluble As species are considered bioavailable, controlling contaminant (N, P and As) leachability from PL has been the key strategy. For instance, sodium bisulfate, ferrous sulfate and aluminum sulfate have been found effective to reduce ammonia emission and lower P (and possibly As) in runoff from land fertilized with litter (Blake, 2001a; 2001b; Huff et al., 1984). However, because of the high solubility of these chemicals, costly-high dosages (>2.5%) are often required and the effectiveness lasts only for 3-4 weeks (Huff et al., 1984).

In situ immobilization of environmentally important contaminants in soils or solid/hazardous wastes is an emerging and promising technology (An et al., 2011b; Liu and Zhao, 2007; Xu and Zhao, 2007). To facilitate effective removal/immobilization of arsenic in water and soil, our group developed a new class of polysaccharide-modified magnetite (An et al., 2011b; Liang et al., 2012b) and Fe-Mn binary oxide nanoparticles (An and Zhao, 2011). The starch stabilized magnetite nanoparticles offered a 2.2 times greater As(V) uptake than bare particles (based on the Langmuir capacity coefficient), while CMC (Carboxymethyl Cellulose) stabilized Fe-Mn binary nanoparticles provided 2.4 times greater As(V) and As(III) sorption capacities than those reported for other Fe-Mn products. Further increasing the starch or CMC concentration resulted in fully stabilized/dispersed nanoparticles, which can be potentially used for *in situ* immobilization of As in contaminated soil and sediment. Our previous research indicated that amending As-laden soil with the Fe-Mn nanoparticles reduced leachable arsenic by more than 90%. The overall goal of this study was to preliminarily test the effectiveness of polysaccharide modified magnetite and Fe-Mn binary oxide particles for reducing arsenic

leachability from PL. the specific objectives were to: (1) Prepare starch or CMC modified magnetite and Fe-Mn binary oxide particles that are most suitable for immobilization of As in PL; (2) Test the effectiveness of the modified particles for reducing leachability of As in the PL through bench-scale batch and column experiments; and 3) Examine the effects of pH and polymer modifiers on the treatment effectiveness.

4.2 Materials and Methods

4.2.1 Chemicals

CMC (sodium salt, molecular weight = 90000), a water soluble potato starch (hydrolyzed for electrophoresis), and ferrous sulfate heptahydrate ($FeSO_4 \cdot 7H_2O$) were obtained from Acros Organics (Pittsburgh, PA, USA). Sodium arsenate heptahydrate ($Na_2HAsO_4 \cdot 7H_2O$) was purchased from Sigma Aldrich (St. Louis, MO, USA). Ferric chloride ($FeCl_3$) and sodium hydroxide (NaOH) were obtained from Fisher Scientific (Pittsburgh, PA, USA). Hydrochloric acid and nitric acid were purchased from Mallinckrodt Chemical (St. Louis, MO, USA). The PL sample with the trade mark Black Hen was a processed fertilizer purchased from a local store Lowes (Opelika, AL).

4.2.2 Preparation of starch or CMC modified magnetite and Fe-Mn binary oxides

All solutions were prepared using Milli-Q (18.2 megaohm-cm resistivity) deionized (DI) water deoxygenated by sparging with N_2 gas. The modified magnetite nanoparticles were prepared following the aqueous-phase coprecipitation of ferrous-ferric ions by a base with starch as a stabilizer preventing particle aggregation (Liang et al., 2012b). In brief, in a 250 mL flask and at room temperature, 10 mL of an $FeSO_4 \cdot 7H_2O$ stock solution and 10 mL of an $FeCl_3$ stock solution were added to 100 mL of a stabilizer solution to yield a desired concentration of Fe^{2+}-Fe^{3+} (kept at an Fe^{2+}:Fe^{3+} molar ratio of 1:2) and starch (or CMC). The mixture was then purged

with N_2 and under magnetic stirring for 15 min to ensure complete mixing and formation of the Fe^{2+}-Fe^{3+}- stabilizer complexes. The desired magnetite nanoparticles were then formed through co-precipitating Fe^{2+}-Fe^{3+} as Fe_3O_4 by adding 4 mL of a 5 N sodium hydroxide solution (introduced at one shot) under N_2 purging. The mixture was subsequently sealed and aged for 24 hours without exposure to air. Then the suspension pH was lowered to pH 7 using 0.1 M hydrochloric acid.

The CMC modified Fe-Mn binary oxide nanoparticles were prepared following the approach described in An et al., 2011's work (An and Zhao, 2011). In brief, 10 mL of an ferrous stock solution was added to a stabilizer solution (22 mL of 1 wt% CMC or 33 mL of 1% of starch) to achieve a final concentration for 0.19 g/L as Fe. Then 10 mL of a $KMnO_4$ stock solution was added at an Fe:Mn molar ratio of 3:1 to the Fe^{2+}-stabilizer solutions under vigorous mixing. Finally, the pH of resultant suspensions was adjusted to 7~8, and the suspensions were allowed to age under shaking 200 rpm for 1 hour before use.

4.2.3 Preparation and analysis of poultry litter samples

The commercial PL sample (Black Hen) was first air-dried, sieved through a 2-mm screen and used in the experiments without further processing. All litter extractions were performed on the less than 2-mm size fraction to ensure a homogeneous sample medium and to facilitate comparison in column tests.

The litter samples were sent to the Laboratory for Environmental Analysis of University of Georgia for determining the total arsenic concentration and arsenic speciation. The elemental analysis of the Black Hen PL was determined by microwave-heated EPA method 3050B. Microwave heating was employed to digest the PL samples, which is superior to the conventional hot plate heating for enhanced reaction control and thus improved precision

(Lorentzen and Kingston, 1996). Briefly, PL samples (0.5 g each) were digested in sealed Teflon containers in a microwave with 1 mL H_2O_2 followed by 5 mL of nitric acid and taken up with water after digestion. Elemental analysis was then carried out with an inductively coupled plasma-mass spectrometry (Perkin-Elmer Elan 6000 ICP-MS) for As, Pb, P, C, N and S. The detection limit of the ICP-MS system was 0.4 μg/L for As.

The soluble arsenic species in the raw PL samples were determined using an ion chromatography (IC) ─ ICP-MS system. The arsenic species were separated by gradient elution in a 2% methanol mobile phase. Two grams of each litter sample were shaken with 20 mL of 2% methanol in water for 2 hours, centrifuged at 2200 rpm for 30 minutes. The aqueous phase was then decanted and subjected to the IC-ICP/MS analysis.

4.2.4. Water and acid leachable As in PL

Water leachable As in the PL was determined through extraction tests by mixing air-dried PL with DI water at a constant solid-to-water ratio of 2 g of PL to 200 mL of DI water in 250 mL glass flasks. The PL and water mixtures were then placed on a platform shaker operated at 200 rpm. The mixtures were then sampled at pre-determined time intervals, filtered with 0.025 μm to separate colloids, and analyzed the filtrates for water leachable arsenic using a Perkin Elmer Graphite Atomic Absorption Spectrometer 3110 (equipped with an HGA 600 and EDL system 2).

Acid leachable or total As on the PL samples was determined per EPA method 3050B. Briefly, a 0.2-g each of a litter sample was treated with concentrated HNO_3 and heated on a hot plate at 95±5ºC, refill the concentrated HNO_3 until no more brown fume was generated (~3 hours). After cooling down, 10 mL of a 30% H_2O_2 solution was added to the residual aliquots. The mixture was continually heated at 95±5 ºC for two hours to dryness. Then the solid residue was dissolved

with 100 mL of DI water and analyzed for As by a Perkin Elmer Graphite Atomic Absorption Spectrometer (GAAS).

4.2.5 Immobilization of PL-laden As: batch tests

The effectiveness of the two types of polysaccharide modified nanoparticles for immobilization of PL-laden As was tested through batch As-desorption tests in the absence or the presence of the nanoparticles. To test the dosage effect, magnetite particles were prepared at a fixed starch concentration of 0.4 wt% but with an Fe concentration of 0.5, 1.0, 2.5 and 5.0 g/L, respectively; and Fe-Mn particles were also synthesized at a fixed CMC concentration of 0.14 wt% but with an Fe concentration of 0.19, 0.37, 0.5, 1.0 and 2.5 g/L, respectively. The batch desorption tests were initiated by mixing 2 g of an air-dried PL sample with 200 mL of a suspension of the starch coated magnetite nanoparticles or the CMC modified Fe-Mn oxide particles. The pH of the mixtures was kept at 6.8±0.4 during the course of the tests through intermittent adjustment using 0.1M hydrochloric acid and 0.1M sodium hydroxide. The mixtures were continuously mixed on a platform shaker operated at 200 rpm at room temperature (21±1°C). At predetermined times, the supernatant of suspension was sampled and filtered through a 25 nm membrane of mixed cellulose esters (Millipore Corp., Billerica, MA, USA). The membrane was able to completely remove the nanoparticles, but did not remove the soluble arsenic. The filtrates were then acidified to pH < 2.0 with 1N HNO_3 and then analyzed for total As using GAAS.

4.2.6 Effect of pH

To test the effects of pH on immobilization of As, the batch desorption kinetic tests for As from PL were carried out the presence of modified nanoparticles and at pH 4 and pH 10. The tests were carried out following the same procedures as described above at a fixed nanoparticle

concentration of 0.5 mg/L as Fe using magnetite (with 0.2% starch) and Fe-Mn (with 0.2% CMC) oxide nanoparticles.

4.2.7 Effect of stabilizers

To test the effects of type and concentration of the stabilizers, the sorbent particles were prepared at a fixed concentration of 0.5 g/L as Fe but with a range of starch concentration from 0.05 to 0.5 wt% for magnetite and 0.005 to 0.25 wt% of CMC for Fe-Mn oxide particles. At equilibration time (96 hrs), the supernatant of suspension was sampled and filtered through a 25 nm membrane of mixed cellulose esters (Millipore Corp., Billerica, MA, USA). The filtrates were then acidified to pH < 2.0 with 1N HNO_3 and then analyzed for total As using GAAS.

4.2.8 Leachability of nanoparticle immobilized As upon land application: Column tests

Assuming that the nanoparticle amended PL is to be applied to the top of soil as a fertilizer column tests were carried to examine the transport behavior of nanoparticle immobilized As upon land application and under simulated runoff or groundwater flow conditions. The experimental setup includes a solution reservoir containing 0.84 mM NaCl and 0.16 mM $NaHCO_3$ (pH 7.5), Teflon tubing, a Plexiglas column (inner diameter = 10 mm, length = 100 mm, Omnifit, Cambridge, UK), an HPLC pump (Series II), and a fraction collector (Eldex Laboraries, Napa, CA, USA). Before the column tests, 2 grams of PL samples were treated by either 2.5 g/L as Fe of 0.4 wt% starch modified magnetite or 2.5 g/L as Fe of 0.14 wt% CMC modified Fe-Mn oxide nanoparticle suspension for 96 hours in the same way as in the batch tests. After the treatments, the solid and aqueous phases were separated by carefully decanting the liquid and then retrieving the soil. Arsenic concentration in aqueous phase was measured. The solid samples were air dried and mixed with an As-free sandy soil at a PL-to-soil ratio of 1:2 by weight. Then, the mixture was wet-packed in the column. Column elution tests were then

initiated by pumping a simulated groundwater with a chemical composition of 7 mM NaCl + 0.86 mM $CaSO_4$ at pH 6.5) through the PL-soil bed in the down-flow mode (flow rate = 0.06 mL/min). The effluent was sampled by the fraction collector, acidified at pH 3.0 and analyzed for total As and iron. For comparison, arsenic elution curves were also acquired with untreated PL and under identical operating conditions. To facilitate a fair comparison, the total mass of As in the PL-soil beds was equal in all cases.

4.2.9 Chemical analysis

Total As was analyzed using a Perkin Elmer Graphite Atomic Absorption Spectrometer (GAAS) 3110 (connected with an HGA 600 and EDL system 2). The detection limit was ~5 µg/L. Total iron concentration was analyzed with a VARIAN 220FS Flame Atomic Absorption Spectrometer (detection limit = 0.1 mg/L).

4.3 Results and Discussions

Table 4-1 presents the salient elemental compositions. The total arsenic concentration in the litter was determined to be 25 mg/kg, which is in the range of 12-30 mg/kg reported in the literature (Arai et al., 2003). Soluble As was determined by extracting PL samples with 2% methanol in DI water. Two grams of a PL sample was mixed with 20 mL of DI water and shaking for 2 hours, upon centrifuging at 2200 rpm for 30 minutes. As in the aqueous phase was analyzed using IC-ICP/MS. The fraction of soluble arsenic species in the Black Hen PL leachate with 2% methanol (to improve ICP-MS signal (Jackson and Bertsch, 2001)) was 17.99 wt%. The distribution of arsenic species in soluble arsenic compounds is as follows: roxarsone = 77.05 wt%, dimethylarsinate (DMA) = 20.83 wt%, monomenthylarsonic acid (MMA) = 0.30 wt%, arsenate [As(V)] = 1.67 wt%, and arsenite [As(III)] = 0.15 wt%. Similar arsenic speciation in PL leachate was reported by others (Garbarino et al., 2003; Jackson and Bertsch, 2001). However, if the extraction time is prolonged and PL is fresh, much higher (indicated in the controls of **Figure 4-3**) percentage of the total As would leach from water extraction. It was reported (Garbarino et al., 2003) that a much higher percentage (between 70 and 90%) of the total As in fresh dried PL can be mobilized with water. The As speciation and water leachability can be affected by litter processing practices, storage time, exposure to sunlight, air temperature, and the associated photochemical and biological reactions, which are responsible for transforming roxarsone to As(V) (Garbarino et al., 2003).

Table 4-1 Elemental composition of poultry litter sample

Element	Poultry Litter Sample
As (mg/kg)	24.52±1.98
Pb (mg/kg)	1.44±0.04
P (mg/kg)	14359±778
C (%)	3.65±0.01
N (%)	0.45±0.01
S (%)	0.14±0.01

Trace element data given as mean of duplicates and errors refer to deviation from the mean. Litter was obtained from black hen fertilizer sold in Lowes store. Litter was digested by microwave digestion and analyzed by inductively coupled plasma atomic emission spectrometry.

4.3.1 Sorption of arsenic in litter leachates

The PL leachates contain high concentrations of dissolved organic matter (around 77 wt% of PL is organic matter (Jackson et al., 2003)) and phosphate, which are expected to inhibit the sorption/immobilization of arsenic from the leachates. **Figure 4-1** shows the arsenic desorption kinetic data during batch desorption experiments in the presence of various dosages of modified magnetite or Fe-Mn oxide nanoparticles. For magnetite, 0.4 wt% of starch was used in all cases, whereas 0.14 wt% of CMC was applied to modify Fe-Mn oxide particles. For comparison, control tests with the same concentrations of starch or CMC were also carried out in the absence of the nanoparticles. **Figure 4-1a** indicates that at a magnetite dose of 2.5 g/L as Fe, the leachable As was reduced by ~97% from ~150 mg/L to < 5 mg/L at equilibrium. **Figure-1b** shows that at a dose of 0.5g and 1.0g/L as Fe, the Fe-Mn oxide nanoparticles lowered the leachable As by ~93% and 99%, respectively. Both types of nanoparticles displayed relatively fast kinetics with an equilibrium time less than 24 h. In the control tests, both starch and CMC solutions eluted about the same levels of As (~150 mg/L) from the PL samples.

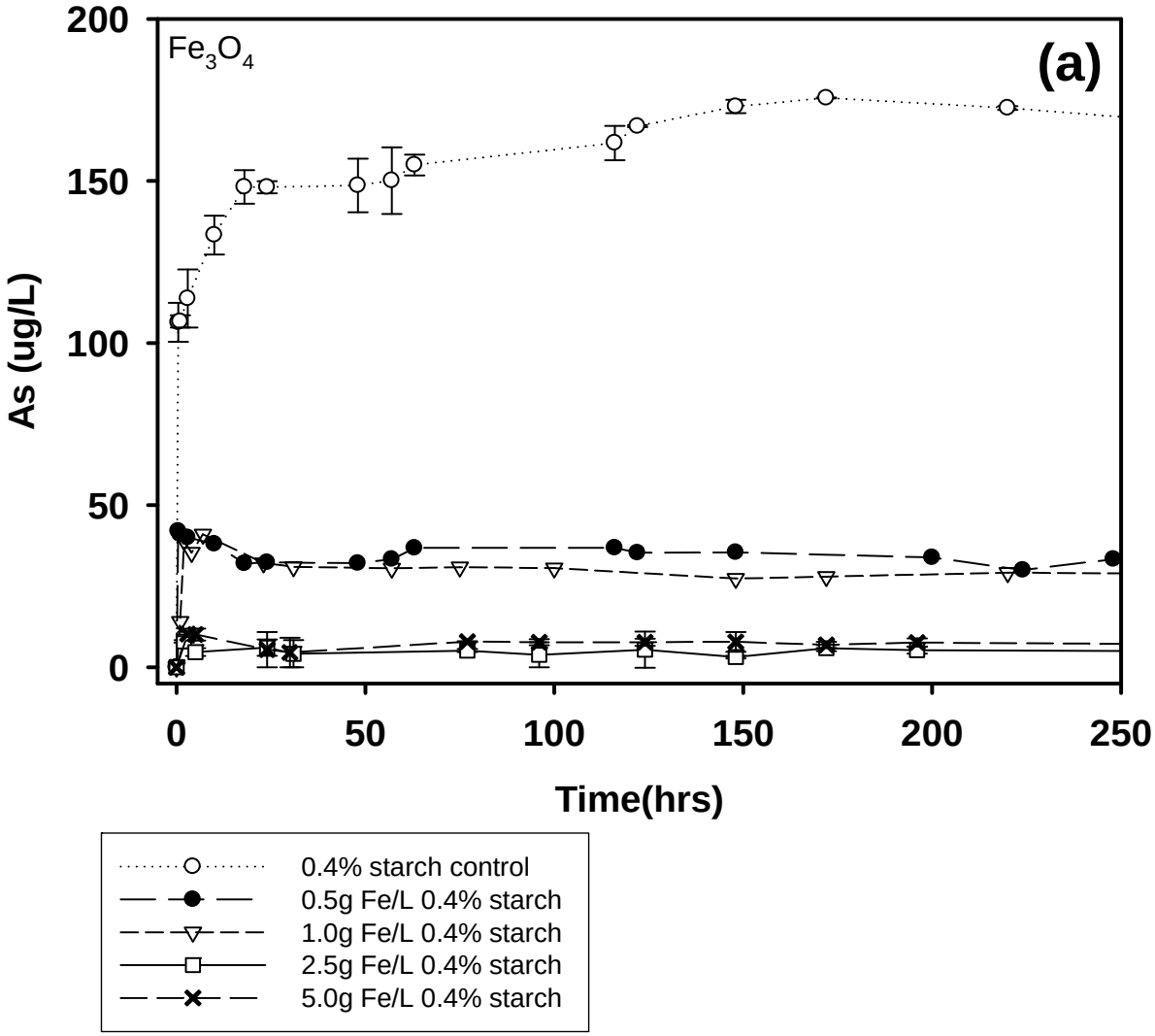
200
150
100
50
0
As (ug/L)
Fe3O4
(a)
0
50
100
150
200
250
Time(hrs)
0.4% starch control
0.5g Fe/L 0.4% starch
1.0g Fe/L 0.4% starch
2.5g Fe/L 0.4% starch
5.0g Fe/L 0.4% starch

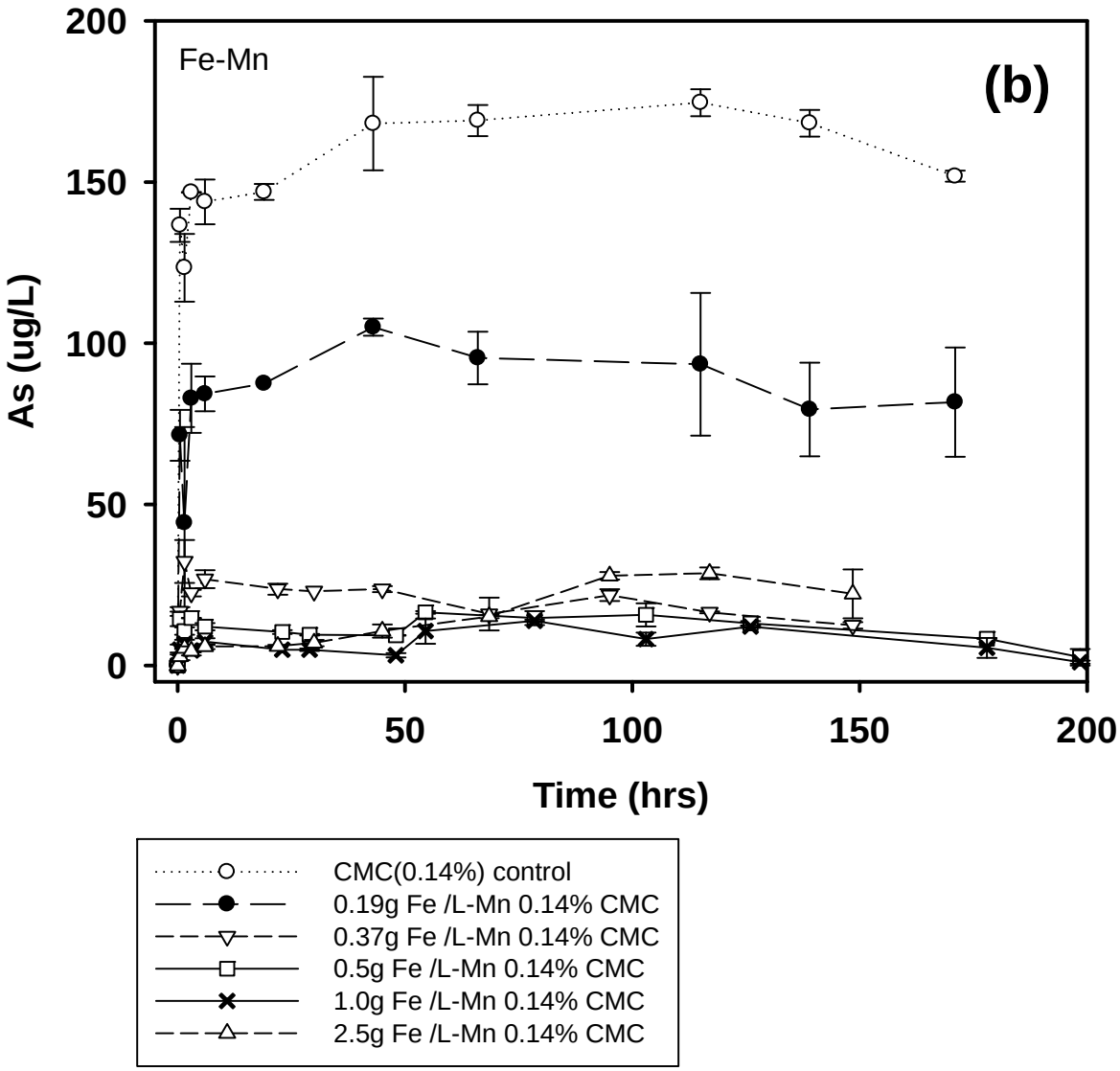

Figure 4-1. The variation of arsenic concentration in PL leachates (solid to liquid ratio = 1g : 100 mL) as a function of time at various dosages of: **(a)** 0.4 wt% of starch-modified magnetite, and **(b)** 0.14 wt% CMC modified Fe-Mn binary oxide nanoparticles at an initial pH of ~7.0 and final pH was 6.5-7.0. Data given as mean of duplicates and error bars refer to standard deviation from the mean to show data reproducibility.

It is noteworthy that the Fe-Mn oxide particles appeared to be more effective than the magnetite particles. Similar observations were reported by others who studied As(III) and As(V) removal from water and brine using stabilized magnetite and Fe-Mn oxide nanoparticles. The starch stabilized magnetite nanoparticles offered 62.1 mg/g As(V) uptake at pH 6.8 ± 0.4 (based on the Langmuir capacity coefficient), while CMC stabilized Fe-Mn binary nanoparticles provided the sorption capacities of 272 mg/g for As(V) and 338 mg/g for As(III) at pH = 5.1 (An and Zhao, 2011; Liang et al., 2012b). The enhanced removal of As by the Fe-Mn oxide particles is attributed to oxidizing effect of manganese dioxide. Researchers (An and Zhao, 2011; Deschamps et al., 2005) observed that Fe-Mn binary oxides offered much higher As(III) uptake than As(V) at pH >5.0 and confirmed per FTIR and stoichiometric studies that As(III) was partially oxidized to As(V) by manganese dioxide and taken up through inner sphere complexation in the form of Fe-O-As.

The researchers also claimed that particle dissolution of MnO_2 opens up more accessible surface sorption sites for binding with more arsenic species. For our case here, roxarsone accounts for 77%, and DMA for 20.8%, of the total soluble arsenic. Therefore, it is plausible that MnO_2 was able to transform at least a part of roxarsone and/or DMA to As(V) (Thirunavukkarasua et al., 2002). All the arsenic originally present in the litter eventually would be transformed to inorganic As(V) (Garbarino et al., 2003). Thus, the enhanced As sorption of the Fe-Mn oxide particles could be attributed to the oxidation of As(III), roxarsone as well as other organic arsenic compounds to As(V), the subsequent uptake of As(V), and creation of additional sorption sites at the solid surface upon partial dissolution of Mn^{2+}. At the experimental pH of range of 6.5-7.0, sorption of As(V) is more favorable than that of As(III)

(Deschamps et al., 2005; Zhang et al., 2007). Therefore, conversion of other As species to As(V) favors the overall uptake of As by both types of the nanoparticles.

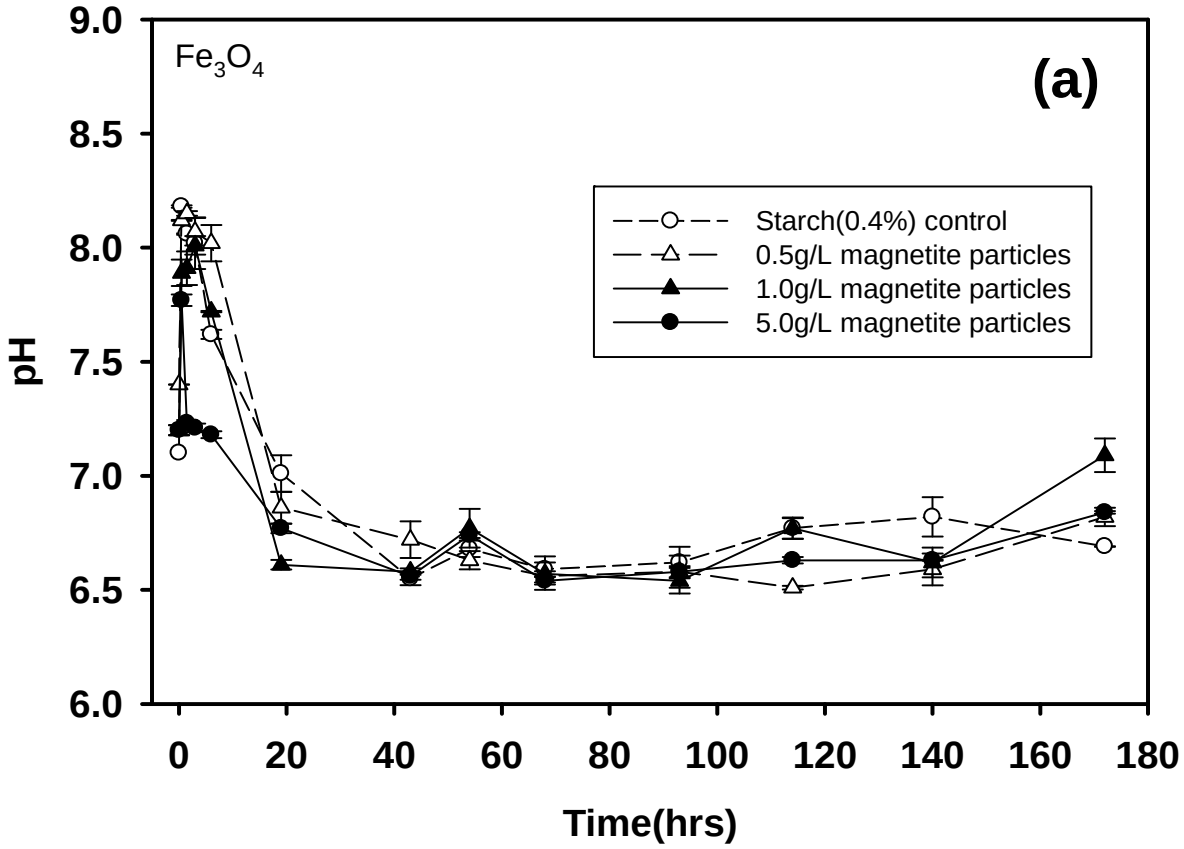

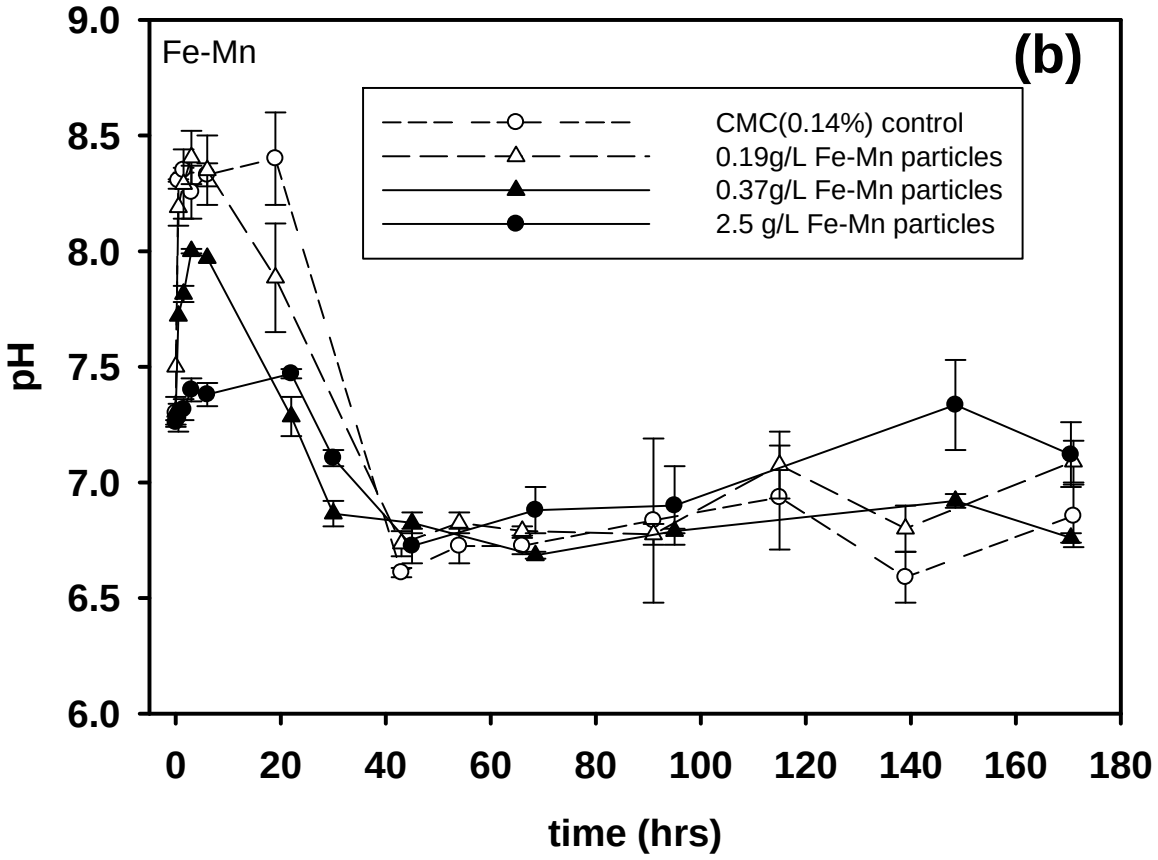

Figure 4-2. The profile of pH in PL leachates (solid to liquid ratio = 1g : 100 mL) as a function of time at various dose of 0.4 wt. % of starch coated magnetite (a) and 0.14 wt. % CMC coated Fe-Mn binary oxides (b). Data given as mean of duplicates and errors refer to standard deviation from the mean.

On the other hand, roxarsone could be directly adsorbed by metal oxide, similar to those of inorganic arsenate and monomethylated arsenate (Chen and Huang, 2012). Chen et al. (2012) observed that the arsenate acid group of roxarsone is mainly responsible for the adsorption to take place. Roxarsone and inorganic arsenate share many chemical properties including the same oxidation state (+V) for As, the arsenate acid group, and three acidity constants associated with the arsenate acid group. It is thus possible that the sorption mechanism of roxarsone is similar to that of arsenate (Chen and Huang, 2012).

4.3.2 Effects of pH

Solution pH can affect arsenic speciation, oxidation of roxarsone and DMA, and surface potential of the nanoparticles. **Figure 4-2** displays the profile of pH in PL leachates (solid to liquid ratio = 1 g: 100 mL) as a function of time at various doses of 0.4 wt% starch coated magnetite and 0.14 wt% of CMC coated Fe-Mn oxides. The pH of PL leachates at the presence of both magnetite and Fe-Mn oxides started at around 7.0, immediately climbed up to the peak value at around 8.2-8.5 within 5 hrs, and eventually leveled off at 6.5-7.0 within 40 hrs. Typical litter pH remained relatively constant at 8 (Bednar et al., 2003; Moore et al., 1999). In a study, the litter pH for the control birds remained at 8 throughout the study, while the reduction in pH was seen after aluminum sulfate (alum) application due to the influence of this dry acid (Moore et al., 1999). In our case, it is believed that the peak value of pH (~8) at the beginning is resulted from the wetting and dissolving of PL, representative of typical PL leachates; the slight drop of pH in **Figure 4-2** is resulted from the influence from the pH of magnetite and Fe-Mn aliquots.

Figure 4-3 shows arsenic desorption kinetic data at pH 4 and pH 10 with or without the magnetite (a) and Fe-Mn oxide (b) nanoparticles. In both cases, the nanoparticles offered greater arsenic removal at pH 4 than at pH 10. At a magnetite dosage of 0.5 g/L as Fe, the equilibrium

aqueous As level was ~50 μg/L at pH 10, compared to ~ 20 μg/L at pH 4. Similarly, at a dosage of 0.5 g/L as Fe, the Fe-Mn nanoparticles lowered the aqueous As concentration to ~40 μg/L at pH 10 and <10 μg/L at pH 4. Based on mass balance calculations, 28% more As was leached out from the PL at pH 10 than pH 4 by DI water.

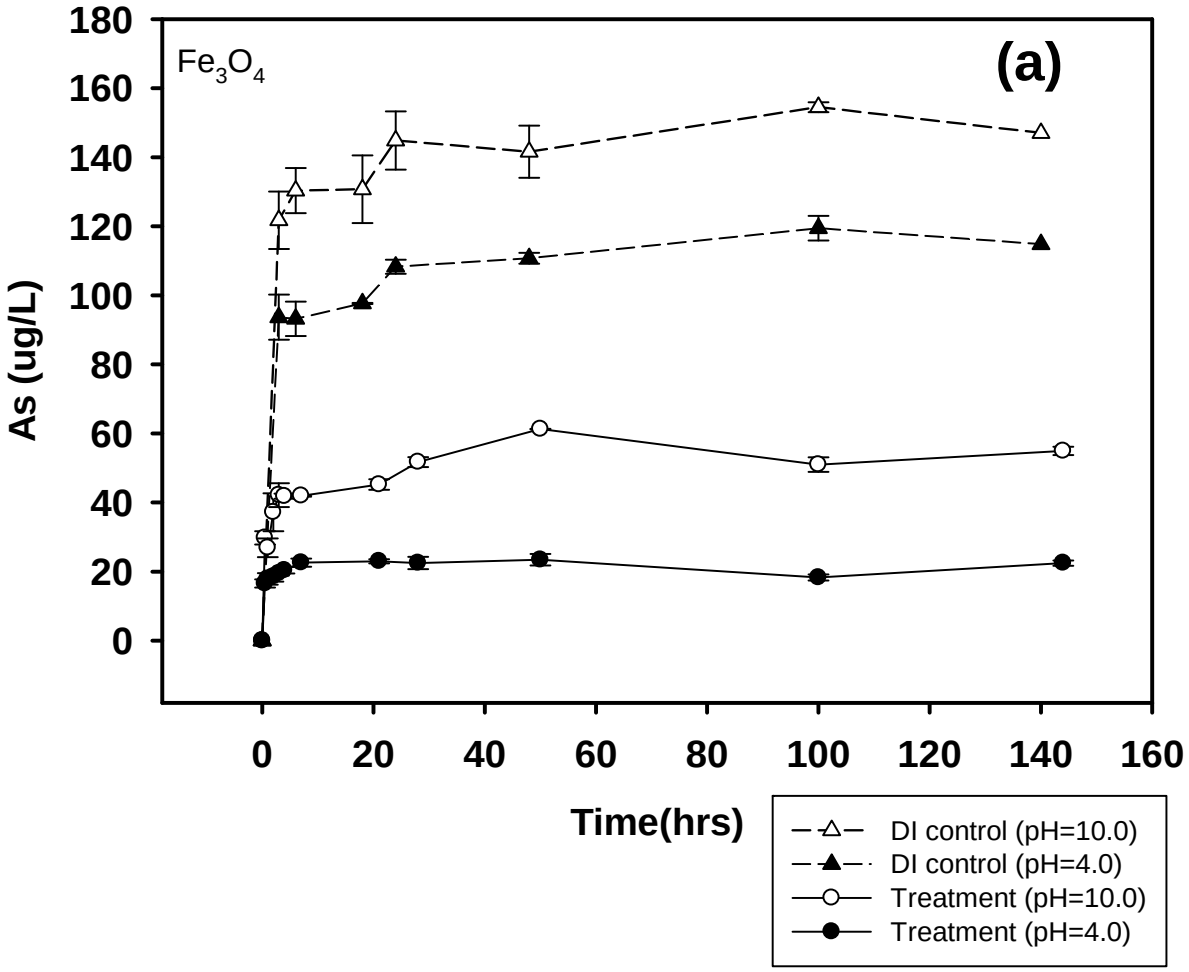

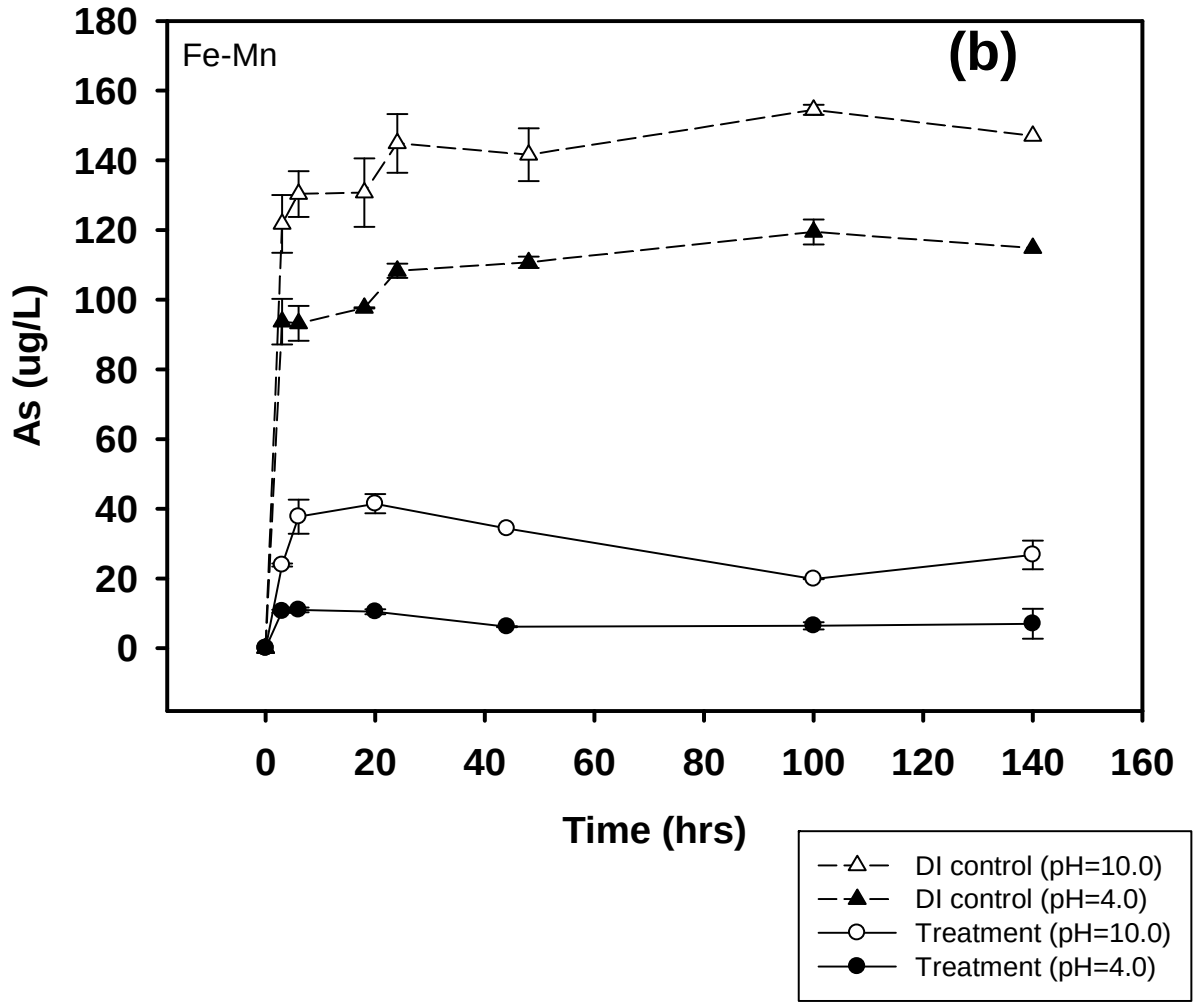

Figure 4-3. Arsenic desorption from PL as a function of time at pH 4 and pH 10: **(a)** in the presence of 0.4 wt% starch modified magnetite, and **(b)** 0.14 wt% CMC modified Fe-Mn binary oxide nanoparticles. PL:Solution Ratio = 1g : 100 mL, Nanoparticle dosage = 0.5 g/L as Fe for both type of nanoparticles. Data given as mean of duplicates and errors refer to standard deviation from the mean.

The observed pH-dependent desorption behavior could be attributed to a number of factors. First, at elevated pH, more negatively charged arsenic species become predominant. For instance, at pH 10, roxarsone (pK_{a1} = 3.43, pK_{a2} = 6.48, pK_{a3} = 9.67) becomes predominately -3 charged species, and As(V) (pK_{a1} = 2.20, pK_{a2} = 6.97, pK_{a3} = 11.53) turns to $HAsO_3^{2-}$. On the other hand, the surface of the nanoparticles becomes more negatively charged. The ζ potential of starch coated magnetite particles remained neutral over a pH range of 2-9 (negative at pH>9), while ζ potential of Fe-Mn in the presence of 0.16 wt% CMC was substantially lowered to below -50 mV throughout the pH range (< -65 mV at pH>5) (An and Zhao, 2011; Liang et al., 2012b). As a result, the surface turns more unfavorable for sorption of anionic organoarsenicals and the arsenic oxyanions. Second, solution pH can affect transformation of organic arsenic species and As(III) to As(V). For example, As(III) oxidation has been reported in solution of pH>9, however, it is kinetically slow though thermodynamically favorable (Jackson and Bertsch, 2001; Jackson and Miller, 2000; Manning and Goldberg, 1997). Because OH^- is generally an effective extractant for all arsenic species and leads to substantial oxidation of As(III) with and without an Fe oxide solid phase present (Jackson and Bertsch, 2001; Jackson and Miller, 2000). Lastly, at elevated pH, the competition of hydroxyl anions for the sorption sites become stronger with the anionic arsenate species , which again diminishes arsenic uptake by the nanoparticles at pH 10 (Arai et al., 2003).

4.3.3 Effects of starch and CMC stabilizers

Figure 4.4 shows the equilibrium uptake of As in the PL leachates by the magnetite or Fe-Mn oxide particles at a fixed dosage of 0.5 g/L as Fe but prepared in the presence of various concentrations of starch or CMC. For starch modified magnetite particles, increasing starch concentration from 0 to 0.2 wt% increased As removal from 70% to 90% , and the maximum removal continued till a starch concentration reached 0.3 wt.%. However, further increasing starch concentration from 0.3 to 0.5 wt% progressively inhibited As uptake.

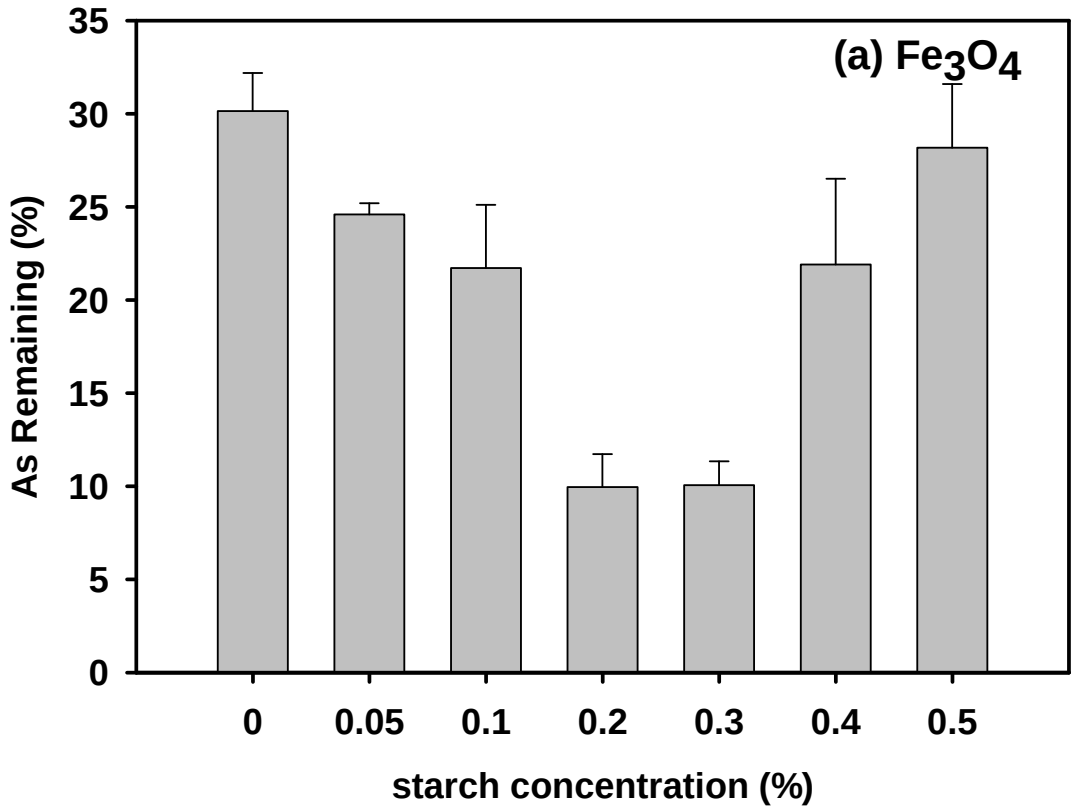

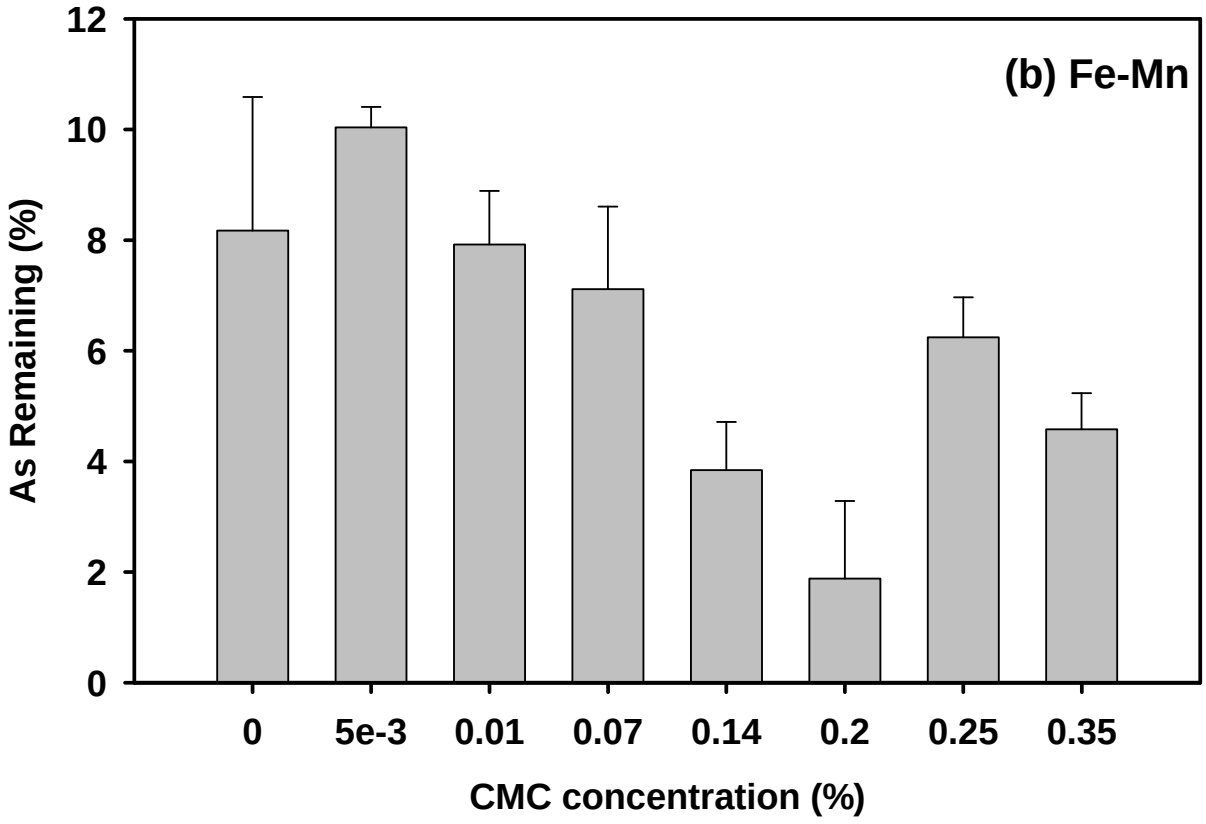

Figure 4-4. Arsenic uptake inform PL leachates by: (a) starch modified magnetite, and (b) CMC modified Fe-Mn binary oxide particles. PL:Solution ratio = 1g : 100 mL, nanoparticle dosage = 0.5 g/L as Fe for both cases, and pH was kept at 6.8±0.4. Data given as mean of duplicates and errors refer to standard deviation from the mean.

For the Fe-Mn oxide particles, the CMC concentration showed a similar effect profile though to a much lesser extent. Increasing CMC concentration from 0.005 to 0.2 wt% increased As removal from 92% to 98%, and the trend was reversed when CMC concentration as further increased from to 0.25 wt%. Unlike the case of starch-magnetite, the presence of low concentrations of CMC (<0.01 wt%) did not show any capacity enhancement compared to the bare particles.

Based on our prior study [9], the higher the starch concentration, the smaller the magnetite nanoparticles, which results in greater specific surface area and translates into enhanced As sorption capacity. On the other hand, the accumulation of starch on the particle surface can render some inhibitive effects on the sorption of As. First, increased starch coating elevates mass transfer resistance for As uptake and may block some micropores and sorption sites; Second, the higher the starch concentrations, the more sorption sites are occupied by starch molecules, and the fewer available sites for As; Third, accumulation of starch molecules may increase the activation energy for surface complexation and formation of the Fe-O-As complexes. For the case of CMC modified Fe-Mn oxide particles, the CMC coating renders a highly negative surface potential (below -50 mV). As a result, sorption of anionic As species (e.g., arsenate and roxarsone) becomes increasingly unfavorable as CMC concentration increases. Namely, the gain in specific surface area due to CMC-stabilization can be counteracted by the increased surface repulsive forces and elevated energy barrier. Despite the limited gain in the overall As removal, CMC modification provides a means to control the particle size, and thus, can facilitate transport and application of the nanoparticles in the solid wastes such as PL.

4.3.4 Column tests

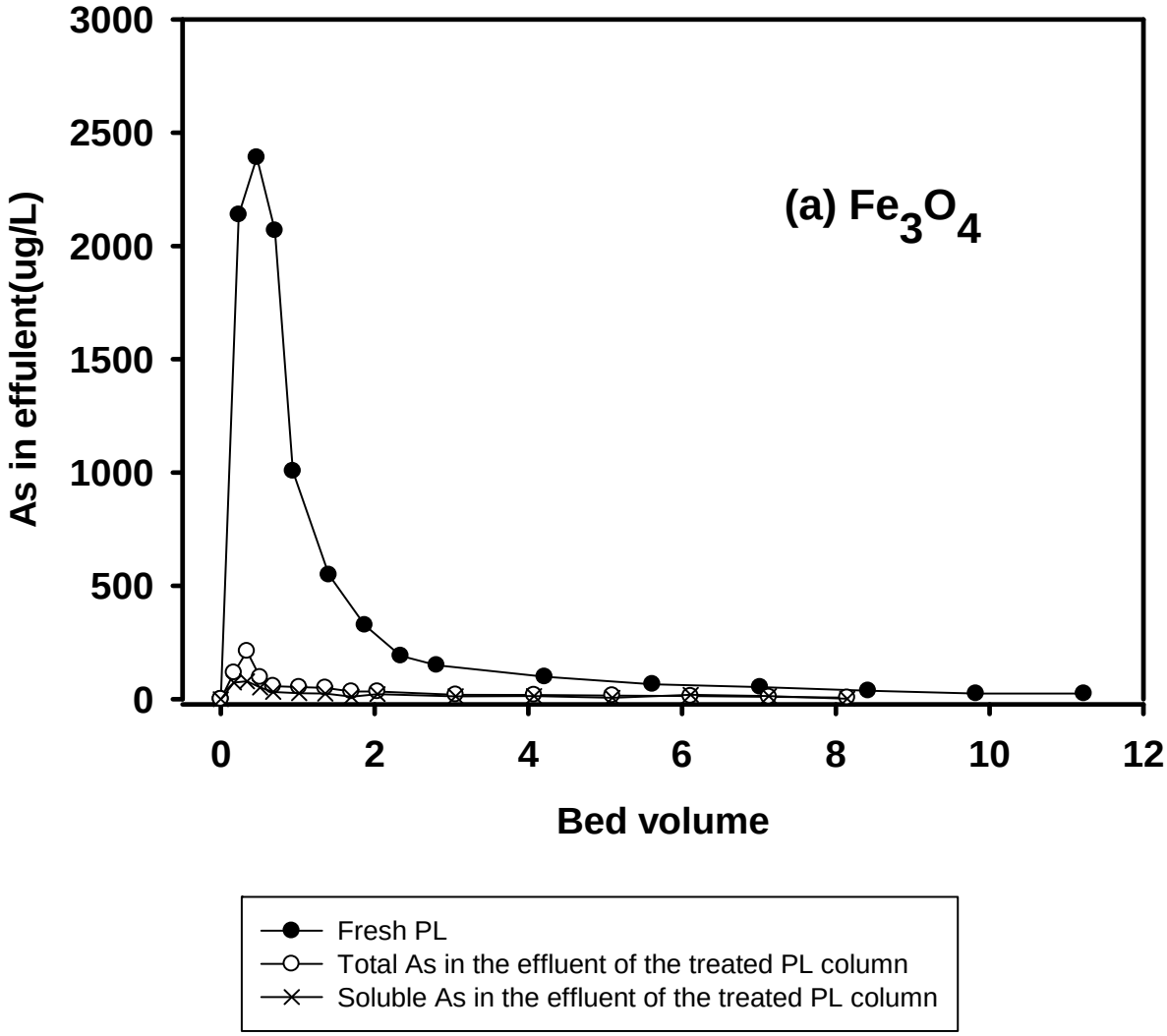

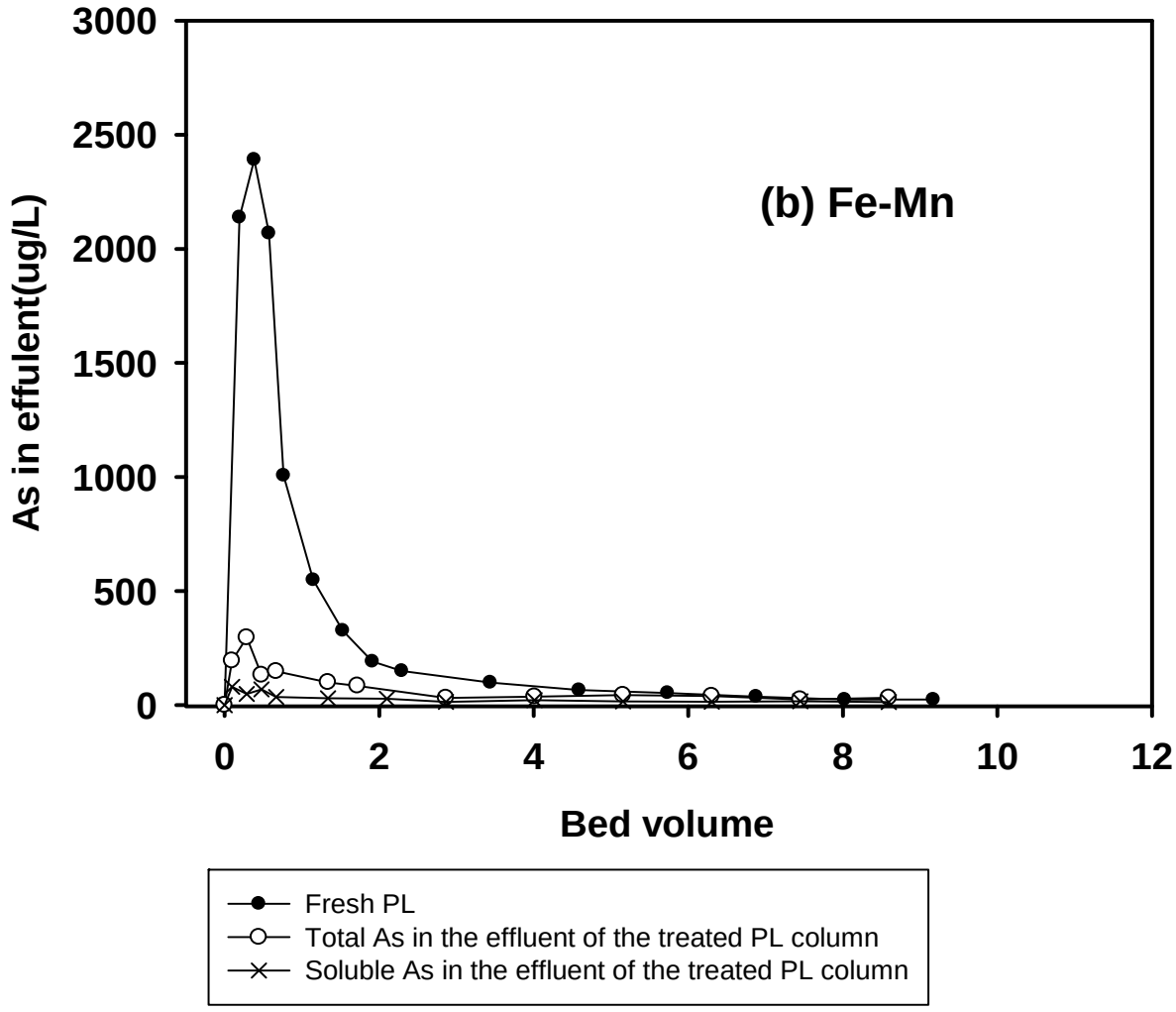

Figure 4-5. Arsenic elution histories from: (a) magnetite nanoparticle treated and (b) Fe-Mn oxide nanoparticle PL treated poultry litter when subjected to a simulated groundwater. For comparison, arsenic elution histories of untreated PL containing the same amount of arsenic were also superimposed. PL:Soil ratio = 1:2. Empty bed contact time (EBCT) = 177 min.

To test the leachability of As from the nanoparticle amended PL, column elution testes were carried out simulating a scenario where the treated PL is to be applied to the top of soil as a fertilizer and is subjected to a groundwater flow or storm water runoff. For comparison, a sandy soil was mixed with 1) untreated PL, 2) magnetite treated PL, and 3) Fe-Mn oxide treated PL. In all cases, the PL:soil ratio was kept at 1:2 and the total As mass was the same in each column bed. **Figure 4-5** shows the elution curves of arsenic from each of the packed columns. For the untreated PL bed, 84.9% of As initially in the bed was eluted to the effluent in 11 bed volumes. For the column with magnetite treated PL, a total of 34% As was eluted, of which 36% was found associated with the nanoparticles, and 64% was in soluble As. For the column with Fe-Mn oxide treated PL, a total of 18% As was eluted, of which 63% was associated with the nanoparticles and 37% was soluble As. It is also noteworthy that the soluble peak As concentration was reduced from ~2500 μg/L for the untreated PL to ~78 μg/L for magnetite treated PL and 80 μg/L for Fe-Mn oxide treated PL. While both types of nanoparticles were able to effectively immobilize arsenic in the PL, CMC-modified Fe-Mn oxide particles appeared more effective than the magnetite particles based on overall mass of As immobilized.

4.4 Conclusions

Our results proposed a promising strategy of applying starch coated magnetite as well as CMC coated Fe-Mn binary oxides particles for poultry litter amendments and As contamination. The primary findings and conclusions are summarized as follows:

High level of As in poultry litter (25 mg/kg in the Black Hen samples in this study) poses an imminent threat to farm crops, livestock and the health of public. We have successfully extended the use of As-sorbents such as starch magnetite and CMC Fe-Mn to controlling As contamination from poultry litter leachates and runoff. To be specific, at a magnetite dose of 2.5

g Fe/L, or Fe-Mn dose of 0.5 g/L, >93% of ~150 mg/L As in PL leachates was removed from solution phrase by sorption at equilibrated time of 24h. Fe-Mn binary oxide, also an oxidizing agent, provides with higher sorption capacities than magnetite by forming fresh sorption sites at the solid surface during the process of oxidation.

The arsenic sorption on magnetite and Fe-Mn from poultry litter leachates displayed a pH-dependent manner. 18% and 12% more of As was removed by magnetite and Fe-Mn, respectively, from aqueous phrase when pH was dropped from 10 to 4. Noteworthy, since the ultimate form of As existed in PL would be As(V) and As(V) ions would be out-competed by hydroxyl ions at high pH, 28% more As would leach to aqueous phrase from poultry litter at pH=10 than pH=4. Luckily, As(V) was usually more favorably sorbed at lower pH (also good for controlling phosphorus runoff), thus the overall arsenic sorption capacities increased as pH decreased from 10 to 4.

The presence of polysaccharide polymer generally enhanced the As removal by magnetite and Fe-Mn binary oxide particles at an extent of 20% and 6%, respectively. The difference between the gains of sorption capacities by these two particles was probably due to the negative surface of CMC, which expels ions of like charge, As(V), the ultimate existing As species in PL. The sorption capacity gain could be attributed to the smaller particle size and thus greater specific surface area, though the gain would be limited because the accumulation of polymer coating would also increase mass transfer resistance and occupy sorption sites.

Column tests of magnetite and Fe-Mn treated PL showed that only 7% of total As content from Fe-Mn treated PL was detected as soluble As compared to 85% from untreated PL, while 22% of As leached from magnetite treated PL.

Chapter 5. Conclusions and Suggestions for Future Research

5.1 Summary and Conclusions

Arsenic is ranked first on the most recent priority list of Superfund site (ATSDR, 2011). The presence of arsenic (As) in soil and water is widespread. Stabilized magnetite nanoparticles were synthesized and tested for enhanced removal of arsenate from water. Two "green" polysaccharides, a water-soluble starch and sodium carboxymethyl cellulose (CMC), were used as stabilizers to enhance arsenate sorption. TEM images and sedimentation tests revealed that the presence of ≥0.04 wt.% starch or ≥0.005 wt.% CMC was able to fully stabilize 0.1 g/L (as Fe) of the nanoparticles; yet, when the stabilizer concentration was below these critical values, the particles were present as larger aggregates bridged by the stabilizer macromolecules. The mean particle size was 75±17 (standard deviation) nm and 2.9±2.0 nm, respectively, when 0.1g/L (as Fe) of the nanoparticles were stabilized with 0.1 wt.% starch and 0.1 wt.% CMC. XRD spectra confirmed the magnetite structure of the stabilized nanoparticles. Over broad pH range (2-11), CMC-stabilized magnetite displayed a highly negative ζ potential (up to -150 mV), while starch-stabilized magnetite showed a nearly neutral surface. For a nanoparticle suspension of 0.1 g/L as Fe, increasing starch concentration from 0 to 0.04% increased arsenate uptake from 26 mg/g to 56 mg/g, yet the nanoparticles remain settleable by gravity. Further increasing the starch concentration to 0.1 wt.% resulted in fully dispersed nanoparticles and an increase in arsenate uptake by 14%. Starch-stabilized magnetite nanoparticles offer much faster arsenate sorption rate than CMC-stabilized or non-stabilized magnetite. The sorption rates can be adequately

modeled using the intraparticle-diffusion model. In the pH range of 3-11, the arsenate sorption capacity follows the sequence of: starch-stabilized magnetite >> CMC-stabilized magnetite > non-stabilized magnetite. The sorption capacity increases with decreasing pH and reaches maximum plateau at pH <6 for the stabilized nanoparticles. The presence of dissolved organic matter at up to 20 mg/L as TOC decreased arsenate uptake by up to 19.1%. Aging of As-laden particles for >1.5 years did not show any arsenate leaching or dissolution of the nanoparticles. A weak external magnetic field was able to completely separate the stabilized nanoparticles from water. The As-laden spent particles were able to pass the TCLP (Toxicity Characteristic Leaching Procedure) test.

Arsenate (As(V)) immobilization using starch-stabilized magnetite (Fe_3O_4) nanoparticles was investigated through a series of batch and column experiments. Batch tests showed that the nanoparticles could effectively immobilize As(V) in As(V)-laden sandy soil with equilibrated As sorption capacity of 4335 μg-As/g-Fe. TCLP (Toxicity Characteristic Leaching Procedure) based As leachability was reduced by 80% at the presence of starch-stabilized Fe_3O_4 nanoparticles. Column tests showed that water-leachable As(V) from the As(V)-laden sandy soil containing 31.45 mg/kg was reduced by ~93% and the TCLP leachability by >83% when the soil was treated with 34 pore volumes (PVs) of a 0.1 g/L Fe_3O_4 nanoparticle suspension. Though Fe_3O_4 nanoparticles are highly mobile and deliverable in sandy soil, the effective travel distance of Fe_3O_4 nanoparticles can be manipulated by controlling the injection flow rate. The experimental results showed that the spent Fe_3O_4 nanoparticles could be retained by the matrix within a limited distance (<10 cm) under natural groundwater condition (velocity $\leq 2.2\times10^{-7}$ cm/s).

Magnetite and Fe-Mn binary particles have been tested for the feasibility of reducing dissolved As in leachates from poultry litter (PL). High level of As in poultry litter (25 mg/kg in

the black hen samples in this study) poses an imminent threat to farm crops, livestock and the health of public. We have successfully extended the use of As-sorbents such as starch magnetite and CMC Fe-Mn to controlling As contamination from poultry litter leachates and runoff. To be specific, at a magnetite dose of 2.5 g Fe/L, or Fe-Mn dose of 0.5 g/L, >93% of ~150 mg/L As in PL leachates was removed from solution phrase by sorption at equilibrated time of 24h. Fe-Mn binary oxide, also an oxidizing agent, provides with higher sorption capacities than magnetite by forming fresh sorption sites at the solid surface during the process of oxidation.

The arsenic sorption on magnetite and Fe-Mn from poultry litter leachates displayed a pH-dependent manner. 18% and 12% more of As was removed by magnetite and Fe-Mn, respectively, from aqueous phrase when pH was dropped from 10 to 4. 28% more As leached to aqueous phrase from poultry litter at pH=10 than pH=4. The presence of polysaccharide polymer generally enhanced the arsenic removal by magnetite and Fe-Mn binary oxide particles at an extent of 20% and 6%, respectively.

Column tests of magnetite and Fe-Mn treated PL showed that only 7% of total As content from Fe-Mn treated PL was detected as soluble As compared to 85% from untreated PL, while 22% of As leached from magnetite treated PL.

5.2 Suggestions for Future Work

The specific recommendations for future work were made as follows:

1. X-ray diffraction (XRD), x-ray photoelectron spectroscopy (XPS), extended x-ray absorption fine structure (EXAFS), and scanning electron microscopy (SEM), and transmission electron micrograph (TEM) image tests on stabilized magnetite nanoparticles synthesized with

CMC and starch before and after arsenic sorption can provide more reliable evidence to elucidate the structure of stabilized nanoparticles, and the mechanisms of arsenic sorption.

2. Field implementation and demonstration of stabilized magnetite nanoparticles in As-contaminated sites would be desired to validate the effectiveness of this in situ remediation technology. The onsite practice would also help us spot any potential limitation in the procedures and methods.

3. More work should be done on the kinetic models that describe the arsenic sorption on stabilized magnetite nanoparticles. Although our preliminary results showed that the sorption kinetics is intraparticle diffusion controlled, more evidences need to be presented to support this claim.

4. There're still a lot of unsolved mysteries in the study of environmental fate and impacts of magnetite and Fe-Mn nanoparticles. More experiments need to be conducted to validate the maximum transport distance. The ultimate fate and the dissolution of spent nanoparticles are interesting research topics that require future work.

References

Abernathy, C.O., Liu, Y.P., Longfellow, D., Aposhian, H.V., Beck, B., Fowler, B., Goyer, R., Menzer, R., Rossman, T., Thompson, C. and Waalkes, M., 1999. Arsenic: Health effects, mechanisms of actions, and research issues. Environmental Health Perspectives, 107(7), 593-597.

Adler, J.J., Rabinovich, Y.I. and Moudgil, B.M., 2001. Origins of the non-DLVO force between glass surfaces in aqueous solution. Journal of Colloid and Interface Science, 237(2), 249-258.

Alley, W.M., Reilly, T.E., Franke, O.L. (1999) Sustainability of ground-water resources (U.S. Geological Survey Circular 1186), U.S. Geological Survey, Denver, Colorado.

Allison, J.D. and Allison, T.L. (2005) Partition coefficients for metals in surface water, soil, and waste. USEPA, O.o.R.a.D. (ed), Washington, DC.

Amini, M., Abbaspour, K.C., Berg, M., Winkel, L., Hug, S.J., Hoehn, E., Yang, H. and Johnson, C.A., 2008. Statistical modeling of global geogenic arsenic contamination in groundwater. Environmental Science & Technology, 42(10), 3669-3675.

An, B., Liang, Q.Q. and Zhao, D.Y., 2011a. Removal of arsenic(V) from spent ion exchange brine using a new class of starch-bridged magnetite nanoparticles. Water Res, 45(5), 1961-1972.

An, B., Liang, Q.Q. and Zhao, D.Y., 2011b. Removal of Arsenic(V) from spent ion exchange brine using a new class of starch-bridged magnetite nanoparticles. Water Research, 45(5), 1961-1972.

An, B., Steinwinder, T.R. and Zhao, D.Y., 2005. Selective removal of arsenate from drinking water using a polymeric ligand exchanger. Water Research, 39(20), 4993-5004.

An, B. and Zhao, D., 2011. Immobilization of As(III) in soil and groundwater using a new class of polysaccharide stabilized Fe–Mn oxide nanoparticles. Journal of Hazardous Materials, 211-212, 332-341.

Arai, Y., Lanzirotti, A., Sutton, S., Davis, J.A. and Sparks, D.L., 2003. Arsenic speciation and reactivity in poultry litter. Environmental Science & Technology, 37(18), 4083-4090.

ATSDR (2011) The ATSDR 2011 Substance Priority List. Registry, A.f.T.S.D. (ed), Atlanta, GA.

Bauer, M. and Blodau, C., 2006. Mobilization of arsenic by dissolved organic matter from iron oxides, soils and sediments. Science of the Total Environment, 354(2-3), 179-190.

Bednar, A.J., Garbarino, J.R., Ferrer, I., Rutherford, D.W., Wershaw, R.L., Ranville, J.F. and Wildeman, T.R., 2003. Photodegradation of roxarsone in poultry litter leachates. Science of the Total Environment, 302(1-3), 237-245.

Bellows, B. (2005) Arsenic in poultry litter: Organic regulations, The National Sustainable Agriculture Information Service.

Belluck, D.A., Benjamin, S.L., Baveye, P., Sampson, J. and Johnson, B., 2003. Widespread arsenic contamination of soils in residential areas and public spaces: An emerging regulatory or medical crisis? International Journal of Toxicology, 22(2), 109-128.

Berg, M., Tran, H.C., Nguyen, T.C., Pham, H.V., Schertenleib, R. and Giger, W., 2001. Arsenic contamination of groundwater and drinking water in Vietnam: A human health threat. Environmental Science & Technology, 35(13), 2621-2626.

Bissen, M. and Frimmel, F.H., 2003. Arsenic - a review. Part II: Oxidation of arsenic and its removal in water treatment. Acta Hydrochimica Et Hydrobiologica, 31(2), 97-107.

Blake, J.P. (2001a) Sodium bisulfate (PLT) as a litter treatment, Alabama Corporative Extension System Publications Homepage, ANR-1208.

Blake, J.P. (2001b) Aluminum sulfate as a litter treatment, Alabama Corporative Extension System Publications Homepage, ANR-1202.

Blake, J.P. and Hess, J.B. (2001) Litter treatment for poultry, Alabama Corporative Extension System Publications Homepage, ANR-1199.

Chapman, H.D. and Johnson, Z.B., 2002. Use of antibiotics and Roxarsone in broiler chickens in the USA: Analysis for the years 1995 to 2000. Poultry Science, 81(3), 356-364.

Chen, D.M., Zhang, H.H., Tao, Y.F., Wang, Y.L., Huang, L.L., Liu, Z.L., Pan, Y.H., Peng, D.P., Wang, X., Dai, M.H. and Yuan, Z.H., 2011. Development of a high-performance liquid chromatography method for the simultaneous quantification of four organoarsenic compounds in the feeds of swine and chicken. Journal of Chromatography B-Analytical Technologies in the Biomedical and Life Sciences, 879(11-12), 716-720.

Chen, J.Y., Ko, C.H., Bhattacharjee, S. and Elimelech, M., 2001. Role of spatial distribution of porous medium surface charge heterogeneity in colloid transport. Colloids and Surfaces a-Physicochemical and Engineering Aspects, 191(1-2), 3-15.

Chen, W.-R. and Huang, C.-H., 2012. Surface adsorption of organoarsenic roxarsone and arsenilic acid on iron and aluminum oxides. Journal of Hazardous Materials, 227-228, 378-385.

Chen, Z.R., Cai, Y., Solo-Gabriele, H., Snyder, G.H. and Cisar, J.L., 2006. Interactions of arsenic and the dissolved substances derived from turf soils. Environmental Science & Technology, 40(15), 4659-4665.

Cheng, R.C., Wang, H.C. and Beuhler, M.D., 1994. Enhanced coagulation for arsenic removal. Journal American Water Works Association, 86(9), 79-90.

Christen, K., 2001. Chickens, manure, and arsenic. Environmental Science & Technology, 35(9), 184A-185A.

Clifford, D.S. (1999) Water quality and treatment, a handbook of community water supplies, McGraw Hill, New York.

Cortinas, I., Field, J., Kopplin, M., Garbarino, J., Gandolfi, A. and Sierra-Alvarez, R., 2006. Anaerobic biotransformation of roxarsone and related N-substituted phenylarsonic acids. Environ. Sci. Technol., 40, 2951-2957.

Crank, J. (1975) The mathematics of diffusion, second edition, Oxford University Press.

deLemos, J.L., Bostick, B.C., Renshaw, C.E., Sturup, S. and Feng, X.H., 2006. Landfill-stimulated iron reduction and arsenic release at the Coakley Superfund Site (NH). Environmental Science & Technology, 40(1), 67-73.

Deschamps, E., Ciminelli, V.S. and Holl, W.H., 2005. Removal of As(III) and As(V) from water using a natural Fe and Mn enriched sample. Water Research, 39(20), 5212-5220.

Deuel, L.E. and Swoboda, A.R., 1972. Arsenic solubility in a reduced environment. Soil Science Society of America Proceedings, 36(2), 276-286.

Dixit, S. and Hering, J.G., 2003. Comparison of arsenic(V) and arsenic(III) sorption onto iron oxide minerals: Implications for arsenic mobility. Environmental Science & Technology, 37(18), 4182-4189.

Environmental Protection Agency, E.P.A. (2001b) Technical fact sheet: final rule for arsenic in drinking water (EPA 815-F-00-016), Office of Research and Development, Washington, DC.

Farquhar, M.L., Charnock, J.M., Livens, F.R. and Vaughan, D.J., 2002. Mechanisms of arsenic uptake from aqueous solution by interaction with goethite, lepidocrocite, mackinawite, and pyrite: An X-ray absorption spectroscopy study. Environmental Science & Technology, 36(8), 1757-1762.

Feinstein, D.T. and Guo, W.X., 2004. STANMOD: A suite of Windows-based programs for evaluating solute transport. Ground Water, 42(4), 482-487.

Frey, M., J.D. Chwirka, S. Kommineni, Z. Chowdhury, R. Marasimhan (2000) Cost implications of a lower arsenic MCL, AWWA Research Foundation, Denver, CO.

Fuller, C.C., Davis, J.A. and Waychunas, G.A., 1993. Surface-chemistry of ferrihydrite .2. Kinetics of arsenate adsorption and coprecipitation. Geochimica Et Cosmochimica Acta, 57(10), 2271-2282.

Garbarino, J.R., Bednar, A.J., Rutherford, D.W., Beyer, R.S. and Wershaw, R.L., 2003. Environmental fate of roxarsone in poultry litter. I. Degradation of roxarsone during composting. Environmental Science & Technology, 37(8), 1509-1514.

Gee, G.W., Or, D. (2002) Methods of Soil Analysis (Part 4): Physical Methods. Dane, J.H., Topp, G.C. (ed), pp. 272-278, Soil Science Society of America, Madison, Wisconsin.

Ghosh, A., Mukiibi, M. and Ela, W., 2004. TCLP underestimates leaching of arsenic from solid residuals under landfill conditions. Environmental Science & Technology, 38(17), 4677-4682.

Gimenez, J., Martinez, M., de Pablo, J., Rovira, M. and Duro, L., 2007. Arsenic sorption onto natural hematite, magnetite, and goethite. Journal of Hazardous Materials, 141(3), 575-580.

Gnanaprakash, G., Mahadevan, S., Jayakumar, T., Kalyanasundaram, P., Philip, J. and Raj, B., 2007. Effect of initial pH and temperature of iron salt solutions on formation of magnetite nanoparticles. Materials Chemistry and Physics, 103(1), 168-175.

Grafe, M., Eick, M.J. and Grossl, P.R., 2001. Adsorption of arsenate (V) and arsenite (III) on goethite in the presence and absence of dissolved organic carbon. Soil Science Society of America Journal, 65(6), 1680-1687.

Gu, B.H., Schmitt, J., Chen, Z., Liang, L.Y. and McCarthy, J.F., 1995. Adsorption and desorption of different organic-matter fractions on iron-oxide. Geochimica Et Cosmochimica Acta, 59(2), 219-229.

Gulledge, J.H. and Oconnor, J.T., 1973. Removal of arsenic (v) from water by adsorption on aluminum and ferric hydroxides. Journal American Water Works Association, 65(8), 548-552.

Guo, X.J., Du, Y.H., Chen, F.H., Park, H.S. and Xie, Y.N., 2007. Mechanism of removal of arsenic by bead cellulose loaded with iron oxyhydroxide (beta-FeOOH): EXAFS study. Journal of Colloid and Interface Science, 314(2), 427-433.

He, F., Zhang, M., Qian, T.W. and Zhao, D.Y., 2009. Transport of carboxymethyl cellulose stabilized iron nanoparticles in porous media: Column experiments and modeling. Journal of Colloid and Interface Science, 334(1), 96-102.

He, F. and Zhao, D.Y., 2005. Preparation and characterization of a new class of starch-stabilized bimetallic nanoparticles for degradation of chlorinated hydrocarbons in water. Environmental Science & Technology, 39(9), 3314-3320.

He, F. and Zhao, D.Y., 2007. Manipulating the size and dispersibility of zerovalent iron nanoparticles by use of carboxymethyl cellulose stabilizers. Environmental Science & Technology, 41(17), 6216-6221.

He, F., Zhao, D.Y., Liu, J.C. and Roberts, C.B., 2007. Stabilization of Fe-Pd nanoparticles with sodium carboxymethyl cellulose for enhanced transport and dechlorination of trichloroethylene in soil and groundwater. Industrial & Engineering Chemistry Research, 46(1), 29-34.

Holm, T.R., 2002. Effects of CO32-/bicarbonate, Si, and PO43- on arsenic sorption to HFO. Journal American Water Works Association, 94(4), 174-181.

Hristovski, K., Baumgardner, A. and Westerhoff, P., 2007. Selecting metal oxide nanomaterials for arsenic removal in fixed bed columns: From nanopowders to aggregated nanoparticle media. Journal of Hazardous Materials, 147(1-2), 265-274.

Huff, W.E., Malone, G.W. and Chaloupka, G.W., 1984. Effect of litter treatment on broiler performance and certain litter quality parameters. Poultry Science, 63, 2167-2171.

Illes, E. and Tombacz, E., 2003. The role of variable surface charge and surface complexation in the adsorption of humic acid on magnetite. Colloids and Surfaces a-Physicochemical and Engineering Aspects, 230(1-3), 99-109.

Jackson, B., Bertsch, P., Cabrera, M., Camberato, J., Seaman, J. and Wood, C., 2003. Trace element speciation in poultry litter. Journal of Environmental Quality, (32), 535-540.

Jackson, B.P. and Bertsch, P.M., 2001. Determination of arsenic speciation in poultry wastes by IC-ICP-MS. Environmental Science & Technology, 35(24), 4868-4873.

Jackson, B.P. and Miller, W.P., 2000. Effectiveness of phosphate and hydroxide for desorption of arsenic and selenium species from iron oxides. Soil Science Society of America Journal, 64(5), 1616-1622.

Jain, A., Raven, K.P. and Loeppert, R.H., 1999. Arsenite and arsenate adsorption on ferrihydrite: Surface charge reduction and net OH- release stoichiometry. Environmental Science & Technology, 33(8), 1179-1184.

Jang, M., Min, S.H., Kim, T.H. and Park, J.K., 2006. Removal of arsenite and arsenate using hydrous ferric oxide incorporated into naturally occurring porous diatomite. Environmental Science & Technology, 40(5), 1636-1643.

Kanel, S.R., Manning, B., Charlet, L. and Choi, H., 2005. Removal of arsenic(III) from groundwater by nanoscale zero-valent iron. Environmental Science & Technology, 39(5), 1291-1298.

Kanel, S.R., Nepal, D., Manning, B. and Choi, H., 2007. Transport of surface-modified iron nanoparticle in porous media and application to arsenic(III) remediation. Journal of Nanoparticle Research, 9(5), 725-735.

Kang, M., Kawasaki, M., Tamada, S., Kamei, T. and Magara, Y., 2000. Effect of pH on the removal of arsenic and antimony using reverse osmosis membranes. Desalination, 131(1-3), 293-298.

Kapaj, S., Peterson, H., Liber, K. and Bhattacharya, P., 2006. Human health effects from chronic arsenic poisoning- A review. Journal of Environmental Science and Health Part a-Toxic/Hazardous Substances & Environmental Engineering, 41(10), 2399-2428.

Kretzschmar, R., Borkovec, M., Grolimund, D. and Elimelech, M., 1999. Mobile subsurface colloids and their role in contaminant transport. Advances in Agronomy, Vol 66, 66, 121-193.

Lecoanet, H.F. and Wiesner, M.R., 2004. Velocity effects on fullerene and oxide nanoparticle deposition in porous media. Environmental Science & Technology, 38(16), 4377-4382.

Lee, J., Isobe, T. and Senna, M., 1996. Preparation of ultrafine Fe3O4 particles by precipitation in the presence of PVA at high pH. Journal of Colloid and Interface Science, 177(2), 490-494.

Li, H., Xin, H.W., Burns, R.T. and Liang, Y. (2006) Reduction of Ammonia Emission from Stored Poultry Manure Using Additives: Zeolite, Al+clear, Ferix-3 and PLT, Oregon Convention Center, Portland, Oregon

Liang, Q.Q., Qian, T.W., Zhao, D.Y., Freeland, K. and Feng, Y.C., 2012a. Effects of Stabilizers and Water Chemistry on Arsenate Sorption by Polysaccharide-Stabilized Magnetite Nanoparticles. Industrial & Engineering Chemistry Research.

Liang, Q.Q., Zhao, D.Y., Qian, T.W., Freeland, K. and Feng, Y.C., 2012b. Effects of stabilizers and water chemistry on arsenate sorption by polysaccharide-stabilized magnetite nanoparticles. Industrial & Engineering Chemistry Research, 51(5), 2407-2418.

Liu, G.J., Zhang, X.R., Talley, J.W., Neal, C.R. and Wang, H.Y., 2008. Effect of NOM on arsenic adsorption by TiO2 in simulated As(III)-contaminated raw waters. Water Res, 42(8-9), 2309-2319.

Liu, R. and Zhao, D., 2007. Reducing leachability and bioaccessibility of lead from soils using a new class of stabilized iron phosphate nanoparticles. Water Research, 41, 2491-2502.

Liu, X.Y., Wazne, M., Christodoulatos, C. and Jasinkiewicz, K.L., 2009. Aggregation and deposition behavior of boron nanoparticles in porous media. Journal of Colloid and Interface Science, 330(1), 90-96.

Lorentzen, E.M.L. and Kingston, H.M., 1996. Comparison of microwave-assisted and conventional leaching using EPA method 3050B. Analytical Chemistry, 68(24), 4316-4320.

Manning, B.A., Fendorf, S.E. and Goldberg, S., 1998. Surface structures and stability of arsenic(III) on goethite: Spectroscopic evidence for inner-sphere complexes. Environmental Science & Technology, 32(16), 2383-2388.

Manning, B.A. and Goldberg, S., 1997. Adsorption and stability of arsenic(III) at the clay mineral-water interface. Environmental Science & Technology, 31(7), 2005-2011.

Manning, B.A., Hunt, M.L., Amrhein, C. and Yarmoff, J.A., 2002. Arsenic(III) and Arsenic(V) reactions with zerovalent iron corrosion products. Environmental Science & Technology, 36(24), 5455-5461.

Marcano-Martinez, E., McBride, M.B., 1989. Comparison of the titration and ion adsorption methods for surface charge measurement in oxisols. Soil Sci. Soc. Am. J., 53, 1040-1045.

Marmier, N., Delisee, A. and Fromage, F., 1999. Surface complexation modeling of Yb(III), Ni(II), and Cs(I) sorption on magnetite. Journal of Colloid and Interface Science, 211(1), 54-60.

Masscheleyn, P.H., Delaune, R.D. and Patrick, W.H., 1991. Effect of reodx potential and pH on arsenic speciation and solubility in a contaminated soil. Environmental Science & Technology, 25(8), 1414-1419.

Mayo, J.T., Yavuz, C., Yean, S., Cong, L., Shipley, H., Yu, W., Falkner, J., Kan, A., Tomson, M. and Colvin, V.L., 2007. The effect of nanocrystalline magnetite size on arsenic removal. Science and Technology of Advanced Materials, 8(1-2), 71-75.

Melitas, N., Wang, J.P., Conklin, M., O'Day, P. and Farrell, J., 2002. Understanding soluble arsenate removal kinetics by zerovalent iron media. Environmental Science & Technology, 36(9), 2074-2081.

Molday, R.S. (1984) Magnetic iron-dextran microspheres, United States Patent.

Moore, P.A., Daniel, T.C. and Edwards, D.R., 1999. Reducing phosphorus runoff and improving poultry production with alum. Poultry Science, 78(5), 692-698.

Morrison, J.L., 1969. Distribution of arsenic from poultry litter in broiler chickens, soil, and crops. Journal of Agricultural and Food Chemistry, 17(6), 1288-&.

Nachman, K.E., Graham, J.P., Price, L.B. and Silbergeld, E.K., 2005. Arsenic: a roadblock to potential animal waste management solutions. Environmental Health Perspectives, 113(9), 1123-1124.

National Research Council, N.R.C. (2001) Arsenic in drinking water: 2001 update, National Academy Press, Washington, DC.

Nordstrom, D.K., 2002. Public health - Worldwide occurrences of arsenic in ground water. Science, 296(5576), 2143-2145.

Peng, F.F. and Di, P.K., 1994. Removal of arsenic from aqueous-solution by adsorbing colloid flotation. Industrial & Engineering Chemistry Research, 33(4), 922-928.

Pierce, M.L. and Moore, C.B., 1982. Adsorption of arsenite and arsenate on amorphous iron hydroxide. Water Research, 16(7), 1247-1253.

Raven, K.P., Jain, A. and Loeppert, R.H., 1998. Arsenite and arsenate adsorption on ferrihydrite: Kinetics, equilibrium, and adsorption envelopes. Environmental Science & Technology, 32(3), 344-349.

Redman, A.D., Macalady, D.L. and Ahmann, D., 2002. Natural organic matter affects arsenic speciation and sorption onto hematite. Environmental Science & Technology, 36(13), 2889-2896.

Roonasi, P., A. Holmgren (2009) A study on the mechanism of magnetite formation based on iron isotope fractionation, San Francisco, California.

Rutherford, D.W., Bednar, A.J., Garbarino, J.R., Needham, R., Staver, K.W. and Wershaw, R.L., 2003a. Environmental fate of roxarsone in poultry litter. part II. Mobility of arsenic in soils amended with poultry litter. Environmental Science & Technology, 37(8), 1515-1520.

Rutherford, D.W., Bednar, A.J., Garbarino, J.R., Needham, R., Staver, K.W. and Wershaw, R.L., 2003b. Environmental fate of roxarsone in poultry litter. Part II. Mobility of arsenic in soils amended with poultry litter. Environmental Science & Technology, 37, 1515-1520.

Saltikov, C.W., Wildman, R.A. and Newman, D.K., 2005. Expression dynamics of arsenic respiration and detoxification in Shewanella sp strain ANA-3. Journal of Bacteriology, 187(21), 7390-7396.

Santra, S., Tapec, R., Theodoropoulou, N., Dobson, J., Hebard, A. and Tan, W.H., 2001. Synthesis and characterization of silica-coated iron oxide nanoparticles in microemulsion: The effect of nonionic surfactants. Langmuir, 17(10), 2900-2906.

Schaefer, A., 2007. Chicken litter and arsenic. Environmental Science and Technology, 41, 668-669.

Shah, S., Westerman, P. and Parsons, J. (2006) Poultry litter amendments, North Carolina State University.

Shipley, H.J., Engates, K.E. and Guettner, A.M., 2011. Study of iron oxide nanoparticles in soil for remediation of arsenic. Journal of Nanoparticle Research, 13(6), 2387-2397.

Shipley, H.J., Yean, S., Kan, A.T. and Tomson, M.B., 2009. Adsorption of arsenic to magnetite nanoparticles: effect of particle concentration, pH, ionic strength, and temperature. Environmental Toxicology and Chemistry, 28(3), 509-515.

Shipley, H.J., Yean, S., Kan, A.T. and Tomson, M.B., 2010. A sorption kinetics model for arsenic adsorption to magnetite nanoparticles. Environmental Science and Pollution Research, 17(5), 1053-1062.

Si, S., Kotal, A., Mandal, T.K., Giri, S., Nakamura, H. and Kohara, T., 2004. Size-controlled synthesis of magnetite nanoparticles in the presence of polyelectrolytes. Chemistry of Materials, 16(18), 3489-3496.

Smedley, P.L. and Kinniburgh, D.G., 2002. A review of the source, behaviour and distribution of arsenic in natural waters. Applied Geochemistry, 17(5), 517-568.

Smith, E., Naidu, R. and Alston, A.M., 1998. Arsenic in the soil environment: A review. Advances in Agronomy, Vol 64, 64, 149-195.

Sparks, D.L. (1989) Kinetics of Soil Chemical Processes, Academic Press, New York.

Stolz, J.E., Basu, P., Santini, J.M. and Oremland, R.S. (2006) Annual Review of Microbiology, pp. 107-130.

Su, C.M. and Puls, R.W., 2001. Arsenate and arsenite removal by zerovalent iron: Effects of phosphate, silicate, carbonate, borate, sulfate, chromate, molybdate, and nitrate, relative to chloride. Environmental Science & Technology, 35(22), 4562-4568.

Su, C.M. and Puls, R.W., 2003. In situ remediation of arsenic in simulated groundwater using zerovalent iron: Laboratory column tests on combined effects of phosphate and silicate. Environmental Science & Technology, 37(11), 2582-2587.

Sun, S.H. and Zeng, H., 2002. Size-controlled synthesis of magnetite nanoparticles. Journal of the American Chemical Society, 124(28), 8204-8205.

Thirunavukkarasua, O.S., Viraraghavana, T., Subramanianb, K.S. and Tanjorec, S., 2002. Organic arsenic removal from drinking water. Urban Water, 4(4), 415-421.

Tufenkji, N. and Elimelech, M., 2004. Deviation from the classical colloid filtration theory in the presence of repulsive DLVO interactions. Langmuir, 20(25), 10818-10828.

USDA (2007) United States Department of Agriculture, US and State Data, USDA, Washington, DC.

USDA (2008a) U.S. Broiler Industry: Background Statistics and Information.

USEPA (1992) Toxicity Characteristic Leaching Procedure, Method 1311, Washington, DC.

USEPA (1996) Acid Digestion of Sediments, Sludges, and Soils, Method 3050B, Washington, DC.

Vaishya, R.C. and Gupta, S.K., 2003. Arsenic removal from groundwater by iron impregnated sand. Journal of Environmental Engineering-Asce, 129(1), 89-92.

Wallinga, D. (2006) Playing chicken: avoiding arsenic in your meat, The Institute for Agriculture and Trade policy, Food and Health Program, Minneapolis, Minnesota, USA.

Waychunas, G.A., Rea, B.A., Fuller, C.C. and Davis, J.A., 1993. Surface-chemistry of ferrihydrite .1. Exafs studies of the geometry of coprecipitated and adsorbed arsenate. Geochimica Et Cosmochimica Acta, 57(10), 2251-2269.

Welch, A.H., Lico, M.S. and Hughes, J.L., 1988. Arsenic in ground-water of the western united-states. Ground Water, 26(3), 333-347.

Welch, A.H., Westjohn, D.B., Helsel, D.R. and Wanty, R.B., 2000. Arsenic in ground water of the United States: Occurrence and geochemistry. Ground Water, 38(4), 589-604.

Wenzel, W.W., Kirchbaumer, N., Prohaska, T., Stingeder, G., Lombi, E. and Adriano, D.C., 2001. Arsenic fractionation in soils using an improved sequential extraction procedure. Analytica Chimica Acta, 436(2), 309-323.

Woo, K., Hong, J., Choi, S., Lee, H.W., Ahn, J.P., Kim, C.S. and Lee, S.W., 2004. Easy synthesis and magnetic properties of iron oxide nanoparticles. Chemistry of Materials, 16(14), 2814-2818.

Woolson, E.A., Axley, J.H. and Kearney, P.C., 1973. Chemistry and phytotoxicity of arsenic in soils. 2. Effects of time and phosphorus Soil Science Society of America Journal, 37(2), 254-259.

World Health Organization, W.H.O. (2000) Air quality guidelines for Europe, 2nd edition. Chapter 6.1 Arsenic.

World Health Organization, W.H.O., 2008. Guidelines for drinking-water quality (Third Edition, incorporating the first and second addenda), Volume 1, 186.

Xiong, Z., He, F., Zhao, D.Y. and Barnett, M.O., 2009. Immobilization of mercury in sediment using stabilized iron sulfide nanoparticles. Water Research, 43(20), 5171-5179.

Xu, Y.H. and Zhao, D.Y., 2007. Reductive immobilization of chromate in water and soil using stabilized iron nanoparticles. Water Research, 41(10), 2101-2108.

Yang, J.K., Barnett, M.O., Jardine, P.M., Basta, N.T. and Casteel, S.W., 2002. Adsorption, sequestration, and bioaccessibility of As(V) in soils. Environmental Science & Technology, 36(21), 4562-4569.

Yavuz, C.T., Mayo, J.T., Yu, W.W., Prakash, A., Falkner, J.C., Yean, S., Cong, L.L., Shipley, H.J., Kan, A., Tomson, M., Natelson, D. and Colvin, V.L., 2006. Low-field magnetic separation of monodisperse Fe_3O_4 nanocrystals. Science, 314(5801), 964-967.

Yean, S., Cong, L., Yavuz, C.T., Mayo, J.T., Yu, W.W., Kan, A.T., Colvin, V.L. and Tomson, M.B., 2005. Effect of magnetite particle size on adsorption and desorption of arsenite and arsenate. Journal of Materials Research, 20(12), 3255-3264.

Zhang, G.S., Qu, J.H., Liu, H.J., Liu, R.P. and Li, G.T., 2007. Removal mechanism of As(III) by a novel Fe-Mn binary oxide adsorbent: Oxidation and sorption. Environmental Science & Technology, 41(13), 4613-4619.

Appendix 1

Film diffusion model

$$\Delta M = \Delta q \cdot W, \qquad q = K_d \cdot C_s + b$$

$$\frac{\Delta q \cdot W}{A \cdot \Delta t} = K_f (C_b - C_s), \qquad a = A/V$$

$$W \cdot \frac{\partial q}{\partial t} = K_f A(C_b - C_s) = K_f \cdot (a \cdot V) \cdot (C_b - C_s)$$

Make K= $K_f A$. Since

$$q \cdot w = V(C_b - C_s), \quad \frac{w}{V} \cdot \frac{\partial q}{\partial t} = -\frac{\partial C_b}{\partial t}$$

$$-\frac{\partial C_b}{\partial t} = K[C_b - \frac{1}{K_d} \cdot \frac{V}{W} (C_0 - C_b) + \frac{b}{K_d}]$$

$$-\frac{\partial C_b}{\partial t} = K[C_b \left(1 + \frac{1}{K_d} \cdot \frac{V}{W}\right) - \frac{1}{K_d} \cdot \frac{V}{W} C_0 + \frac{b}{K_d}]$$

Let $m = 1 + \frac{1}{K_d} \cdot \frac{V}{W}$, $n = \frac{1}{K_d} \cdot \frac{V}{W} C_0 - \frac{b}{K_d}$

$$-\frac{\partial C_b}{\partial t} = K[C_b \cdot m - n] = mKC_b - nK$$

$$\frac{\partial C_b}{\partial t} + mKC_b = nK$$

$$\partial C_b + mKC_b \partial t = nK \partial t$$

$$\partial C_b = (nK - mKC_b) \partial t$$

$$\frac{\partial C_b}{nK - mKC_b} = \partial t$$

$$\int_{C_0}^{C_b} \frac{\partial(nK - mKC_b)}{nK - mKC_b} = -mK \int_0^t \partial t$$

$$\ln(nK - mKC_b) \Big|_{C_0}^{C_b} = -mKt$$

$$\ln(nK - mKC_b) - \ln(nK - mKC_0) = -mKt$$

$$\ln(nK - mKC_b) = \ln(nK - mKC_0) - mKt$$

$$e^{\ln(nK - mKC_b)} = e^{\ln(nK - mKC_0)} / e^{mKt}$$

$$nK - mKC_b = \frac{nK - mKC_0}{e^{mKt}}$$

$$n - mC_b = \frac{n - mC_0}{e^{mKt}}$$

$$C_b = \frac{mC_0 - n}{m \cdot e^{mKt}} + \frac{n}{m}$$

When $= 1 + \frac{1}{K_d} \cdot \frac{V}{W}$, $n = \frac{1}{K_d} \cdot \frac{V}{W}\ C_0 - \frac{b}{K_d}$, K= $K_f A$

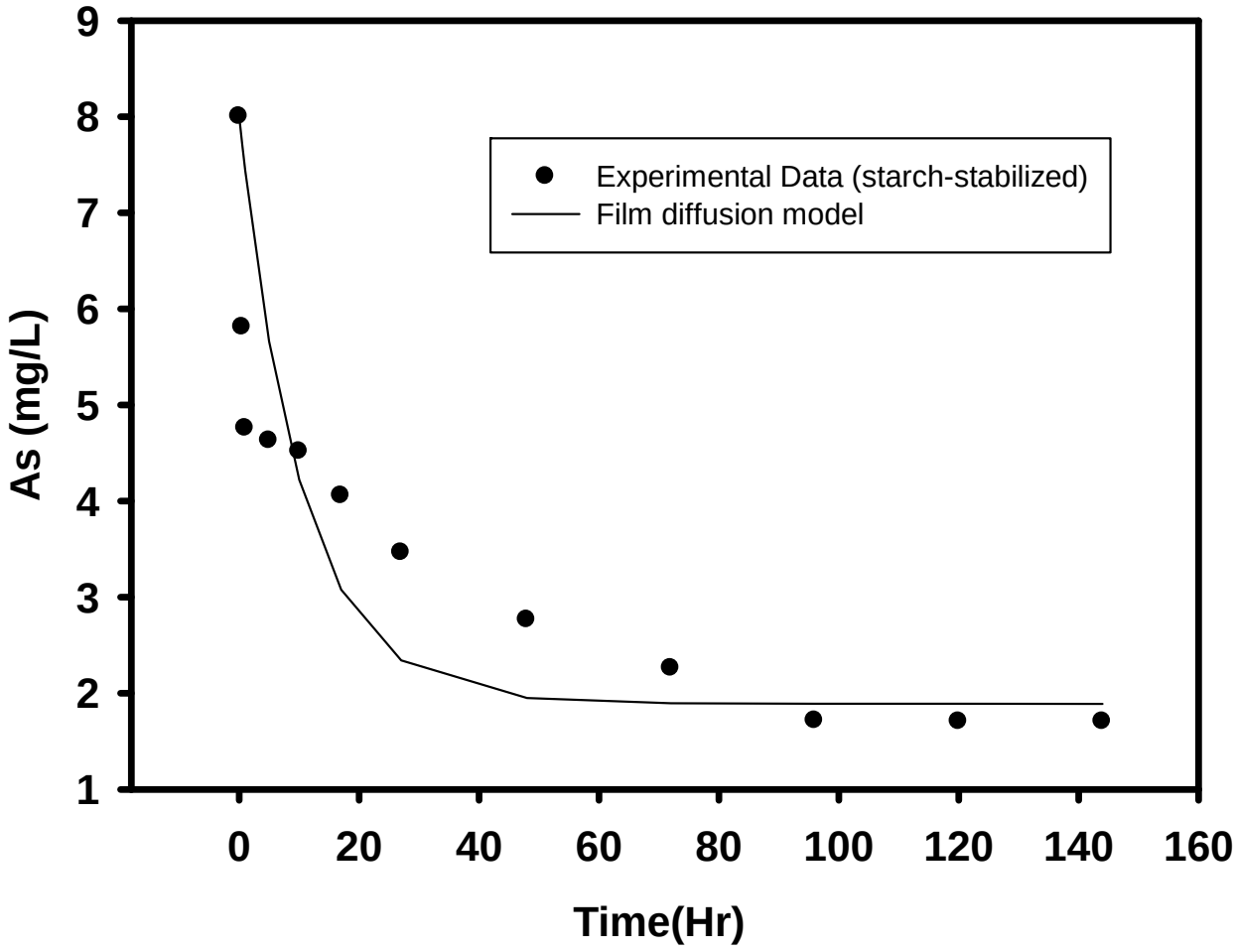

Figure A-1. The sorption kinetics of starch-stabilized magnetite nanoparticles fitted by film diffusion model. Fitting parameter K= 0.0220, the difference Δ= $(C_{experimental} - C_{model})^2 =$ 15.072

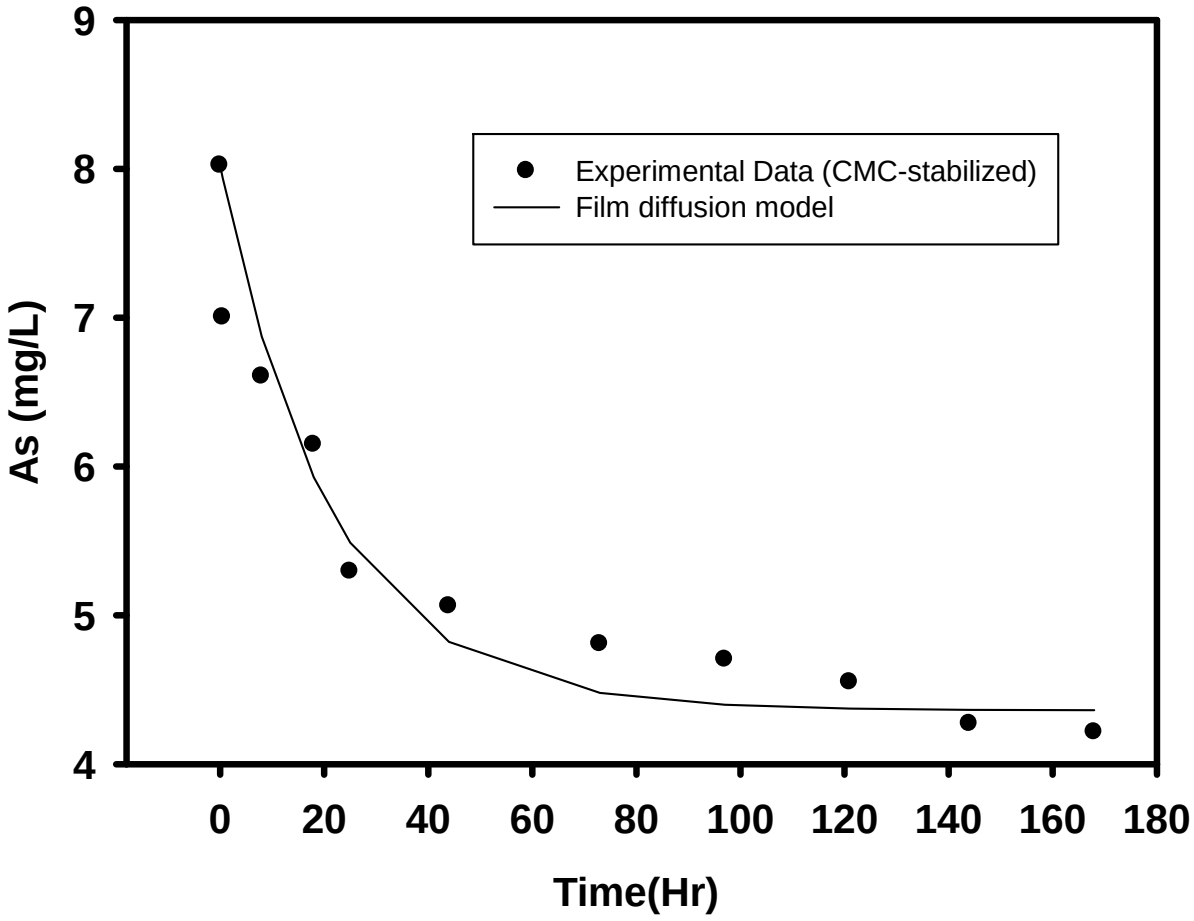

Figure A-2. The sorption kinetics of CMC-stabilized magnetite nanoparticles fitted by film diffusion model. Fitting parameter K= 0.0049, the difference $\Delta = (C_{experimental} - C_{model})^2 =$ 1.3479

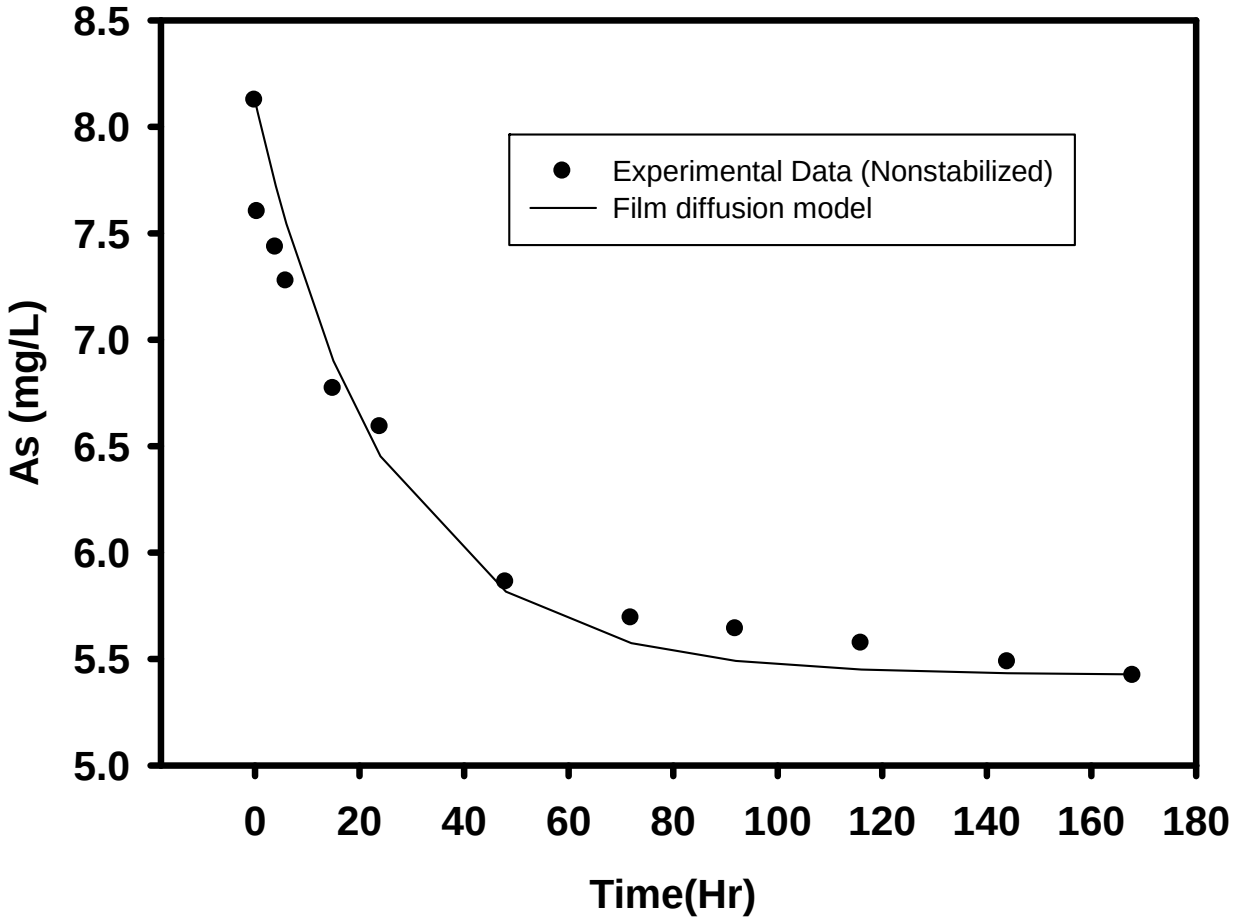

Figure A-3. The sorption kinetics of nonstabilized magnetite nanoparticles fitted by film diffusion model. Fitting parameter K= 0.0011, the difference $\Delta = (C_{experimental} - C_{model})^2 =$ 0.46990

Appendix 2

Intraparticle diffusion model

```
Program DOW3Nkinetic

!       This program is to calcualte the limited volume solution by Crank
!       for DOW 3N-Cu in the presence of sulfate.
!    Notation:
!    PK: partition coefficient (q/C (mg/g)/(mg/L))
!    Unit: q-mg/g; C-mg-P/L; D-um2/hr; t-hr; a-um ; V-L

     integer m, k
     real fmid, t, qn, qq, term, sum, root(1000), x1, dx
     real x0, x2, alpha, Frac, M0, Mt, Ct, C0, V

     Parameter (pi=3.141592694)


     Data a/0.029/, D/1E-7/, alpha/2.00/, M0/0.040529/, V/0.015/
     Data C0/8.1235/


     Fun(z)= tan(z)-3*z/(3+alpha*z**2)


!     alpha=3*V/(4*pi*a**3*PK)  use Minfinite/VC0=1/(1+alpha)


         Open  (Unit=10, FILE='starch_1.dat', STATUS='unknown')

         Write (10, *) 'Time (hour)          Ct'



!    Compute the roots using bisectional method
```

```
      do 10 m=1, 1000

      x1=float(2*(m-1)-1)*(pi/2)
      if (m.eq.1) x1=0.
          x2=float(2*m-1)*(pi/2)
          root(m)=x1
          dx=x2-x1
           do 20 j=1, 200
       dx=0.5*dx
            xmid=root(m)+dx
            fmid=Fun(xmid)
            if (fmid.lt.0.0) root(m)=xmid
            if (ABS(dx).lt.1e-10) goto 10
            if (fmid.eq.0.0) goto 10

20      continue


10     continue



!      the series solution


      DO 50 k=0, 170, 1

      sum=0.
          t=float(k)*10

           do 30 n=1, 500

           qn=root(n+1)
       qq=qn*qn
           term=6.0*alpha*(alpha+1.0)*exp(-D*qq*t/a**2.0)/(9.0+9.0*alpha+qq
     &     *alpha**2.0)

       sum=sum+term


           if (ABS(term).lt.ABS(sum/1.0E6)) goto 40

30     continue

40     Frac=1.0-sum
```

```
      Mt=M0*Frac

          Ct=C0-Mt/V

      write(10, '(1X, I5, F20.5)') k, Ct

50    continue

      close (100)
          end
```

α (alpha) is expressed in terms of the final fractional uptake of arsenate as

$$\frac{Mq_{\infty}}{V_0 C_0} = \frac{1}{1+\alpha}$$

Where V_0 and C_0 are initial solution volume and initial As(V) concentration in solution, respectively.

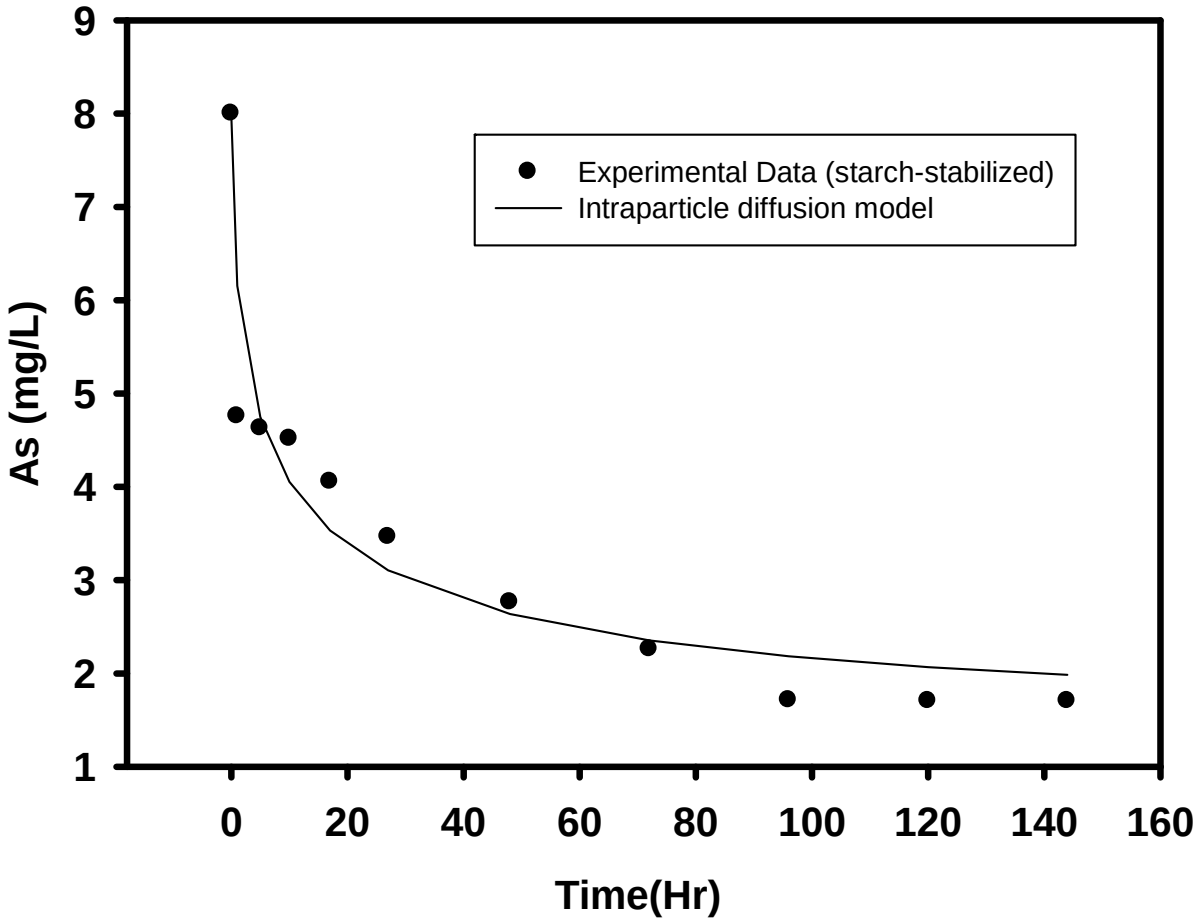

Figure A-4. The sorption kinetics of starch-stabilized magnetite nanoparticles fitted by intraparticle diffusion model. Fitting parameter D= 3.00E-7 μm^2/hr, the difference $\Delta = (C_{experimental} - C_{model})^2 = 3.0426 < 15.072$ (film diffusion). Thus, the intraparticle diffusion model described the arsenate-magnetite adsorption kinetic better than the film diffusion model.

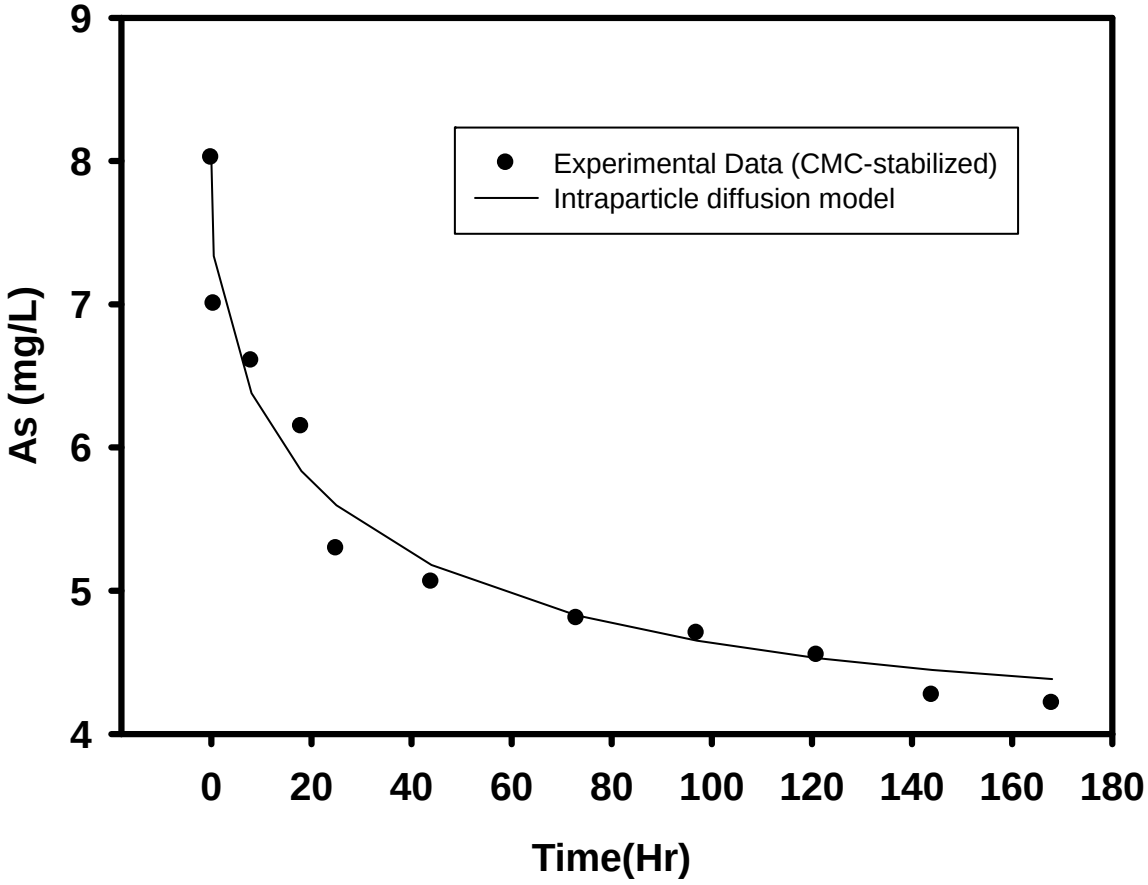

Figure A-5. The sorption kinetics of CMC-stabilized magnetite nanoparticles fitted by intraparticle diffusion model. Fitting parameter D=8.0E-10 μm^2/hr, $\Delta = (C_{experimental} - C_{model})^2 = 0.4287 < 1.3479$ (film diffusion)

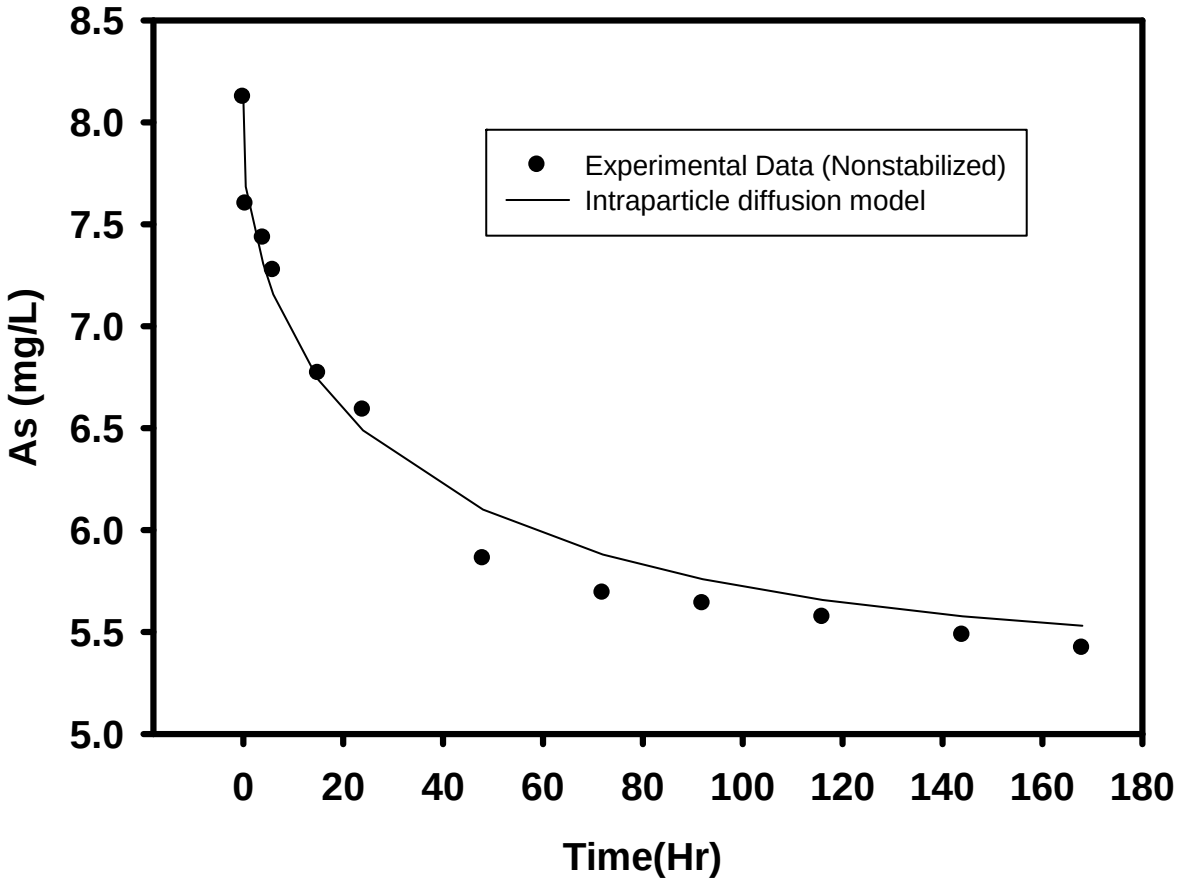

Figure A-6. The sorption kinetics of nonstabilized magnetite nanoparticles fitted by intraparticle diffusion model. Fitting parameter D=1.0E-07 μm^2/hr, $\Delta = (C_{experimental} - C_{model})^2 = 0.1842 < 0.46990$ (film diffusion)